



**“Novel therapeutic targets for the treatment  
of diabetes and obesity:  
potential and risks of D-serine and its transporter Asc-1”**

Lisa Siu-Lan Suwandhi

Vollständiger Abdruck der von der Fakultät für Medizin der Technischen Universität München zur Erlangung des akademischen Grades eines Doktors der Naturwissenschaften genehmigten Dissertation.

Vorsitzender: Prof. Dr. Percy A. Knolle  
Prüfer der Dissertation: 1. Prof. Dr. Matthias Tschöp  
2. Prof. Dr. Martin Klingenspor

Die Dissertation wurde am 22.08.2018 bei der Technischen Universität München eingereicht und durch die Fakultät der Medizin am 08.10.2019 angenommen.

## **Eidesstattliche Erklärung**

Ich erkläre an Eides statt, dass ich die bei der Fakultät für Medizin zur Promotionsprüfung vorgelegte Arbeit mit dem Titel:

### **„Novel therapeutic targets for the treatment of diabetes and obesity: potential and risks of D-serine and its transporter Asc-1”**

am Institut für Diabetes und Adipositas (Helmholtz Zentrum München) unter der Anleitung und Betreuung durch Prof. Dr. Tschöp ohne sonstige Hilfsmittel erstellt und bei der Abfassung nur die gemäß § 6 Abs. 6 und 7 Satz 2 angegebenen Hilfsmittel benutzt habe.

Ich habe keine Organisation eingeschaltet, die gegen Entgelt Betreuerinnen und Betreuer für die Anfertigung von Dissertationen sucht, oder die mir obliegenden Pflichten hinsichtlich der Prüfungsleistungen für mich ganz oder teilweise erledigt.

Ich habe die Dissertation in dieser oder ähnlicher Form in keinem anderen Prüfungsverfahren als Prüfungsleistung vorgelegt.

Die vollständige Dissertation wurde noch nicht veröffentlicht.

Ich habe den angestrebten Doktorgrad noch nicht erworben und bin nicht in einem früheren Promotionsverfahren für den angestrebten Doktorgrad endgültig gescheitert.

Die öffentlich zugängliche Promotionsordnung der TUM ist mir bekannt, insbesondere habe ich die Bedeutung von § 28 (Nichtigkeit der Promotion) und § 29 (Entzug des Doktorgrades) zur Kenntnis genommen. Ich bin mir der Konsequenzen einer falschen Eidesstattlichen Erklärung bewusst.

Mit der Aufnahme meiner personenbezogenen Daten in die Alumni-Datei bei der TUM bin ich einverstanden.

München, den

Lisa Suwandhi

## I Abbreviations

BMI	body mass index	mRNA	messenger RNA
4F2hc	4F2 heavy chain	mTOR	mammalian target of rapamycin
ABC	ATP-binding cassette	NMDA	N-methyl-D-aspartate
aP2	fatty acid binding protein 4	OCR	oxygen consumption rate
ASC-1	alanine serine cysteine transporter 1	P2rx5	purinergic receptor P2rx, ligand-gated ion channel 5
BAT	brown adipose tissue	PAT2	proton-coupled amino acid transporter-2
CAT	cationic amino acid transporter	PBS	Phosphate-buffered saline
CD	chow diet	PEPCK	Phosphoenolpyruvate carboxykinase
CD68	Cluster of Differentiation 68	PFA	paraformaldehyde
CNS	central nervous system	PGC1 $\alpha$	Peroxisome proliferator activated receptor $\gamma$ (PPAR $\gamma$ ) coactivator 1 $\alpha$
CRH	corticosterone releasing hormone	PGF	perigonadal adipose tissue
CSF	cerebrospinal fluid	PPAR $\gamma$	Peroxisome proliferator activated receptor $\gamma$
DAO	D-amino acid oxidase	PRDM16	PR (PRD1-BF1-RIZ1 homologous) domain-containing 16
DXM	Dextromethorphan hydrobromide monohydrate	RER	respiratory exchange quotient
DXO	dextrorphan tartrate	Rosi	rosiglitazone
E.coli	Escherichia coli	SCF	subcutaneous adipose tissue
GLP-1	glucagon-like peptide-1	Scr	scrambled
GSIS	glucose stimulated insulin secretion test	SHMT1	Serine hydroxymethyltransferase 1
GTT/ITT/PTT	Glucose / Insulin / Pyruvate tolerance test	shRNA	short hairpin RNA
GWAS	genome-wide association studies	SLC	solute carrier
H&E	hematoxylin and eosin	SNP	single nucleotide polymorphism
HAT	hetero(di)meric amino acid transporter	SRR	serine racemase
HDL	high-density lipoprotein	T2D	Type 2 diabetes
HFD	high fat diet	TBP	TATA-box binding protein
HSL	hormone sensitive lipase	TBS	tris-buffered saline
i.p.	intraperitoneal	TFAM	mitochondrial transcription factor A
IBMX	3-Isobutyl-1-methylxanthin	TNF $\alpha$	Tumor necrosis factor alpha
IL-6	Interleukin-6	UCP1	Uncoupling protein 1
IP	immunoprecipitation	VLDL	very-low-density lipoprotein
KIM1	Kidney injury molecule-1	WAT	white adipose tissue
MAC-1	macrophage-1 antigen	WHO	world health organization
MALDI FT-ICR MSI	Matrix-assisted laser desorption/ionization Fourier-transform ion cyclotron resonance mass spectrometry imaging	wt/het/ko	wildtype/heterozygous/knockout

## II List of tables

Table 1: Consumables .....	28
Table 2: Chemicals .....	28
Table 3: Amino acids.....	30
Table 4: Antibodies and fluorescent dyes .....	31
Table 5: Enzymes .....	31
Table 6: Genotyping PCR for ASC-1 ko mice .....	33
Table 7: Primers for cloning and sequencing pCDH-Asc-1-HA.....	44
Table 8: Primers for cloning and sequencing pCDH-Asc-1-HA-2a-4f2hc.....	45
Table 9: qPCR primers.....	48

## III List of figures

Figure 1: Projected rates of obesity .....	11
Figure 2: Brown, beige and white adipocytes .....	14
Figure 3: Expression pattern of <i>Asc-1</i> in mice .....	24
Figure 4: Regulation of synaptic D-serine levels by ASCT, ASC-1, SRR and DAO .	26
Figure 5: Loss of ASC-1 changes the intra- and extracellular amino acid profiles....	53
Figure 6: Loss of ASC-1 increases brown adipocyte marker gene expression.....	54
Figure 7: Beige ASC-1 knockdown cells are functional beige adipocytes .....	55
Figure 8: Overexpression of ASC-1 in brown preadipocytes reduces brown adipocyte specific gene expression .....	57
Figure 9: Knockdown of ASC-1 results in spontaneous differentiation .....	58
Figure 10: Early chemical inhibition of ASC-1 induces beige adipocyte differentiation .....	60
Figure 11: <i>Asc-1</i> is differently expressed in subcutaneous single cell clones .....	61
Figure 12: Knockdown of ASC-1 alters intracellular amino acid profile of preadipocytes.....	62
Figure 13: Extracellular D-serine does not alter brown adipocyte identity .....	63
Figure 14: Whole body ASC-1 knockout mice have smaller adipocytes in SCF.....	63
Figure 15: Global loss of ASC-1 induces hepatosteatosis and reduces UCP1 in BAT .....	65
Figure 16: Heterozygous ASC-1 ko mice develop normal upon CD and HFD feeding .....	66
Figure 17: Oral administered D-serine is taken up by various organs .....	68
Figure 18: D-serine prevents from diet induced obesity .....	69

Figure 19: D-serine reduces high fat diet food intake.....	70
Figure 20: D-serine alters gut microbiota composition .....	71
Figure 21: D-serine accumulates in organs but does not induce inflammation .....	73
Figure 22: D-serine reduces adipocyte cell size and prevents from hepatosteatosis upon HFD feeding .....	74
Figure 23: D-serine impairs glucose tolerance.....	76
Figure 24: D-serine alters hepatic one-carbon metabolism.....	77
Figure 25: D-serine impairs insulin secretion from pancreatic beta cells.....	78
Figure 26: DXM supplementation reduces water intake.....	79
Figure 27: D-serine has does not directly impair insulin secretion <i>in vitro</i> . .....	80
Figure 28: D-serine accumulates in the hypothalamus and alters c-Fos expression	81
Figure 29: Inhibition of $\alpha$ 2-adrenergic receptors normalizes glucose tolerance of D-serine supplemented mice.....	82
Figure 30: L-serine has no effect on body weight gain.....	83
Figure 31: L-serine does not alter white adipose tissue morphology.....	84
Figure 32: L-serine alters <i>Shmt1</i> expression in BAT.....	85
Figure 33: L-serine has no impact on glucose tolerance or gut microbiota .....	86
Figure 34: L-serine alters hepatic metabolism .....	87
Supplemental Figure 1: Vector map of pCDH-CMV-MCS-EF1-puro-Asc-1-HA.....	118
Supplemental Figure 2: Vector map of pCDH-CMV-MCS-EF1-puro-Asc-1-HA-2a-4F2hc.....	119

## IV Abstract

Obesity is a major health burden all over the world with increasing prevalence. In addition to obesity, the numbers of its co-morbidities, over all diabetes, are rising. One novel therapeutic approach to treat obesity and diabetes is tissue targeted therapy, which aims to bring drugs specifically to a target tissue. Recently, the amino acid transporter ASC-1 was found to be specifically expressed on the surface of white but not brown adipocytes. Therefore, ASC-1 could display a novel target for the treatment of obesity. Though, the role of this amino acid transporter in white adipose tissue remains unknown so far. Besides white adipose tissue, ASC-1 is expressed in the brain, where its main function is to transport the signaling molecule D-serine. D-serine is a co-agonist of N-methyl-D-aspartate (NMDA) receptors, which are important in neuronal development and learning processes. Dysregulation of NMDARs can result in various diseases, such as depression or schizophrenia. Latter can be treated with D-serine or drugs elevating D-serine levels, however, little is known about the role of D-serine in whole body metabolism.

Here, it is shown that the amino acid transporter ASC-1 is important for maintaining white adipocyte identity. Loss or chemical inhibition of ASC-1 *in vitro* results in spontaneous differentiation into brown-like adipocytes. This may be driven by the accumulation of intracellular D-serine. Nevertheless, supplementation of mice with D-serine does not increase white adipose tissue (WAT) beiging. Instead, it is shown that D-serine has an impact on high fat diet (HFD) food intake and therefore prevents from diet induced weight gain and hepatosteatosis. In contrast to that positive effect, D-serine induces diet-independent hyperglycemia. This is caused by impaired insulin secretion from pancreatic beta cells, which most likely results from altered sympathetic activity. Inhibition of  $\alpha$ 2-adrenergic receptors rapidly restores D-serine caused glycemia and glucose tolerance. Independent of D-serine, supplementation with its proteinogenic enantiomer L-serine alters hepatic metabolism and gluconeogenesis.

Thus, here it is demonstrated that the transporter ASC-1 is a novel therapeutic target for the treatment of obesity whereas its cargo D-serine exhibits a severe risk in the treatment of NMDAR hypocativation, resulting in the development of hyperglycemia.

## V Zusammenfassung

Adipositas ist ein weltweit zunehmendes Gesundheitsproblem mit vielen verschiedenen Begleiterkrankungen wie beispielsweise Diabetes. Eine neue Möglichkeit zur Behandlung von Adipositas und Diabetes ist die Gewebs-spezifische Therapie. Diese hat das Ziel, Medikamente spezifisch zum Wunschgewebe zu bringen und dabei Nebenwirkungen zu reduzieren. Vor einiger Zeit wurde festgestellt, dass der Aminosäuretransporter ASC-1 spezifisch auf der Oberfläche von weißen, aber nicht von braunen Fettzellen exprimiert wird. Daher könnte ASC-1 ein innovatives Zielmolekül für die Gewebs-spezifische Therapie darstellen, allerdings ist dessen spezielle Funktion im Fettgewebe bisher nicht bekannt. Neben weißem Fett wird ASC-1 auch im Gehirn exprimiert, wo es der Haupt-Transporter des Neurotransmitters D-serin ist. D-serin ist ein Co-Agonist von N-methyl-D-aspartate (NDMA) Rezeptoren, die wichtig für neuronale Entwicklung sowie Lernprozesse sind. Deregulierung von NMDA-Rezeptoren kann Krankheiten wie Depression oder Schizophrenie verursachen. Letztere kann mit D-serin oder D-serin-erhöhende Medikamente behandelt werden, aber die Rolle von D-serin auf den Gesamtmetabolismus ist bisher nicht bekannt.

In dieser Arbeit wird gezeigt, dass der Aminosäuretransporter ASC-1 wichtig für die Identität von weißen Fettzellen ist. Verlust oder chemische Inhibierung von ASC-1 führt *in vitro* dazu, dass weiße Präadipozyten spontan in beige Adipozyten differenzieren. Dies könnte durch eine intrazelluläre Akkumulierung von D-serin verursacht sein, obwohl bei Mäusen eine orale Gabe von D-serin im Trinkwasser keine Auswirkungen auf die Anzahl beiger Adipozyten in weißem Fett hat. Im Gegenteil dazu reduziert D-serin die Futteraufnahme von fettreichem Futter und schützt Mäuse daher vor Diät-induziertem Übergewicht sowie einer Fettleber. Im Gegenteil zu diesen positiven Effekten wird außerdem gezeigt, dass D-serin, unabhängig von der Art des Futters, zu erhöhten Blutzuckerwerten führt. Dies wird dadurch verursacht, dass die Insulin-Sekretion von pankreatischen Betazellen verringert ist. Es wird vermutet, dass D-serin dies indirekt über eine veränderte sympathische Aktivität reguliert, da eine Inhibierung von  $\alpha$ 2-adrenergen Rezeptoren die Blutzuckerwerte normalisieren konnte. Unabhängig von D-serin wirkt eine Gabe von dessen Enantiomer L-serin vorwiegend auf die Leber und verändert deren Metabolismus.

Im Ganzen wird hier gezeigt, dass der Aminosäuretransporter ASC-1 ein gutes Ziel für die Behandlung von Adipositas wäre, während dessen Cargo D-serin ein ernst zu nehmendes Risiko bei der Behandlung von Schizophrenie-Patienten darstellt.

# Index of contents

<b>I Abbreviations</b>	<b>2</b>
<b>II List of tables</b>	<b>3</b>
<b>III List of figures</b>	<b>3</b>
<b>IV Abstract</b>	<b>5</b>
<b>V Zusammenfassung</b>	<b>6</b>
<b>1 Introduction</b>	<b>11</b>
<b>1.1 Obesity, its causes and consequences</b>	<b>11</b>
1.1.1 Type 2 Diabetes	12
<b>1.2 The role of adipose tissue in the development of obesity and insulin resistance</b>	<b>13</b>
1.2.1 The function of white adipose tissue	14
1.2.1.1 Consequences of white adipose tissue dysregulation	15
1.2.2 Brown adipose tissue	15
1.2.2.1 Function of classical brown adipocyte marker genes	16
1.2.3 Beige adipocytes	18
1.2.4 Brown and beige adipocytes in mice and men	19
<b>1.3 Treatments to reduce body weight</b>	<b>20</b>
1.3.1 Diet induced weight loss	20
1.3.2 Bariatric surgery induced weight loss	21
1.3.3 Weight loss by activation of brown and beige adipocytes	21
1.3.4 Tissue targeted treatment of obesity	22
<b>1.4 The solute carrier superfamily</b>	<b>23</b>
1.4.1 ASC-1 and 4F2HC	23
1.4.2 Importance of ASC-1 activity in the brain	24
1.4.2.1 D-serine in the regulation of NMDA receptors	25
<b>2 Aims of this thesis</b>	<b>27</b>
<b>3 Material and Methods</b>	<b>28</b>
<b>3.1 Animal experiments</b>	<b>32</b>
3.1.1 ASC-1 <sup>-/-</sup> strain	32
3.1.1.1 Genotyping	32
3.1.2 D/L-serine supplementation	33
3.1.3 Metabolic phenotyping	33



3.1.3.1	Body composition	33
3.1.3.2	GTT, ITT, GSIS, PTT	33
3.1.3.3	Indirect calorimetry	34
3.1.3.4	Food preference test	34
3.1.4	Sacrifice and organ withdrawal	34
<b>3.2</b>	<b>Ex vivo measurements</b>	<b>35</b>
3.2.1	Isolation of pancreatic $\beta$ -cells	35
3.2.1.1	Insulin secretion from pancreatic $\beta$ -cells	35
3.2.1.2	Islet membrane potential measurement (Collaboration)	35
3.2.2	Bomb calorimetry	36
3.2.3	Measurement of gut microbiota (Collaboration)	36
3.2.4	Measurement of metabolic parameters	37
3.2.4.1	Serum metabolites	37
3.2.4.2	Liver triglyceride and glycogen content	37
3.2.4.3	Liver metabolites (Collaboration)	37
<b>3.3</b>	<b>Histology</b>	<b>39</b>
3.3.1	Paraffin embedding	39
3.3.1.1	H&E staining	39
3.3.1.2	Picosirius red staining	39
3.3.2	c-Fos staining (Collaboration)	40
3.3.3	Immunohistochemistry	40
3.3.4	Agarose embedding	41
3.3.5	Cryoembedding and triple staining of pancreata	41
3.3.6	Immunohistochemistry of cultured cells	42
3.3.7	Imaging	42
3.3.7.1	Cell size assessment (Collaboration)	42
3.3.8	MALDI FT-ICR MSI (Collaboration)	42
<b>3.4</b>	<b>Bacterial culture</b>	<b>43</b>
3.4.1	Cloning of ASC-1 overexpression constructs	43
3.4.1.1	pCDH-CMV-MCS-EF1-puro-Asc-1-HA	43
3.4.1.2	pCDH-CMV-MCS-EF1-puro-Asc-1-HA-2a-4F2hc	44
3.4.2	Transformation of Escherichia coli	45
3.4.2.1	Isolation of plasmids	46
<b>3.5</b>	<b>Cell culture</b>	<b>46</b>
3.5.1	Isolation and immortalization of stromal vascular fraction	46
3.5.2	Cell line maintenance	46
3.5.3	Differentiation	47

3.5.4	Seahorse measurements	47
<b>3.6</b>	<b>Transcriptional and protein analysis</b>	<b>48</b>
3.6.1	RNA isolation	48
3.6.1.1	cDNA synthesis	48
3.6.1.2	qPCR	48
3.6.2	Protein isolation from cells or tissue	49
3.6.2.1	SDS Page and Western Blot	49
3.6.3	Immunoprecipitation	50
<b>3.7</b>	<b>Amino acid analysis (Collaboration)</b>	<b>50</b>
3.7.1	D-serine quantification	50
3.7.2	Measurement of free amino acids	51
<b>3.8</b>	<b>Statistics</b>	<b>52</b>
<b>4</b>	<b>Results</b>	<b>53</b>
<b>4.1</b>	<b>Depletion of ASC-1 remodels genetic predisposition and enables beige over white adipocyte differentiation</b>	<b>53</b>
4.1.1	Loss of ASC-1 induces beige adipocyte differentiation <i>in vitro</i>	53
4.1.2	Overexpression of ASC-1 reduces brown adipocyte gene expression in brown adipocytes	56
4.1.3	Depletion of ASC-1 re-programs preadipocytes resulting in spontaneous differentiation into beige adipocytes	58
4.1.4	Beiging of ASC-1 knockdown cells could be caused by accumulation of intracellular D-serine	59
4.1.5	Whole body loss of ASC-1 results in hepatosteatosis and reduced UCP1 expression in BAT	63
<b>4.2</b>	<b>D-serine regulates insulin secretion and weight gain</b>	<b>67</b>
4.2.1	D-serine supplementation ameliorates diet induced obesity and preference to HFD	67
4.2.2	D-serine induced changes in gut microbiota do not mediate reduced weight gain on HFD	71
4.2.3	D-serine accumulates in metabolically important organs without inducing tissue inflammation	72
4.2.4	D-serine administration induces diet independent glucose intolerance but not insulin resistance	75
4.2.5	D-serine supplementation alters hepatic one-carbon metabolism but not gluconeogenesis	77
4.2.6	D-serine impairs insulin secretion from pancreatic beta cells	78
4.2.7	D-serine regulates insulin secretion via the sympathetic nervous system	80
<b>4.3</b>	<b>L-serine remodels hepatic metabolism</b>	<b>83</b>

4.3.1	L-serine supplementation has no effect on body weight or adipose tissue morphology	83
4.3.2	L-serine increases hepatic PEPCCK but has no effect on glucose tolerance	85
4.3.3	L-serine alters hepatic metabolism	86
<b>5</b>	<b><i>Discussion</i></b>	<b>88</b>
<b>5.1</b>	<b>Depletion of ASC-1 remodels genetic predisposition and enables beige over white adipocyte differentiation</b>	<b>88</b>
5.1.1	ASC-1 as important regulator of adipocyte identity	88
5.1.2	Depletion of ASC-1 re-programs preadipocytes resulting in changes of intracellular amino acids and spontaneous differentiation into beige adipocytes	89
5.1.3	Whole body loss of ASC-1 results in hepatosteatosis and reduced UCP1 expression in BAT	91
<b>5.2</b>	<b>D-serine supplementation regulates insulin secretion and HFD induced weight gain</b>	<b>93</b>
5.2.1	D-serine induced changes in food preference are independent of changes in gut microbiome	93
5.2.2	D-serine alters hepatic one-carbon cycle but does not induce tissue damage or inflammation	94
5.2.3	D-serine regulates insulin secretion and glucose homeostasis	95
5.2.4	D-serine in the therapy of schizophrenia	96
<b>5.3</b>	<b>L-serine supplementation remodels hepatic metabolism</b>	<b>98</b>
5.3.1	L-serine supplementation alters serine catabolism in brown adipose tissue	99
5.3.2	L-serine does not impact glucose tolerance	99
5.3.3	L-serine supplementation alters hepatic gluconeogenesis and metabolism	100
<b>6</b>	<b><i>Conclusion and Outlook</i></b>	<b>101</b>
<b>VI</b>	<b><i>References</i></b>	<b>104</b>
<b>VII</b>	<b><i>Acknowledgements</i></b>	<b>117</b>
<b>VIII</b>	<b><i>Supplements</i></b>	<b>118</b>
<b>IX</b>	<b><i>Curriculum Vitae</i></b>	<b>120</b>

# 1 Introduction

## 1.1 Obesity, its causes and consequences

Obesity is a global disease caused by excessive accumulation of fat in the body. It is defined as a body mass index (BMI) of 30 kg/m<sup>2</sup> or higher. Once, obesity was associated with high-income countries but nowadays it also is prevalent in low- and middle-income countries (WHO 10 Facts about obesity, October 1017; <http://www.who.int/features/factfiles/obesity/en/>). Since 1975, the prevalence of obese people has nearly tripled (WHO Obesity and overweight, October 1017; <http://www.who.int/en/news-room/fact-sheets/detail/obesity-and-overweight>).

Projected rates of obesity show a further increase and predict about 50 % of the US citizens being obese (**Figure 1**) by 2030 (OECD, obesity update 2017, <https://www.oecd.org/els/health-systems/Obesity-Update-2017.pdf>).

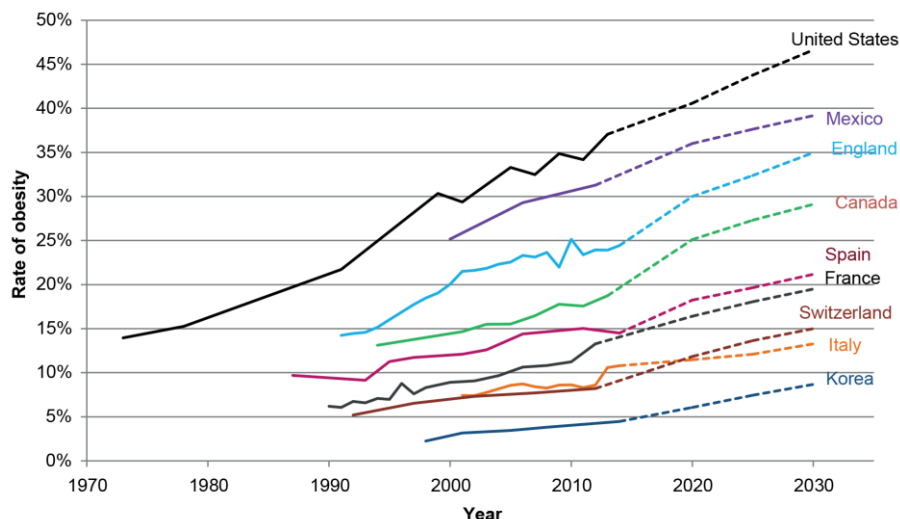


**Figure 1: Projected rates of obesity.** Obesity is defined as Body Mass Index (BMI)  $\geq 30$  kg/m<sup>2</sup>. Projections assume that BMI will continue to rise as a linear function of time. Adapted from OECD analysis of national health survey data.

Obesity is caused by an imbalance between energy intake and expenditure. While the availability of energy-dense foods that are rich in sugar and fat is increasing, the physical activity decreases due to changing transportation systems and the sedentary nature of many forms of work (WHO Obesity and overweight, October 1017; <http://www.who.int/en/news-room/fact-sheets/detail/obesity-and-overweight>). However, unhealthy diets and lack of physical activity are not the only cause of obesity. Human genome-wide association studies (GWAS) identified around 240 genetic loci for obesity (Castillo et al., 2017) which revealed that obesity is primarily

driven by changes in the central nervous system (CNS) (Locke et al., 2015; Willer et al., 2009).

Obesity is a major risk factor for several diseases such as heart disease and ischemic stroke or musculoskeletal disorders as osteoarthritis (Calenzani et al., 2017; Rexrode et al., 1997). In addition, it can increase the mortality of cancers of the esophagus, colon, rectum, liver, gallbladder, pancreas and kidney (Calle et al., 2003). Obesity is part of the metabolic syndrome which is defined as a cluster of at least 3 out of 5 risk factors that are hypertension, insulin resistance, high serum triglycerides and reduced serum high-density lipoprotein (HDL) (Paley and Johnson, 2018). Due to those severe co-morbidities, obesity is associated with a decreased life expectancy (Peeters et al., 2003) and today, overweight takes more lives, than underweight does (WHO Obesity and overweight, October 1017; <http://www.who.int/en/news-room/fact-sheets/detail/obesity-and-overweight>).

### **1.1.1 Type 2 Diabetes**

One risk of obesity is the development of type 2 diabetes (T2D). Usually, blood glucose levels are highly regulated in the body, as dysregulation can have severe effects. For example, hypoglycemia (low blood glucose levels) can induce palpitations, hunger, sweating, confusion, loss of consciousness and in worst case coma and death (Rehni and Dave, 2018). In contrast, chronic hyperglycemia (high blood glucose levels) can result in cardiovascular disease (Sarwar et al., 2010), kidney disease (diabetic nephropathy), nerve disease (diabetic neuropathy) or eye disease (diabetic retinopathy) (International diabetes federation, May 2018; <https://www.idf.org/aboutdiabetes/what-is-diabetes.html>).

The main regulator of glucose homeostasis is insulin, which is secreted by pancreatic beta cells in response to raising blood glucose levels. Insulin acts on many different tissues in the body facilitating glucose uptake (Rowe, 1923). Two main disorders can interrupt this highly regulated system: deficiency in insulin secretion or insulin resistance of the target tissues. Type 1 diabetes is caused by a deficiency in insulin secretion due to damage of the pancreatic beta cells. Therefore, type 1 diabetes usually is diagnosed early in life and patients need to inject insulin regularly to control their blood glucose level (Chiang et al., 2014). In contrast, type 2 diabetes is caused by insulin resistance especially in muscle, liver and adipose tissue and can be triggered by accumulation of fat. Insulin resistant cells have an impaired reaction to insulin, causing increased insulin secretion from pancreatic beta cells and hyperinsulinemia (Groop, 2000). Ongoing hyperinsulinemia worsens the insulin

resistance of target tissues, leading to increased blood glucose levels and the diagnosis of pre-diabetes (Bacha et al., 2010). Chronic elevation of insulin secretion can result in collapse of pancreatic beta cells, accompanied by a reduction in insulin secretion. Hence, blood glucose levels rise and a patient is considered as diabetic, when fasted glucose levels are over 126 mg/dl (American Diabetes Association, November 2016; <http://www.diabetes.org/diabetes-basics/diagnosis/>).

Besides obese diabetic patients, there also exist lean people with T2D (Yang et al., 2016). Therefore, obesity is a driver, but not the only cause of T2D. It has been shown that T2D is a multifactorial disease driven by a complicated interplay of genetic predisposition and environmental factors (Castillo et al., 2017; Ussar et al., 2016). Human GWAS identified more than 100 genetic loci associated with T2D (Ndiaye et al., 2017). Analysis revealed that T2D strongly is associated with alterations in genes modulating pancreatic beta cell function (Pasquali et al., 2014). In addition to genetic predisposition, lifestyle and nutrition can contribute to the development of T2D (Horton, 1983). For example, it is known that physical activity reduces blood glucose levels by promoting glucose uptake into the muscle. Though, together with increasing prevalence for obesity, also the prevalence for type 2 diabetes doubled since 1980 (Mathers and Loncar, 2006).

## ***1.2 The role of adipose tissue in the development of obesity and insulin resistance***

Besides liver and muscle, one of the main organs contributing to insulin-dependent glucose uptake is adipose tissue. In the body, several distinct types of adipose tissue depots exist that differ in their specific region and function. The two main adipose tissue subtypes are white and brown adipose tissue. White adipose tissue mainly stores fatty acids in form of triglycerides and can release those fatty acids in times of need. In contrast, brown adipose tissue primarily dissipates energy and thereby produces heat. Both, white and brown adipocytes differ in their morphology and gene expression (**Figure 2**). Upon several stimuli, brown-like adipocytes can develop within white adipose tissue, forming the third group of adipocytes: “beige” or “brite” (brown in white) adipocytes (Wang and Seale, 2016).

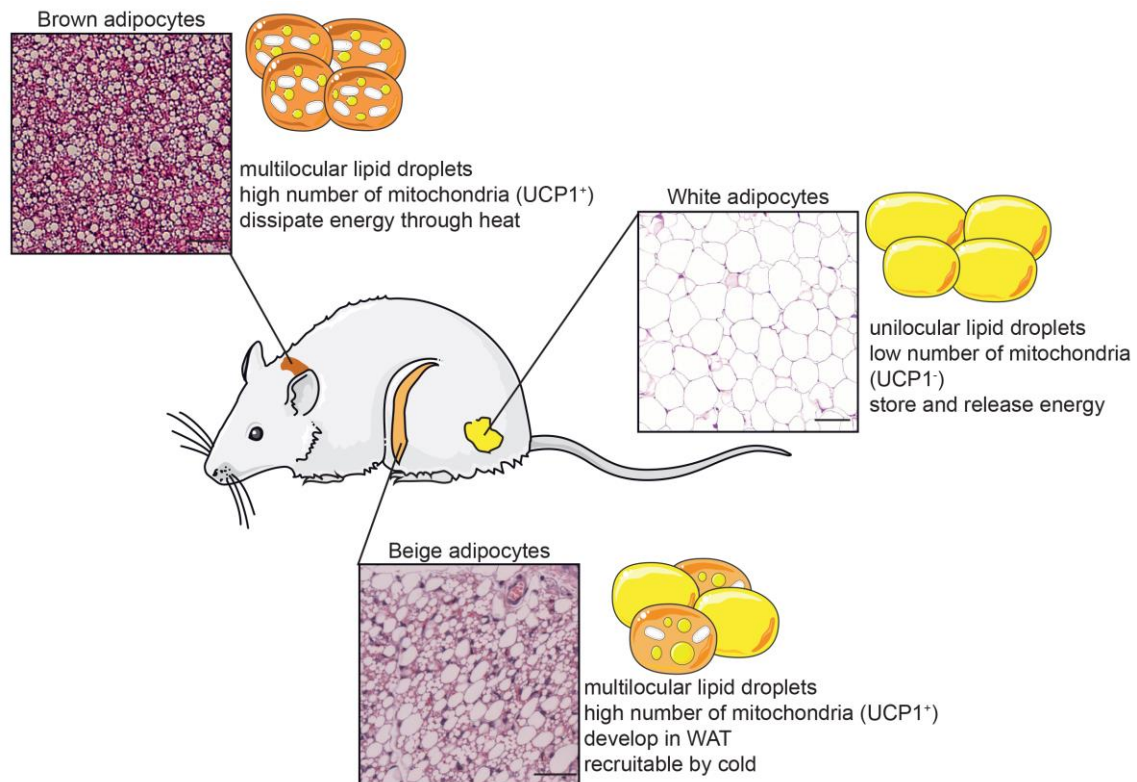


**Figure 2: Brown, beige and white adipocytes.** In mice, brown and white adipocytes form distinct tissues. Beige adipocytes can develop within white adipose tissue due to cold or other stimuli. Adapted from Wang and Seale, 2016.

### 1.2.1 The function of white adipose tissue

The main function of white adipose tissue (WAT) is storing energy in form of triglycerides. In periods of positive energy balance, white adipose tissue expands whereas its size reduces upon negative energy balance (Trayhurn and Beattie, 2007). Besides its role in energy storage, WAT has an important role in thermal isolation and protection from mechanical damage (Toner et al., 1989; Wang et al., 2003). Another main function of WAT is the secretion of a multitude of hormones, through which it can contribute to whole body metabolism and glucose homeostasis (Ouchi et al., 2011). The first discovered adipokine secreted by WAT was leptin, a hormone that regulates food intake by action in the brain (Campfield et al., 1995; Zhang et al., 1994). Through secretion of other proteins and peptides, WAT is involved in the regulation of lipoprotein metabolism, fatty acid uptake, blood pressure and inflammatory responses (Cook et al., 1987; Murray et al., 1999a; Murray et al., 1999b; Trayhurn and Beattie, 2007; Zhou and Qin, 2012). In addition, several cytokines secreted by WAT are known to be involved in the development of insulin resistance (Hotamisligil et al., 1993; Stepan et al., 2001; Wieser et al., 2013).

### **1.2.1.1 Consequences of white adipose tissue dysregulation**

The central regulators of adipocyte function are the sympathetic nervous system and insulin (Dimitriadis et al., 2011; Klemm et al., 2001; Rayner, 2001). Sympathetic stimulation can mobilize fatty acids from adipose tissue and regulate the production of leptin (Dimitriadis et al., 2011). In contrast, insulin is essential for adipocyte differentiation and promotes glucose uptake and lipogenesis (Klemm et al., 2001). It is produced and secreted by pancreatic  $\beta$ -cells due to rising glucose concentrations. Upon starvation, white adipocytes induce lipolysis and secrete free fatty acids. To prevent excessive release of free fatty acids, most of the fatty acids are re-esterified to triglycerides (Van Harmelen et al., 1999). For this, glycerol-3-phosphate is essential as it serves as backbone for the triglycerides. White adipocytes are not able to convert glycerol into glycerol-3-phosphate and therefore need glucose, pyruvate, lactate or amino acids as alternative substrates (Forest et al., 2003; Watford, 2000). This highly regulated system can be interrupted by excessive accumulation of triglycerides. Impaired adipose tissue function can result in altered adipokine secretion, tissue inflammation, local and systemic insulin resistance and spillover of lipids into other organs as skeletal muscle and liver (Schoettl et al., 2018). Those fatty acids can have severe effects on whole body metabolism. In muscle, an acute overload of fatty acids can be managed by increasing muscle activity and thereby using excess fatty acids as fuel. In contrast, the liver can store a few amount of triglycerides or produce and secrete very-low-density lipoproteins (VLDLs) which are less toxic than un-oxidized free fatty acids. Other cells can adapt to increased free fatty acid influx by increasing  $\beta$ -oxidation (Unger and Orci, 2002), but chronic overload with un-oxidized fatty acids results in overaccumulation of lipids (steatosis) which leads to cellular stress, malfunction and ultimate death (lipoapoptosis) of non-adipose tissue (Unger and Orci, 2002).

### **1.2.2 Brown adipose tissue**

Morphologically, brown adipose tissue (BAT) differs from WAT by the presence of multilocular lipid droplets and a high number of mitochondria (Hilton et al., 2015). The main function of BAT is to burn substrates like fatty acids and glucose to produce heat, which is termed adaptive or non-shivering thermogenesis (Wang and Seale, 2016). BAT is highly vascularized in order to enable substrate and oxygen delivery on one hand, but on the other hand allow heat distribution into the body (Wang and Seale, 2016). The activity of brown adipose tissue is highly regulated, as chronic heat dissipation causes hyperthermia which has the potential to cause organ failure and



death (Sharma et al., 2014). The main regulator of BAT activity is the sympathetic nervous system. Therefore, BAT is densely innervated by nerves and various nerve fibers directly synapse onto brown adipocytes (Cannon and Nedergaard, 2004; Wang and Seale, 2016). Upon cold exposure, sympathetic outflow stimulates  $\beta$ -adrenergic receptors located on brown adipocytes (Wang and Seale, 2016), thereby activating the tissue. In addition to cold, fasting or changes in the metabolic environment have been identified as BAT activating stimuli (Migliorini et al., 1997; Villarroya and Vidal-Puig, 2013).

### **1.2.2.1 Function of classical brown adipocyte marker genes**

Due to accumulation of mitochondria and its special function in heat production, BAT expresses various genes that are specific for brown compared to white adipocytes. Through measuring the amount of those proteins, brown and white adipocytes can easily be distinguished from each other.

#### UCP1

Uncoupling protein 1 (UCP1) is a member of the mitochondrial carrier protein family which is localized on the inner membrane of brown adipocyte mitochondria (Cannon and Nedergaard, 2004). Mitochondria are cell organelles that are known as powerhouse of the cells since long time (McBride et al., 2006). Proteins of the electron transport chain pump protons from the matrix into the mitochondrial intramembrane space and thereby create a proton motive force across the inner membrane. Re-entry of protons into the matrix through ATP synthase couples the release of energy to ATP production (Jastroch et al., 2010). In contrast to “usual” mitochondria, the mitochondria of brown adipocytes have reduced levels of ATP synthase but high levels of UCP1 instead (Nedergaard et al., 2001). Upon activation by fatty acids, UCP1 catalyzes the leak of protons across the mitochondrial membrane uncoupling the oxidative respiratory chain from ATP synthesis (Fedorenko et al., 2012; Klingenspor et al., 2008). The energy is dissipated as heat to defend body temperature upon cold or to combust excess food energy in response to diets of high caloric density (Klingenspor et al., 2008). The expression of UCP1 is primarily regulated via adrenergic signaling from the brain (Galmozzi et al., 2014).

### PRDM16

PR (PRD1–BF1–RIZ1 homologous) domain-containing 16 (PRDM16) is a transcription factor which is crucial for brown adipocyte cell fate (Wang and Seale, 2016). By binding to chromatin and thereby altering its structure, PRDM16 activates genes that are expressed in brown adipocytes, such as peroxisome proliferator activated receptor  $\alpha$  (PPAR $\alpha$ ) and peroxisome proliferator activated receptor  $\gamma$  (PPAR $\gamma$ ) coactivator 1  $\alpha$  (PCG1 $\alpha$ ) (Harms et al., 2015). In addition, PRDM16 was shown to regulate the activity of super-enhancers that drive the expression of cell identity genes (Harms et al., 2015).

### PGC1 $\alpha$

PGC1 $\alpha$  is a transcriptional coactivator that has an important role in mitochondrial biogenesis. Therefore, its expression is not limited to brown adipocytes, but is higher in brown, compared to white adipocytes due to their higher content of mitochondria (Austin and St-Pierre, 2012). In 1998, PGC1 $\alpha$  was shown to play an important role in cold-induced thermogenesis (Puigserver et al., 1998), by directly regulating the expression of UCP1. Later it was shown that, in addition to PPAR $\gamma$  and UCP1, PGC1 $\alpha$  also activates several other transcription factors that are involved in mitochondrial biogenesis and thermogenesis (Sharma et al., 2014).

### TFAM

The mitochondrial transcription factor A (TFAM) is a transcription factor that induces mitochondrial biogenesis. Similar to PGC1 $\alpha$ , TFAM is expressed in several cell types, but its expression level is higher in brown compared to white adipocytes as BAT is rich in mitochondria (Jeremic et al., 2017). TFAM is encoded in the nucleus but acts in mitochondria, where it enhances mitochondrial DNA copy number and gene expression by binding, unwinding and bending mitochondrial DNA (Falkenberg et al., 2007; Jeremic et al., 2017). If DNA binding occurs together with mitochondrial RNA polymerase, transcription is activated. Therefore, TFAM is an important regulator of maintaining mitochondrial DNA copy number, mitochondrial biogenesis and cellular metabolism (Collu-Marchese et al., 2015).

### P2RX5

The family of the purinergic receptor P2RX is a family of seven receptors that control the flow of sodium, potassium and calcium across cellular surface membranes (Haines et al., 1999). Upon activation by ATP, these receptors produce changes in membrane potential that initiate a variety of physiological functions, including smooth muscle contraction, neuroendocrine secretion and synaptic transmission (Haines et al., 1999). The receptors form homo- or hetero-oligomers, thereby creating a channel with different affinities to ATP and distinct biophysical profiles (Haines et al., 1999; Le et al., 1997). One of the members, the purinergic receptor P2rx, ligand-gated ion channel 5 (P2RX5) recently was identified to be higher expressed in brown compared to white adipose tissue and therefore is a good surface marker for brown adipocytes (Ussar et al., 2014).

### PAT2

The proton-coupled amino acid transporter-2 (PAT2) belongs to the family of solute carrier proteins (SLC26A2). As the name indicates, amino acid transport by PAT2 is proton-coupled and pH dependent. PAT2 transports small, unbranched amino acids like glycine, alanine, L- and D-proline (Thwaites and Anderson, 2011). Together with P2RX5, PAT2 was identified as a surface marker for brown adipocytes with little expression in white adipose tissue, but nearly no expression in other tissues. Therefore, PAT2 may be the most adipose tissue-selective surface marker known so far (Ussar et al., 2014).

### **1.2.3 Beige adipocytes**

Beige adipocytes are brown-like adipocytes that are localized in white adipose tissue without any separation by a distinct layer of connective tissue (Sidossis and Kajimura, 2015). Similar to the activation of brown adipocytes, the formation of beige adipocytes depends on specific signals. These are chronic cold, noradrenergic signaling, environmental changes such as intermittent fasting, exercise, specific expression of transcriptional regulators or endocrine hormones and metabolites (Harms and Seale, 2013; Li et al., 2017; Seale et al., 2008; Sidossis and Kajimura, 2015). Upon those stimuli, white adipocytes may trans-differentiate into beige adipocytes (Cinti, 2002; Lee et al., 2015). Alternatively, beige adipocytes can develop from precursor cells different to classical brown preadipocytes (Wang et al., 2013; Wang and Seale, 2016). Thus, beige adipocytes might have a flexible switching between energy storage and heat production (Wang and Seale, 2016).

Dependent on their localization, different WAT depots are divided into intra-abdominal (around abdominal organs) and subcutaneous (under the skin) depots (Hamdy et al., 2006; Pond, 1992). Several studies could show that subcutaneous white adipose tissue is higher susceptible for “beiging” (the development of beige adipocytes in WAT) than perigonadal white adipose tissue (Schottl et al., 2015; Wang and Seale, 2016). This observation fits to the fact that accumulation of subcutaneous adipose tissue (=pear shape) is associated with a low metabolic risk for the development of type 2 diabetes and cardiovascular diseases, while the accumulation of visceral adipose tissue (=apple shape) is associated with a high metabolic risk (Gesta et al., 2007).

#### **1.2.4 Brown and beige adipocytes in mice and men**

In rodents and human infants, BAT depots are located in inter- and subscapular, axillary and cervical areas (de Jong et al., 2015; Lidell et al., 2013). Whereas rodents keep their BAT, human classical brown adipocyte depots disappear with age (Heaton, 1972). It was believed for many years that adult humans lack thermogenic adipose tissue, but several years ago PET scans uncovered the presence of thermogenic fat in adult humans in the neck and in supraclavicular regions (Cypess et al., 2009; Saito et al., 2009). There, brown adipocytes are mixed with white adipocytes (Sidossis and Kajimura, 2015). Genome-wide analysis based on RNA sequencing of isolated adipocytes from human BAT revealed that the cells possess molecular signatures that resemble beige adipocytes rather than classical brown (Sidossis and Kajimura, 2015).

In mice, it was known since a long time that especially subcutaneous white fat can undergo browning. Though, it was unclear whether this was true for human WAT as well. In 2015, Bartesaghi et al. could show that human adipose-derived stromal progenitor cells isolated from adult subcutaneous fat depots could be differentiated efficiently into thermogenic beige adipocytes when treated with the PPAR $\gamma$  agonist rosiglitazone (Bartesaghi et al., 2015). Recent studies with patients revealed that human WAT can undergo browning, for example under extreme conditions after severe burn injuries, where the body was exposed to prolonged adrenergic stress with increased norepinephrine levels (Kiefer, 2017).

## **1.3 Treatments to reduce body weight**

As described above, excessive accumulation of triglycerides can have severe effects on whole body metabolism. Therefore, there exist many approaches to reduce body weight in order to maintain adipose tissue function.

### **1.3.1 Diet induced weight loss**

To reduce obesity, a negative energy balance must be evoked. For that, several forms of caloric restriction and diets are available, for example low-fat, low-calorie, low-carbohydrate (high protein), very-low-carbohydrate diets and combinations thereof (Hjorth et al., 2017; Strychar, 2006). Though, there is intense discussion about what types of diets are the most effective for weight loss (Sacks et al., 2009). It recently was published that the effectiveness of a diet is dependent on the glucose metabolism of the patient (Hjorth et al., 2017). In this study it has been shown that diabetic patients lose more weight upon a high fat and low carbohydrate diet, while normoglycemic patients lose more weight upon a low-fat and high-carbohydrate diet. In general, exercise in combination with diet was shown to have beneficial effects on weight loss through increasing energy expenditure. Muscle contractions lead to the production of Interleukin-6 (IL-6), which has several beneficial effects on glucose and fat metabolism as well as anti-inflammatory effects (Scheller et al., 2011; Strasser and Fuchs, 2016).

However, it was recently shown that obesity leaves a genetic fingerprint especially in the liver and adipose tissue, predisposing for the development of insulin resistance and glucose intolerance upon weight regain (Fischer et al., 2018). In addition, excessive dieting can have negative effects on metabolism. Especially very-low-carbohydrate diets are associated with more frequent side effects, such as mood swings (Strasser and Fuchs, 2016). This may be caused by a lack of carbohydrates which are important for the transport of the amino acid tryptophan into the brain, where it serves as precursor for serotonin (Paredes et al., 2009). Therefore, eating a low carbohydrate meal reduces the amount of tryptophan entering the brain, contributing to symptoms of depression, such as mental fatigue and low mood.

As a consequence, calorie-restricted weight loss diets, especially if based on low carbohydrate and high in protein, prompt many dieters to return to their old eating habits, eating more and consuming carbohydrate-rich foods. This is accompanied by the fact that weight loss leads to compensatory changes in the homeostatic processes, including alterations in energy expenditure, substrate metabolism, and

hormone pathways involved in appetite regulation that result in increased hunger and energy storage (Strasser and Fuchs, 2016). All in all, this could lead to the so-called yoyo-effect and fast regain of weight after diet induced weight loss

### **1.3.2 Bariatric surgery induced weight loss**

Especially for the treatment of morbid obesity (BMI  $\geq 40$  kg/m<sup>2</sup>), exercise and diet are not sufficient to prevent co-morbidities (Golzarand et al., 2017). In the 1950s, first methods for bariatric surgery were developed but patients were afraid of invasiveness, risks of death, complications and unknown long-term effects (O'Brien, 2010). To date, bariatric surgery is a well-established and relatively safe technique to treat morbid obesity (Flum et al., 2009). Besides several irreversible methods to reduce stomach size and digestion time, there exists the method to put an adjustable gastric band around the stomach, which is reversible and easy to control (O'Brien, 2010). There is discussion about the effectiveness of the different methods, as all of them have pros and cons, but in general, bariatric surgery has been shown to improve glucose metabolism, hypertension, dyslipidemia, steatohepatitis, asthma and depression, thereby improving whole body health and life expectancy (Andersson et al., 2014; Dadson et al., 2016; O'Brien, 2010).

### **1.3.3 Weight loss by activation of brown and beige adipocytes**

A novel, non-invasive approach to burn excessive calories is the activation of brown and beige adipocytes. Several natural nutrients are known to activate BAT or to induce beiging of WAT. Upon those, capsaicin, an ingredient of hot pepper, contents of green tea or resveratrol, a compound of the skin of grapes have been identified to be beneficial for energy expenditure (Kiefer, 2017; Okla et al., 2017). Though, those ingredients are low concentrated in foods and patients would need to consume large amounts of it. Therefore, many different pharmacological drugs have been developed, aiming either to activate beige and brown adipocytes, reduce nutrient absorption, or to enhance satiety (Giordano et al., 2016).

Although those anti-obesity drugs can help in weight loss, the effects only occur as long as the therapy does and can have various side effects. For example, many of the drugs act in the central nervous system and can have severe effects on mood, blood pressure, concentration, memory, cancer or CNS toxicity (Giordano et al., 2016). In addition to drugs acting in the central nervous system, also various  $\beta$ -adrenergic stimuli were tested for their role in BAT activation. Mirabegron, a  $\beta$ 3-

agonist was shown to activate BAT and elevate energy expenditure in humans similar to cold exposure (Kiefer, 2017). However, the drug primarily was approved for the treatment of overactive bladder and could have negative effects in healthy patients. As a more severe risk,  $\beta$ 3-agonists have the potential of cardiovascular side effects which limits the use of those drugs in humans (Kiefer, 2017).

### **1.3.4 Tissue targeted treatment of obesity**

To circumvent those side effects, novel and more selective drugs are needed. Tissue targeted therapy aims to bring a specific drug directly to the target tissue and thereby reduce off-target effects. One approach to realize that is the use of dual agonists, which bring drugs to specific tissues as for example the glucagon-like peptide-1 (GLP-1)-estrogen conjugate. Estrogens are steroid hormones that modulate energy expenditure and feeding behavior and therefore are a good tool to treat obesity and T2D (Finan et al., 2012). Though, pharmacological treatment with estrogens remains limited as it promotes the development of cancer. GLP-1 is a gut-derived hormone that acts on various tissues and delays gastric emptying, stimulates insulin secretion and mediates satiety. The glucagon-like peptide-1 (GLP-1)-estrogen conjugate was shown to improve estrogen action by direct delivery to GLP-1 receptor expressing cells (Finan et al., 2012). This results in body weight loss, improved glycaemic control and insulin sensitivity without tumorigenic effects (Finan et al., 2012; Sanchez-Garrido et al., 2017). Nevertheless, this and other agonists are still in development. Therefore, the pharmacological relevance in humans remains unknown. A more tissue-specific approach would be by targeting tissue cells through their unique surface proteins as target molecules. Especially for the approach of pharmacologically targeting fat tissue, it is important to distinguish between white and brown adipocytes. As mentioned above, both types of adipocytes have different functions and it therefore is important to bring the right drug to the right cell. Recently, surface markers for white, beige and brown adipocytes have been identified (Ussar et al., 2014), but before targeting those proteins, their specific role needs to be examined. One of those identified markers was the alanine serine cysteine transporter 1 (ASC-1, SLC7A10), an amino acid transporter that is expressed on the surface of white adipocytes (Ussar et al., 2014).

## **1.4 The solute carrier superfamily**

Transporters in general are membrane-bound proteins that are localized on the cell surface or on membranes of intracellular compartments. Through mediation of transport of various substrates across those membranes, they are important for maintaining cellular homeostasis. Transporters are divided into two major superfamilies named ATP-binding cassette (ABC) superfamily and solute carrier (SLC) superfamily (Lin et al., 2015). Whereas ABC transporters hydrolyze ATP for transport activity, SLC transporters transport small molecules without the need of ATP (Lin et al., 2015).

Family seven of the SLC superfamily is divided into two subgroups named cationic amino acid transporters (CAT) and hetero(di)meric amino acid transporters (HAT). CATs transport cationic amino acids, especially L-arginine and thereby are important regulators of NO synthesis (Verrey et al., 2004). In contrast to CATs, HATs, to which ASC-1 belongs to, are unglycosylated and need to form a heteromer with a glycoprotein for their surface expression (Fukasawa, 2000; Verrey et al., 2004). HATs have 12 transmembrane domains and mostly function as exchangers (Verrey et al., 2004). Among the HATs, there exist several sub-groups with different substrate selectivities. One of these sub-groups is the ASC system that transports small neutral amino acids (Verrey et al., 2004).

### **1.4.1 ASC-1 and 4F2HC**

The 4F2 heavy chain (4F2HC) was identified in 1981 as a complex with 4F2 light chain, which later was proved to be the amino acid transporter LAT1 (Kageyama et al., 2000; Mannion et al., 1998). The *4F2hc* gene contains a single hydrophobic putative transmembrane domain with which it is anchored in the cell membrane (Leiden et al., 1989). *4F2hc* is highly expressed in proliferating cells but itself has no function for amino acid transport (Verrey et al., 2004).

ASC-1, also known as SLC7A10, has been identified as amino acid transporter with 12 predicted transmembrane domains (Fukasawa, 2000). Between membrane domains 3 and 4, there exists a conserved cysteine residue in the extracellular loop which is presumed to be linked to the glycoprotein 4F2HC via disulfide bond (Mastroberardino et al., 1998). Compared to other amino acid transporters, ASC-1 has a high sequence identity with the transporters LAT1 (45 %) and LAT2 (65%) (Fukasawa, 2000). Amino acid transport by ASC-1 occurs predominantly as exchange mode, but facilitated diffusion also is possible. The transport of small



neutral amino acids like glycine, L-alanine, L-serine, L-threonine, L-cysteine or D-serine is independent of Na<sup>+</sup> or pH (Fukasawa, 2000; Nakauchi et al., 2000).

Except D-serine, the other amino acids transported by ASC-1 are proteinogenic amino acids. L-serine and L-threonine can be phosphorylated and therefore are important regulators for the activity of proteins (Huttlin et al., 2010; Metcalf et al., 2018). Besides its important function in protein synthesis, L-serine serves as precursor for many other metabolites, amino acids, lipid messenger molecules and the neuromodulators glycine and D-serine (de Koning et al., 2003; Metcalf et al., 2018). L-alanine is important for hepatic gluconeogenesis (Felig, 1973) and can stimulate antioxidant defense proteins (Grosser et al., 2004). Via the production of glutathione, hydrogen sulfide, and taurine, L-cysteine can regulate nutrient metabolism, oxidative stress, and physiologic signaling pathways (Yin et al., 2016).

In humans, messenger RNA (mRNA) of ASC-1 was detected in brain, heart, placenta, skeletal muscle and kidneys (Verrey et al., 2004). Human ASC-1 is 91% identical to mouse *Asc-1* (Nakauchi et al., 2000), which is expressed in brain, placenta, lung, small intestine, and white adipose tissue (**Figure 3**). Though, highest *Asc-1* expression is in brain and white adipose tissue (Fukasawa, 2000; Ussar et al., 2014).

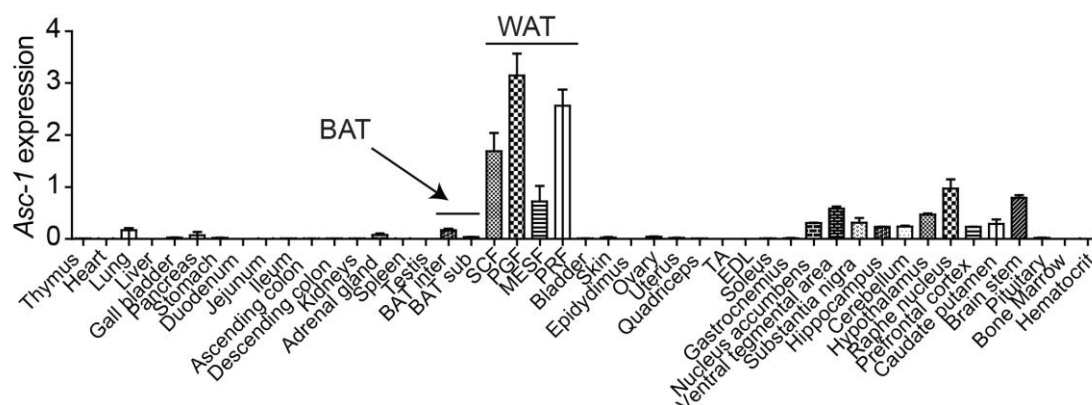


**Figure 3: Expression pattern of *Asc-1* in mice.** (Ussar et al., 2014)

### 1.4.2 Importance of ASC-1 activity in the brain

Besides ASC-1, there exist three other amino acid transporters of the ASC system named ASCT1, ASCT2, and ASC-2, but only the first two are expressed in the brain (Arriza et al., 1993; Chairoungdua et al., 2001; Helboe et al., 2003; Utsunomiya-Tate et al., 1996). There, ASCT1 is expressed equally, ASCT2 is restricted to astrocytes and ASC-1 is limited to neuronal structures and mainly located at presynaptic terminals (Arriza et al., 1993; Broer et al., 1999; Helboe et al., 2003; Van Horn et al.,

2013). The main characteristic, in which ASC-1 differs from ASCT1 and ASCT2, is its high affinity to D-serine, which is a neurotransmitter that acts as NMDA (N-methyl-D-aspartate) receptor co-agonist. ASC-1 has a  $K_m$  of 22.8  $\mu$ M to D-serine, which is close to physiological D-serine concentrations in the brain (Nakauchi et al., 2000). Besides ASC-1, D-serine is also transported, though in a much lower affinity, by ASCT2 (Rutter et al., 2007; Utsunomiya-Tate et al., 1996). Various studies demonstrated an important role of ASC-1 in the transport of D-serine *in vitro* (Sakimura et al., 2016; Sason et al., 2016) and *in vivo* (Rutter et al., 2007). According to those observations, whole body ASC-1 knockout mice have been shown to be smaller in size already 2 weeks after birth. They move in an ataxic gait and show hind-feet claspings when suspended by their tail. After 3 weeks of birth, homozygous mice develop severe seizures and tremors which lead to early postnatal death (Rutter et al., 2007; Safory et al., 2015; Xie et al., 2005). Treatment with the NMDA antagonist MK-801 reduces the tremors, indicating that NMDA receptor over-activation is responsible for the phenotype (Xie et al., 2005). In contrast, D-serine injection does not normalize the hind-foot claspings, whereas glycine and L-serine do (Safory et al., 2015). This indicates that the phenotype of whole body ASC-1 knockout mice is complex and may be caused by overlapping effects of several different amino acids.

#### **1.4.2.1 D-serine in the regulation of NMDA receptors**

NMDA receptors (NMDAR) are heterotetrameric calcium channels that are involved in neuronal development, learning processes and neuronal plasticity (Avellar et al., 2016; Basu et al., 2009). For complete activation, they need binding of their agonist glutamate and one of the co-agonists D-serine or glycine (Cheriyann et al., 2015). Normally, 90% of D-serine in the brain is synthesized by astrocytes or neurons via serine racemase (SRR) (Basu et al., 2009; Wolosker et al., 1999). The remaining 10% are taken up from the food or provided by gut microbiota (Sasaki et al., 2016; Silbernagl et al., 1999). Excessive D-serine is degraded by D-amino acid oxidase (DAO) to prevent over-activation of NMDA receptors (**Figure 4**). Dysregulation of SRR, ASC-1 or DAO lead to increased or decreased synaptic D-serine levels and in turn to deregulation of NMDAR activity. Elevated synaptic D-serine levels can result in diseases like Alzheimer's disease, amyotrophic lateral sclerosis or depression (Lee et al., 2017; Madeira et al., 2015; Otte et al., 2013). In contrast, a reduction of D-serine levels caused by over-activity of DAO, single nucleotide polymorphisms

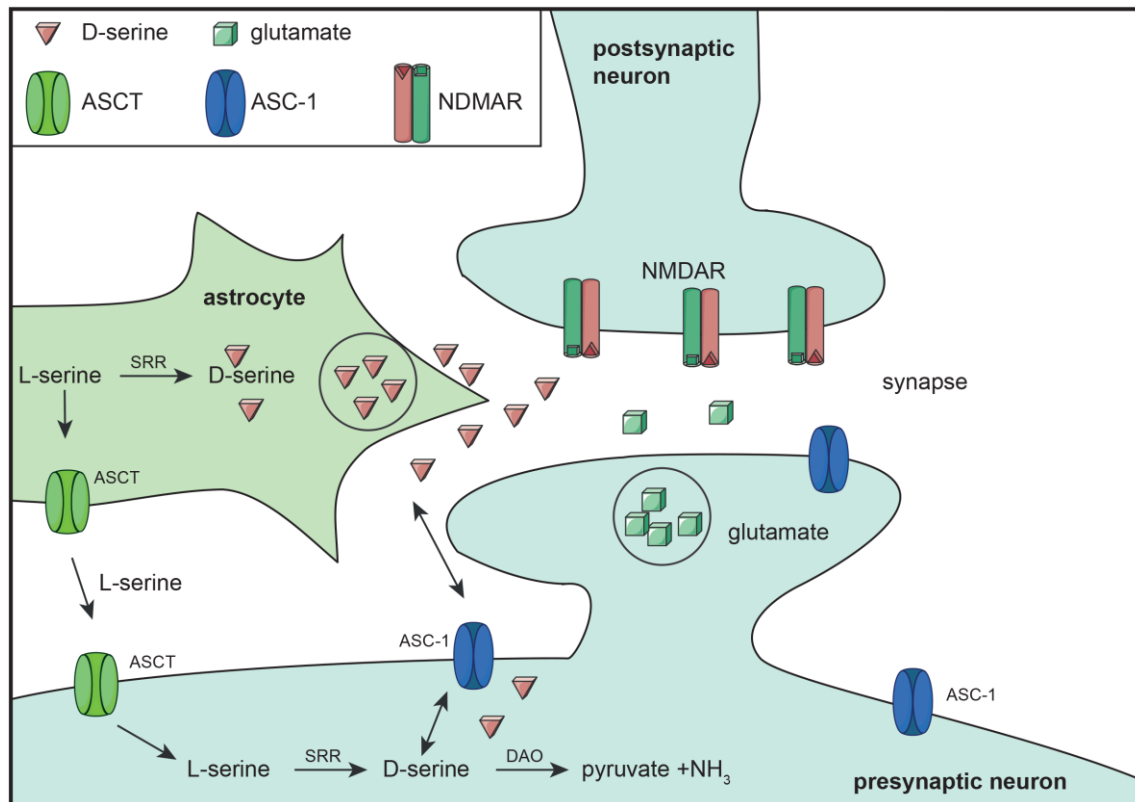


**Figure 4: Regulation of synaptic D-serine levels by ASCT, ASC-1, SRR and DAO.**  
Adapted from van Horn et al., 2013.

(SNPs) or loss of function in SRR are associated with schizophrenia (Burnet et al., 2008; Labrie et al., 2009; Labrie et al., 2010). Schizophrenia is a psychotic disease with motoric and cognitive defects that affects more than 21 million people worldwide (WHO, fact sheet on schizophrenia, April 2018; <http://www.who.int/en/news-room/fact-sheets/detail/schizophrenia>). D-serine levels in the cerebrospinal fluid (CSF) as well as in the serum of schizophrenic patients are significantly reduced compared to healthy subjects (Bendikov et al., 2007; Yamamori et al., 2014). Importantly, clinical studies demonstrated that orally administered D-serine as monotherapy or in combination with antipsychotics improves total psychopathology especially negative and cognitive symptoms (Kantrowitz et al., 2015; Tsai et al., 1998).

## 2 Aims of this thesis

To find novel targets for the treatment of obesity and its co-morbidities, surface markers for target tissues need to be identified. It recently was published, that the amino acid transporter ASC-1 is expressed on the surface of white but not brown adipocytes. Therefore, ASC-1 could be a novel target for tissue-specific treatment of obesity. However, the function of ASC-1 in white adipocytes remains elusive. Therefore, **the first aim of this thesis was to unravel the role of ASC-1 in white adipose tissue.** The outstanding feature that makes ASC-1 special compared to all other amino acid transporters is its high affinity to D-serine. Therefore, the role of ASC-1 in white adipose tissue may be coupled to D-serine. Previously it was shown that, besides the brain, D-serine is abundant in kidneys, liver, testis and muscle, suggesting a role of D-serine in the periphery (Horio et al., 2011; Nishimura et al., 2014). In the therapy of schizophrenia, D-serine supplementation was shown to improve negative and cognitive symptoms (Kantrowitz et al., 2015), but its effect on whole body metabolism has not been addressed so far. Thus, **the second aim of this thesis was to investigate the effects of D-serine supplementation on adipose tissue and whole body metabolism.** In contrast to D-serine, its enantiomer L-serine is an important proteinogenic amino acid. Several different tissues were shown to express SRR, the enzyme responsible for the conversion from L- to D-serine and the other way round. To distinguish the effects caused by supplementation with D-serine from those caused by its conversion to L-serine, **the third aim was to examine the effects of L-serine supplementation on whole body metabolism.**

### 3 Material and Methods

In this work, data are presented that were obtained by successful collaborations with other laboratories. Each method performed by collaboration partners is clearly marked. Materials and chemicals used by collaboration partners are listed together with the method it was used for. All other material is listed below.

**Table 1: Consumables**

<b>material</b>	<b>provider</b>
96 v-bottom well plate	Thermo Scientific
96 well PCR plates	Santa Cruz Biotechnology
96 well plate for Seahorse	Seahorse
96 well plates for assays (white, black and transparent)	Greiner bio-one
384 well qPCR plates	Bio-Rad
Bacteria plates	Greiner bio-one
Cell strainer (70 and 100 µm)	Corning
Cell culture chamber slides (8 well)	Thermo Scientific
CEA <sup>®</sup> RP New Medical X-Ray Screen Film Blue Sensitive	CEA Group
Cell culture plates 10 cm, 15 cm	Thermo Scientific
Cell culture plates 6, 12, 24 and 96 well	Sarstedt
CL high performance chemiluminescence film	GE Healthcare Life Sciences
Combitips (0.1, 1, 5, 10 ml)	Schubert und Weiss
Cover slips	Thermo Scientific
Cryotubes	Greiner bio-one
Cuvettes for OD measurement	Sarstedt
Filters	NeoLab
Microscope slides (SuperFrost R plus)	Thermo Scientific
Needles	B.braun
PCR tubes	Sarstedt
Pipette Filter Tips (10 µl)	Star Lab
Pipette Filter Tips (1250, 1000, 200 µl)	Kisker Biotech
Pipette Filter Tips (20 µl)	Biozym
Pipette Tips (10, 200, 1000 µl)	Biozym
Pipettes 2, 5, 10, 25 ml	Greiner bio-one
PVDF filter 0.2 µm	Carl Roth
PVDF membrane (0.22 µm)	Carl Roth
Syringes	Th.Geyer
Tubes (1, 2, 5 ml)	Sarstedt, Eppendorf
Tubes (15, 50 ml)	Corning
Tubes (PCR, Serum and bacteria culture 14 ml)	Sarstedt
Whatman paper	NeoLab

**Table 2: Chemicals**

<b>Chemical</b>	<b>provider</b>	<b>Chemical</b>	<b>provider</b>
2-3,3'-5 Triiodothyroninesodium salt (T3)	Merck Millipore	Isopropanol	Sigma-Aldrich
2-Deoxy-D-glucose	Alfa Aesar	Kalium chloride (KCl)	Carl Roth
3-Isobutyl-1-methylxanthin (IBMX)	Sigma-Aldrich	Ketamin (10 %)	Pharmanovo GmbH
4',6-Diamidino-2-phenyl-indoldihydrochlorid (DAPI)	Merck Millipore	Luria/Miller (LB) broth	Carl Roth

5-bromo-4-chloro-3-indolyl-beta-D-galactopyranoside (X-Gal)	Peqlab	Magnesium chloride (MgCl <sub>2</sub> *6 H <sub>2</sub> O)	Carl Roth
Acetic acid glacial	Sigma-Aldrich	Methanol	Merck Millipore
Agar-Agar	Carl Roth	Oligomycin	Sigma-Aldrich
Agarose	Sigma-Aldrich	Optiprep™ Density Gradient Medium (60 %)	Sigma-Aldrich
Agarose low gelling temperature	Sigma-Aldrich	Paraffin	Carl Roth
Albumin Fraktion V	Carl Roth	Paraformaldehyde	Carl Roth
Amino acid free medium	Genaxxon bioscience	PCR clean H <sub>2</sub> O	Millipore
Ammonium persulfate (APS)	Serva	Penicillin-Streptomycin (PenStrep)	Thermo Scientific
Ampizillin Sodiumsalt	Carl Roth	phosphatase-inhibitor cocktail II	Sigma-Aldrich
Antimycin A	Sigma-Aldrich	phosphatase-inhibitor cocktail III	Sigma-Aldrich
BMS-466442	Aobious	Picrosirius (Direct Red80)	Sigma-Aldrich
Bovine serum albumin (BSA) fraction V	Carl Roth	Picric acid	Omnilab
BRL44408	Abcam	Pierce® IP lysis buffer	Thermo Scientific
Calcium chloride (CaCl <sub>2</sub> )	Carl Roth	Platinum Green master mix (2x)	Life Technologies
Chlorform	Carl Roth	Polyethylene glycol (PEG) 300 monodisperse solution	Fluka
Chromotrope II R (Eosin)	Alfa Aesar	PolyFect	Qiagen
Collagenase IV	Life Technologies	Potassium dihydrogen phosphate (KH <sub>2</sub> PO <sub>4</sub> )	Carl Roth
Collagenase P	Roche	protease-inhibitor cocktail	Sigma-Aldrich
CutSmart™ Buffer	New England BioLabs	Puromycin hydrochloride	Biomol
Dexamethasone	VWR Lifesciences	QIAzol	Qiagen
Dextromethorphan hydrobromide monohydrate (DXM)	Sigma-Aldrich	Rosiglitazone	Santa Cruz Biotechnology
Dextrorphan tartrate (DXO)	Sigma-Aldrich	Rotenone	Sigma-Aldrich
Dimethylsulfoxid (DMSO)	Carl Roth	Roti®-Histokitt II	Carl Roth
Dithiothreitol (DTT)	VWR Lifesciences	Rotiphorese® Gel 30	Carl Roth
dNTPs	BioLabs	RPMI Medium 1640	Gibco by life technologies
Donkey serum	Abcam	Sample buffer (4x)	Life technologies
Dulbecco's Modified Eagle Medium (DMEM)	Life Technologies	SDS Pellets	Carl Roth
EDTA disodium salt dihydrate	Carl Roth	Sodium chloride (NaCl)	Carl Roth
Ethanol (99 %)	Merck Millipore	NaCl solution (0.9 %; for injection)	Fresenius Kabi Deutschland
FBS	Life technologies	Sodium hydrogen carbonate (NaHCO <sub>3</sub> )	Carl Roth
FCCP	Tocris bioscience	Sodium hydroxide (NaOH)	Carl Roth
Fluorescent mounting medium	Dako	Sodium phosphate (Na <sub>2</sub> HPO <sub>4</sub> )	Acros organics
Formaldehyde solution (37 %)	Carl Roth	Sodium pyruvate (for seahorse)	Life Technologies
Glucose (20 %; for injection)	B.braun	Sodium pyruvate (powder)	Sigma-Aldrich
Glucose (45 %; for <i>in vitro</i> GSIS)	Sigma-Aldrich	β-mercaptoethanol	Carl Roth
Glycerol	Sigma-Aldrich	SuperSignal® West FEMTO Max. Sensitivity	Thermo Fisher Scientific

		Substrate	
Glycine	Carl Roth	Temed	AppliChem
Hank's Balanced Salt Solution (HBSS) with Phenol Red	Lonza	Tissue-Tek® O.C.T.™ compound	Serva
Hematoxylin (Mayer)	Merck	TRIS Pufferan®	Carl Roth
Hematoxylin (Weigert)	Carl Roth	Tri-sodium citrate dihydrate	Carl Roth
Hepes-Na	Merck Millipore	Triton™ X-100	Sigma-Aldrich
Hydrochloric acid (HCl 37 %)	Sigma-Aldrich	Trypton	Carl Roth
Hydrogen peroxide (H <sub>2</sub> O <sub>2</sub> )	Carl Roth	Tween-20	Santa Cruz Biotechnology
Immobilon™ Western Chemiluminescent HRP Substrate	Merck Millipore	XF Assay Medium Modified DMEM (for seahorse)	Seahorse
Indomethacine	Santa Cruz Biotechnology	Xylacin as hydrochloride (20 mg/ml)	Belapharm
Insulin (Actrapid® Penfill®; for injections)	Novo Nordisk	Xylol	Carl Roth
Insulin (for cell culture)	Sigma-Aldrich	Yeast Extract	Carl Roth
IPTG	Sigma-Aldrich		

**Table 3: Amino acids**

<b>Amino acid</b>	<b>provider</b>	<b>Ref number</b>
<sup>13</sup> C-D-serine	Cambridge Isotope Laboratories, Inc	CLM-7759-PK
D-serine	Sigma-Aldrich	S4250-25G
Glycine	Sigma-Aldrich	410225-50G
L-alanyl-L-glutamine	Biochrom	BCHRK0302
L-arginine hydrochloride	Sigma-Aldrich	SIALA5131-10G
L-cysteine	Sigma-Aldrich	168149-25G
L-histidine hydrochloride H <sub>2</sub> O	Carl Roth	1697.1
L-isoleucine	ALFA (AESAR)	A13699.09
L-leucine	Sigma-Aldrich	L8000-25G
L-lysine hydrochloride	Sigma-Aldrich	L5626-100G
L-methionine	Sigma-Aldrich	M9625-5G
L-phenylalanine	Serva Electrophoresis	32191.01
L-serine	Sigma-Aldrich	84959-100G
L-threonine	Serva Electrophoresis	36382.02
L-tryptophan	AppliChem	A3445,0025
L-tyrosine	Carl Roth	T207.1
L-valine	Carl Roth	4879.1

**Table 4: Antibodies and fluorescent dyes**

antibody	Provider	Ref number
Alexa Fluor® 546 Phalloidin (1:100)	Life Technologies	A22283
Alexa Fluor™ 647 Phalloidin (1:100)	Life Technologies	A22287
Anti-goat Alexa 555 (1:800)	Invitrogen	A27017
Anti-guinea pig Alexa 647 (1:800)	Invitrogen	A-21450
Anti-HA (staining; 1:10)	Intern, 2017	-
Anti-HA-HRP (WB; 1:1000)	Cell signaling	2999
Anti-rabbit Alexa 488 (1:500)	Life Technologies	A21206
Anti-rabbit Alexa 594 (1:400)	Dianova	111-585-144
Anti-rabbit HRP (WB; 1:10.000)	Cell signaling	7074S
Anti-rat Alexa 488 (1:400)	Life Technologies	A-11006
Anti-rat Alexa 568 (1:400)	Life Technologies	A-11077
Anti-β-Actin-HRP (WB; 1:10.000)	Santa Cruz Biotechnology	sc-47778
Bodipy™ 493/503 (1:1000)	Life Technologies	D3922
Goat anti-Nkx6.1 (staining; 1:300)	R&D Systems	AF5857
Guinea pig anti-Glucagon (staining; 1:2500)	TakaRa	M182
Rabbit anti-ASC-1 (WB; 1:1000)	FabGennix	ASC-101AP
Rabbit anti-HSL (WB; 1:1000)	Cell Signaling	4107
Rabbit anti-insulin (Immunohistochemistry; 1:200)	Santa Cruz biotechnology	Sc-9168
Rabbit anti-insulin (Immunofluorescence; 1:300)	Cell Signaling	3014
Rabbit anti-p-HSL (WB; 1:1000)	Cell Signaling	4139
Rabbit anti-PPARγ (WB; 1:2000)	Cell Signaling	2435
Rabbit anti-UCP-1 (agarose sections 1:250 paraffin sections 1:500)	Abcam	ab10983
Rabbit anti-UCP1 (WB; 1:1000)	Cell signaling	14670
Rabbit anti-UCP1 Otto3 (WB; 1:15.000)	Custom (Jastroch et al., 2012)	-
Rat anti-ASC-1 10A11 (WB; 1:10)	Intern, 2017	-
Total OxPhos Complex WB Kit (WB; 1:2000)	Novex	458099

**Table 5: Enzymes**

enzyme	provider	Ref Number
DreamTaq™ Hot Start Green DNA Polymerase	Thermo scientific	EP1711
EcoRI-HFR®	New England BioLabs	R31015
NotI-HF®	New England BioLabs	R31896
NheI-HF®	New England BioLabs	R31315
BamHI-HF®	New England BioLabs	R31362
XbaI	New England BioLabs	R01455



### **3.1 Animal experiments**

All mice were kept in groups of at least 4 under a 12h light: 12 hour dark cycle and an ambient temperature of  $22 \pm 2$  °C and fed a standard laboratory chow diet (CD; Altromin 1314) or a 58 % high fat diet (HFD; Research Diets D12331) *ad libitum*. Animal experiments were conducted in accordance with the German animal welfare law and performed with permission and in accordance with all relevant guidelines and regulations of the district government of Upper Bavaria (Bavaria, Germany), protocol numbers ROB-55.2Vet-2532.Vet\_02-14-33 and ROB-55.2-2532.Vet\_02-16-52.

#### **3.1.1 ASC-1<sup>-/-</sup> strain**

Heterozygous ASC-1 knockout mice were purchased from Deltagen (B6;129P2-Slc7a10<sup>tm1Dgen</sup>/H). A whole body knockout of ASC-1 has been shown to reduce body weight and body size already 1 week after birth. After two weeks of birth, whole body knockout mice develop severe seizures and tremors and die due to those reasons (Rutter et al., 2007; Xie et al., 2005). For maintaining the mouse strain, heterozygous animals were mated with wildtype animals. Het/het matings only were set up when knockout pups were needed for experiments.

##### **3.1.1.1 Genotyping**

Eartags were obtained from mice with an age of 3 weeks or, for litters from het/het matings, with an age of 1 week. DNA was isolated by boiling the eartags for 30 min in 100 µl 50 mM NaOH at 95 °C (ThermoMixer C, Eppendorf). Afterwards, 10 µl 1 M EDTA was added to normalize the pH. 0.5 µl of the mixture was used for the genotyping PCR (vapo.protect, Eppendorf) together with 2x Platinum Green master mix and 1µM of each primer.

Following primers were used for the genotyping PCR:

genoAsc-1 ko fwd:	ctctcgtgggatcattgttttct
genoAsc-1 wt fwd:	ccacaggaacatcattggct
genoAsc-1 ko rev:	gctgccagataccacttcgct

**Table 6: Genotyping PCR for ASC-1 ko mice**

PCR step	Temperature [°C]	Time	cycles
Denaturation	95	2 min	1
Amplification	94	30 s	32
(Melting, Annealing,	60	30 s	
Polymerization)	72	30 s	
Polymerization	72	10 min	1
Cooling	12	∞	

PCR was loaded on a 2 % agarose gel and ran in TAE buffer (2 M Tris, 1 M glacial acetic acid, 0.5 M EDTA). Expected band sizes were 346 bp for a homozygous knockout and 292 bp for a wildtype allele.

### 3.1.2 D/L-serine supplementation

Male C57BL/6N-Rj mice were purchased from Janvier at an age of 3 or 7 weeks. Germfree C57BL/6 mice were bred at the HZI in Braunschweig in collaboration with Till Strowig. For D- and L- serine supplementation experiments, mice received either normal water or water supplemented with 0.1, 0.5 or 1 % D- or L-serine or/and 0.3 % Dextromethorphan hydrobromide monohydrate (DXM) *ad libitum*. To study acute oral uptake of D-serine, eight week old male C57BL/6 mice were gavaged with 100 mg/kg body weight D-serine. For assessment of D-serine distribution, mice were fasted for 4h and gavaged with 100 mg/kg <sup>13</sup>C-labelled D-serine.

### 3.1.3 Metabolic phenotyping

#### 3.1.3.1 Body composition

Body composition (fat and lean mass) was analyzed with a non-invasive magnetic-resonance whole-body composition analyzer (EchoMRI).

#### 3.1.3.2 GTT, ITT, GSIS, PTT

Glucose tolerance tests (GTT) and insulin tolerance tests (ITT) were carried out in mice fasted for 4 h. 2 g glucose/kg body weight or 0.75 U insulin/kg were injected intraperitoneally (i.p.) and glucose concentrations were measured in blood collected from the tail before and 15, 30, 60, 90, and 120 min after the injection using a FreeStyle Freedom Lite glucometer (Abbott). To study acute effects of D-serine, mice were fasted for 2 h and injected intraperitoneally with 2 or 4 g D-serine/kg body

weight. Mice were fasted for 2 hours after D-serine injection and GTT was performed as described. Glucose stimulated insulin secretion (GSIS) was assessed in mice fasted for 4 h prior to the i.p. injection of 5 mg/kg BRL44408 and/or 4 g/kg glucose. Blood was collected from the tail vein before and 5, 10, 15, and 30 min after the injection. At the same time points, glucose concentrations were measured. Serum was prepared by centrifugation (5 min, 10.000 xg, 4 °C) and serum insulin concentrations were determined using the mouse ultrasensitive insulin ELISA kit (Alpco). For the pyruvate tolerance test (PTT), mice were fasted for 16 hours. 5 mg/kg sodium pyruvate was injected i.p. and glucose concentrations were measured before and 15, 30, 60, and 120 min after the injection.

### **3.1.3.3 Indirect calorimetry**

Energy expenditure, food and water consumption, locomotor activity, and respiratory exchange quotient (RER) were measured with an indirect calorimetric system (TSE PhenoMaster). Mice were single housed and different treatment groups were randomly arranged in the cabinets to guarantee equal exposure to potential technical differences between cabinets. During measurement, the health status of the mice was monitored daily.

### **3.1.3.4 Food preference test**

Mice were starved for 16 hours in groups and afterwards separated into single cages with a known amount of CD and HFD. After three hours, mice were put back into their group and left over food was weighed, to calculate the amount of consumed CD and HFD per mouse.

### **3.1.4 Sacrifice and organ withdrawal**

Mice were sacrificed by cervical dislocation or by overdose of Ketamine/Xylazine (400 µl Ketamine, 150 µl Xylazine in 2 ml 0.9 % NaCl). Immediately, organs were collected and frozen at -80 °C or processed for histology (see chapter 3.3)

## **3.2 Ex vivo measurements**

### **3.2.1 Isolation of pancreatic $\beta$ -cells**

Mice were sacrificed by cervical dislocation and the bile duct was clamped. 4 ml of cold collagenase solution (1 mg/ml Collagenase P in G-solution (1 % BSA, 1 % PenStrep in HBSS)) was injected into the duct. The pancreas was removed and incubated in 6 ml collagenase solution for 12 min at 37 °C. After half incubation time, the pancreas was shaken hardly. 10 ml of cold G-solution was added to the digested pancreas and centrifuged 2 min at 290 xg. Pellet was washed with 10 ml G-solution and re-suspended in 11 ml 15 % Optiprep (60 % Optiprep, 3.75 mM Hepes, 10 % RPMI in HBSS+PenStrep). Gradient was pipetted (5 ml 15 % Optiprep, 11 ml cell suspension, 12 ml G-solution) and centrifuged 15 min at 226 xg without break. The Islet containing phase was filtered (70  $\mu$ m strainer), islets were picked and cultured in RPMI over-night.

#### **3.2.1.1 Insulin secretion from pancreatic $\beta$ -cells**

10 islets per well were incubated in a 96 v-bottom well plate at 37 °C for 1 hour in 100  $\mu$ l Krebs-Ringer-Buffer (KRB: 120 mM NaCl, 4.8 mM KCl, 2.5 mM CaCl<sub>2</sub> x 2H<sub>2</sub>O, 1.2 mM MgCl<sub>2</sub>, 5 mM Hepes, 24 mM NaHCO<sub>3</sub>, 0.1 % BSA) containing 2 mM glucose and combinations of 400  $\mu$ M D-serine and 10  $\mu$ M dextrorphan tartrate (DXO). After 1 h, the supernatant was discarded and islets were incubated with the same conditions for 1 h. Supernatant was collected (low glucose), and islets were incubated for 1 h at 37 °C with KRB containing 16.7 mM glucose and supplements as described above. The supernatant was collected (high glucose), the remaining islets lysed in 500  $\mu$ l Acid-Ethanol (70 % Ethanol + 1.5 % HCl) using the sonicator (Model 150 V/T; Biologics) and incubated at 4 °C over-night. Lysed cells were centrifuged (7000 rpm, 4 °C, 10 min), and the supernatant transferred into a new tube. Insulin concentrations were determined using the Mouse insulin ELISA (AppliChem), and secreted insulin was normalized to total insulin content.

#### **3.2.1.2 Islet membrane potential measurement (Collaboration)**

All experiments for measurement of islet membrane potential were performed by Elizabeth Haythorne and Guy Rutter (Section of Cell Biology and Functional Genomics, Department of Medicine, Imperial College London, London, UK)

Pancreatic islets were dissociated into single  $\beta$ -cells and plated onto glass coverslips, as previously described (Tarasov et al., 2012). Electrophysiological recordings were performed in perforated patch-clamp configuration using an EPC9 patch-clamp amplifier controlled by Pulse acquisition software (Heka Elektronik).  $\beta$ -cells were identified morphologically and by depolarization of the membrane potential in response to 16.7 mM glucose.  $\beta$ -cells were constantly perfused at 32-33 °C with normal saline solution (mM): 135 NaCl, 5 KCl, 1 MgCl<sub>2</sub>, 1 CaCl<sub>2</sub>, 10 HEPES, and 16.7 glucose (pH 7.4). Recording electrodes had resistances of 8-10 M $\Omega$  and were filled with a solution comprised of (mM): 140 KCl, 5 MgCl<sub>2</sub>, 3.8 CaCl<sub>2</sub>, 10 HEPES, 10 EGTA (pH 7.2), and 20–25  $\mu$ g/ml amphotericin B (Sigma-Aldrich).

### **3.2.2 Bomb calorimetry**

Fecal caloric content was measured from dried fecal pellets using a bomb calorimeter. Feces were collected from cages containing 2-3 animals for 7 days and dried in a drying oven (Lab. Companion SI-300R) at 50 °C. Dried feces were homogenized in a TissueLyser and 1 g of feces was pelletized. Each pellet was completely burned under high oxygen pressure (30 bar) using a 6300 Oxygen Bomb Calorimeter (Parr Instrument Technology) kindly provided by Prof. Dr. M. Klingenspor (Chair of Molecular Nutritional Medicine; School of Life Sciences, Technical University Munich, Weihenstephan).

### **3.2.3 Measurement of gut microbiota (Collaboration)**

All experiments regarding gut microbiota were performed by Eric Gálvez and Till Strowig (Research Group Microbial Immune Regulation, Helmholtz Centre for Infection Research, Braunschweig, Germany).

Mouse fecal pellets were collected and DNA was isolated using an established protocol (Thiemann et al., 2017). Briefly, the samples were suspended in 500  $\mu$ l of extraction buffer (200 mM Tris, 20 mM EDTA, 200 mM NaCl, pH 8.0), 200  $\mu$ l of 20 % SDS, 500  $\mu$ l of phenol:chloroform:isoamyl alcohol (24:24:1), and 100  $\mu$ l of zirconia/silica beads (0.1 mm diameter). Bacterial cells were disrupted with a bead beater (BioSpec) 2x 2min. After isopropanol precipitation, crude DNA extracts were resuspended in TE Buffer with 100  $\mu$ g/ml RNase I and column purified (BioBasic). PCR amplification targeting the V4 region (F515/R806) of the 16S rRNA gene was performed according to previously described protocols (Caporaso et al., 2011). In short, 25 ng DNA were used per PCR reaction (30  $\mu$ l; 30 s at 98 °C and 25 cycles of

10 s at 98 °C, 20 s at 55 °C, 20 s at 72 °C. After normalization, PCR amplicons were sequenced on an Illumina MiSeq platform (PE250). Obtained reads were assembled, quality controlled, and clustered using Usearch8.1 software package (<http://www.drive5.com/usearch/>). Briefly, reads were merged using `-fastq_mergepairs` `-with fastq_maxdiffs 30` and quality filtering was done with `fastq_filter` (`-fastq_maxee 1`), minimum read length 200 bp. The OTU clusters and representative sequences were determined using the UPARSE algorithm (Edgar, 2013), followed by taxonomy assignment using the Silva database v128 (Quast et al., 2013) and the RDP Classifier (Wang et al., 2007) with a bootstrap confidence cutoff of 80 %. The OTU absolute abundance table and mapping file were used for statistical analyses and data visualization in the R statistical programming environment (R Core Team 2016) package phyloseq (McMurdie and Holmes, 2013).

### **3.2.4 Measurement of metabolic parameters**

#### **3.2.4.1 Serum metabolites**

Serum insulin levels were determined using the Mouse ultrasensitive insulin ELISA kit (Alpco). C-peptide was measured with usage of the C-peptide (mouse) ELISA kit (Biocat).

#### **3.2.4.2 Liver triglyceride and glycogen content**

Liver triglyceride content was measured with the triglyceride quantification Colorimetric/Fluorimetric Kit (BioVision). Liver glycogen content was quantified with the starch assay (r-biopharm).

#### **3.2.4.3 Liver metabolites (Collaboration)**

All experiments regarding liver metabolites were conducted by Silke Heinzmann and Philippe Schmitt-Kopplin (Research Unit Analytical BioGeoChemistry, Department of Environmental Sciences, Helmholtz Center Munich 85764 Neuherberg, Germany).

For determination of the liver metabolomics, metabolites from 50 mg of liver tissue were extracted with an aqueous extraction procedure. 1 ml of H<sub>2</sub>O was added to the sample with ceramic beads (NucleoSpin, Macherey-Nagel, Dueren, Germany) and homogenized for 3 min at 30 1/s in a TissueLyser II (Qiagen, Hilden, Germany). Samples were centrifuged (5 min, 13000 xg), and the supernatant was taken as aqueous extract. 100 µl of the extract was mixed with 50 µl NMR buffer (90 % D<sub>2</sub>O,

500 mM PO<sub>4</sub> buffer with 0.1 % trimethylsilyl-tetradecuteropropionic acid [TSP], pH 7.4), and analyzed immediately by NMR spectroscopy.

All samples were transferred to 3 mm outer diameter NMR Bruker Match tubes (Hilgenberg GmbH) and analyzed in a randomized order. NMR spectra were acquired on a Bruker 800 MHz spectrometer (Bruker Biospin) operating at 800.35 MHz with a quadruple inverse (QCI) cryogenic probe. For an overview of all molecules present in the sample, a standard one-dimensional (1D) pulse sequence [recycle delay (RD), 90°, t<sub>1</sub>, 90°, mixing time (t<sub>m</sub>), 90°, acquire FID] was acquired, with water suppression irradiation during an RD of 2 s, the t<sub>m</sub> set on 200 ms, and a 90° pulse set to 9 μs, which collected 512 scans into 64 K data points with a spectral width of 12 ppm. A representative sample of each gut section underwent 2D NMR analysis for detailed metabolite analysis and metabolite identification. For the 2D 1H–13C HSQC spectra, phase-sensitive ge-2D HSQC using PEP and adiabatic pulses for inversion and refocusing with gradients were used. For each 2D spectrum, 4096 × 1024 data points were collected using 64 scans per increment, an acquisition time of 0.25 s, and 16 dummy scans. The spectral widths were set to 12 and 230 ppm in the proton and carbon dimensions, respectively. For the 2D 1H–1H TOCSY spectra, phase sensitive sensitivity-improved 2D TOCSY with WATERGATE (3-9-19) and DIPSI-2 were acquired. For each 2D spectrum, 19 228 × 1024 data points were collected using 16 scans per increment, an acquisition time of 1 s, and 16 dummy scans. The spectral widths were set to 12 and 12 ppm in the F<sub>2</sub> and F<sub>1</sub> dimensions, respectively. Processing of the spectra was carried out in a TopSpin 3.2 (Bruker BioSpin). FIDs were multiplied by an exponentially decaying function corresponding to a line broadening of 0.3 Hz before the Fourier transformation. All spectra were manually phased, baseline corrected, and calibrated to TSP (δ 0.00). Data were imported into Matlab (Mathworks) and further processed (i.e., the water region was removed). Quantification of selected metabolites was done by integration of their area under the curve (AUC) and referencing to the AUC of TSP (in mmol) and the liver wet weight (in kg).

## **3.3 Histology**

### **3.3.1 Paraffin embedding**

Tissues were fixed in 4 % PFA/PBS (10x PBS buffer: 1.37 M NaCl, 27 mM KCl, 100 mM NaHPO<sub>4</sub>, 18 mM KH<sub>2</sub>PO<sub>4</sub>, pH 7.4) overnight, and transferred into 70 % EtOH for at 1 h at RT, or longer at 4 °C. Afterwards, tissues were incubated each for 1 h in 70 %, 80 %, 90 % and twice in 100 % EtOH, followed by 3 times of 30 minutes incubation in Xylol. Tissues were transferred to melted paraffin for two times 1 h at 65 °C. The third paraffin step was performed overnight. Tissues were embedded (Leica EG 1150 C), sectioned (Leica VT1000 S) with a thickness of 2-5 µm and immobilized on slides.

#### **3.3.1.1 H&E staining**

For hematoxylin and eosin (H&E) staining, paraffin sections were dewaxed for two times 5 min in xylol and rehydrated for 2 min each in 100 %, 96 %, 90 %, 80 %, 70 % EtOH followed by 2 minutes in deionized water. Sections were stained in Mayer's solution (filtered) for approximately 1 min and washed with tap water 3 times for 2 minutes. Sections were dehydrated in 96 % and 100 % EtOH for 3 min each and stained with chromotrope II R (100 mg chromotrope II R + 100 ml 100 % ethanol + 100 µl acetic acid, filtered) for 3 min. Slides were washed in 96 % and 100 % EtOH for each 1 min and incubated for 5 min two times in xylol. Afterwards, slides were mounted and dried at room temperature.

#### **3.3.1.2 Picrosirius red staining**

For picrosirius red staining, paraffin sections were dewaxed each 2 minutes in 2x Xylol, 100, 90, 70 % EtOH and H<sub>2</sub>O. Sections were stained with hematoxylin (Weigert) for 20 min, washed with tap water for 5 min and stained in picrosirius red solution (0.1 g picrosirius red in 100 ml saturated picric acid) for 1 h. Afterwards, slides were washed 2 times in acidified water (0.5 % acetic acid in H<sub>2</sub>O) and 2x in 100 % EtOH. Slides were incubated for 5 min in fresh 100 % EtOH, 2x 2 min each in Xylol and mounted in Roti-Histokitt.



### 3.3.2 c-Fos staining (Collaboration)

All c-Fos stainings were performed by Tim Gruber and Cristina García Cáceres (Institute for Diabetes & Obesity, Helmholtz Center Munich, 85748 Garching, Germany).

90 minutes after injections of either glucose (2 g/kg bodyweight) or vehicle (0.9 % NaCl), mice were euthanized by CO<sub>2</sub>. Animals were transcardially perfused with saline (0.9 % NaCl) followed by 4 % paraformaldehyde (PFA) in phosphate buffered saline (pH 7.4) cooled to 4 °C. Brains were removed and post-fixed in 4 % PFA at 4 °C before being equilibrated for 48 h with 30 % sucrose in Tris-buffered saline (TBS; pH 7.2). Brains were coronally cut into 40 µm sections at a cryostat. For immunohistochemistry, brain sections were first washed in TBS and then incubated overnight with primary antibody anti-c-Fos (rabbit polyclonal, 1:500, Santa Cruz Biotechnology, Inc, TX, US) diluted in SUMI (gelatin 0.25 % and TritonX-100 0.5 % in TBS) at 4 °C. After serial washes in TBS, sections were incubated with alexa fluor 647 donkey-anti-rabbit (1:1000, Molecular Probes, Life Technologies GmbH, Darmstadt, Germany) secondary antibody diluted in SUMI. Sections were washed with TBS, mounted on gelatin-pre-coated glass slides, and kept at dark and 4 °C for drying. Dried sections were mounted with a coverslip using mowiol-based mounting solution containing the anti-fading agent DABCO (*elvano*). Images were captured as z-stacks with 2 µm steps at 10X magnification by a Leica TCS SP5 II confocal microscope (Leica Microsystems, Wetzlar, GER). Quantification of c-Fos immunoreactive (c-Fos+) cells was performed using ImageJ software.

Maximum projections of confocal scans were automatically thresholded and the number of c-Fos+ cells per each hypothalamic nucleus according with the mouse brain atlas (PVN, ARC, DMN, VMN and LH) was determined. All morphometric analyses were performed without previous knowledge of the experimental group and nuclear staining was counted in blinded fashion.

### 3.3.3 Immunohistochemistry

For immunohistochemistry staining, slides were dewaxed 2x 5 minutes in Xylol and incubated each 2 min in 100, 90, 70 % EtOH and H<sub>2</sub>O. Afterwards, slides were boiled for 10 minutes in 10 mM tri sodium citrate dihydrate buffer and let cool down to RT. Slides were incubated for 5 min each in TBST (1.21 g Tris, 5.5 g NaCl in 1l H<sub>2</sub>O, pH 7.4 + 0.1 % Tween20) + 3 % H<sub>2</sub>O<sub>2</sub> and in distilled water. Afterwards, slides were blocked for 1 h at RT in goat-serum (VECTASTAIN® ABC HPRT Kit (Vector

Laboratories; PK-4001)) (2 drops in 6ml TBST) and incubated overnight at 4 °C in primary antibody. On the next day, slides were washed 5 min with TBST and incubated in secondary antibody (VECTASTAIN® ABC HPRT Kit (Vector Laboratories; PK-4001) 1:200) for 30 min at RT. After washing with TBST, ABC-solution (VECTASTAIN® ABC HPRT Kit (Vector Laboratories; PK-4001)) was added for 30 min at RT and removed by washing with TBST. Slides were stained for 0.5 - 3 min with DAB solution (DAB Peroxidase (HRP) Substrate Kit (Vector Laboratories; SK-4100) 2.5 ml H<sub>2</sub>O, 1 drop buffer, 1 drop H<sub>2</sub>O<sub>2</sub>, 2 drops DAB stock). Reaction was stopped by washing in H<sub>2</sub>O and counterstain with hematoxylin was performed for 1 min. Slides were washed 2 min under running tap water and dehydrated for each 2 min in 70, 90, 100 % EtOH and 2x 5 min in Xylo. Slides were mounted and dried.

### **3.3.4 Agarose embedding**

After dissection, tissue was fixed in 4 % PFA over night at 4 °C. Tissue was washed 3x 5 min with PBS. Parallel, 4 % low gelling temperature agarose was boiled until dissolved, cooled down to approximately 55 – 60 °C and subsequently tissue was embedded. After cooling down and set, tissue was cut with a vibratome (Microm HM 355S, Thermo Scientific) into 70 – 100 µm sections. Settings for the vibratome were speed 5.0 and frequency 6.0. Free float staining was performed in cell culture plates. Slices were blocked with 3 % filtered BSA/PBS for 1 h on a shaker. Sections were incubated in primary antibody at 4 °C over night and washed 3 times 5 min with PBS. Secondary antibody was added together with Bodipy, Phalloidin and DAPI and incubated 1 h at RT. After washing 3 times 5 min each in PBS, sections were transferred to slides and mounted in fluorescent mounting medium.

### **3.3.5 Cryoembedding and triple staining of pancreata**

Directly after dissection, tissue was embedded in OCT and frozen at -80 °C until further processing. To assess  $\alpha$ -,  $\beta$ -, and  $\delta$ - cell distribution, pancreas was cut in 5 µm sections (Leica CM350 S), fixed 10 min in 4 % PFA, washed 3x with PBS, and permeabilized (0,1 M Glycine, 0,2 % TritonX-100 in PBS) for 30 min. After blocking for 1 h in donkey serum, primary antibodies (diluted in donkey block) were added over night at 4 °C. Secondary antibodies (in donkey block) were incubated for 1 h. After washing, stainings were mounted in fluorescent mounting medium.

### **3.3.6 Immunohistochemistry of cultured cells**

To investigate the localization of the overexpressed ASC-1-HA, cells were fixed 10 min in 10 % formalin, washed 3x with PBS, and blocked for 1 h in 3 % BSA/PBS. Primary antibody was incubated overnight at 4 °C, and secondary antibody mixed with Phalloidin for F-actin staining and Dapi was added for 1 hour. Subsequently after washing, cells were mounted in fluorescent mounting medium

### **3.3.7 Imaging**

Images were acquired using a Zeiss scope A1 or a Leica SP5 confocal microscope.

#### **3.3.7.1 Cell size assessment (Collaboration)**

Cell size assessment was performed by Anette Feuchtinger (Research Unit Analytical Pathology, Helmholtz Center Munich 85764 Neuherberg, Germany).

Stained slides were imaged using a Mirax Desk digital slide scanner (Carl Zeiss MicroImaging). Adipocyte size was calculated from measuring all adipocytes per slide after H&E staining and islet size was determined based on the insulin staining using the Definiens Developer XD2 (Definiens AG) software.

#### **3.3.8 MALDI FT-ICR MSI (Collaboration)**

Organs were dissected, immediately frozen in liquid nitrogen and transferred to Achim Buck and Axel Walch (Research Unit Analytical Pathology, Helmholtz Center Munich 85764 Neuherberg, Germany) who performed MALDI FT-ICR MSI (Matrix-assisted laser desorption/ionization Fourier-transform ion cyclotron resonance mass spectrometry imaging).

To gather information about distribution of <sup>13</sup>C-labeled D-serine, frozen tissue samples were cryosectioned into 12 µm thick slices and thaw-mounted onto pre-cooled conductive indium tin oxide-coated glass slides (Bruker Daltonics) pre-coated with a 1:1 mixture of poly-L-lysine and 0.1 % Nonidet P-40 (Sigma-Aldrich). Tissue sections were coated with 9-aminoacridine hydrochloride monohydrate matrix (Sigma-Aldrich) at 10 mg/ml in methanol/H<sub>2</sub>O (7:3, v/v) using a SunCollect sprayer (Sunchrom). Matrix solution was deposited in eight layers onto the tissue section with the flow rates at 10, 20, 30, and 40 µl/min. MALDI MSI was performed in negative ion mode on a Bruker Solarix 7T FT-ICR MS (Bruker Daltonics). Accurate mass measurements were acquired in negative mode using continuous accumulation of selected ions with a mass window of *m/z* 50-150, a 2 M data point transient (0.5243 s

duration) providing a mass resolving power of approximately 300,000 at  $m/z$  100. The Smartbeam-II Nd:YAG (355 nm) laser operated at a frequency of 1000 Hz using 200 laser shots per spot and a lateral resolution of 60  $\mu\text{m}$ . After MALDI-MSI completion, the matrix was removed from slides with 70 % ethanol, and tissue sections were stained using hematoxylin and eosin. The resulting data were analyzed using FlexImaging 4.0 (Bruker Daltonics) with root mean square normalization of the ion images.

## **3.4 Bacterial culture**

### **3.4.1 Cloning of ASC-1 overexpression constructs**

To investigate the function of ASC-1 *in vitro*, overexpressing constructs were created. Therefore, *Asc-1* was tagged with an HA-tag for cellular localization. As ASC-1 forms a heterodimer with the 4F2 heavy chain (Fukasawa, 2000), a second overexpression construct was created, containing *Asc-1* and *4F2hc*. The HA-tagged *Asc-1* was cloned without stop codon, followed by short sequence called T2A element which then was followed by the sequence for *4F2hc* and a final stop codon. The T2A element is a short sequence that induces ribosome skipping which induces a separation of the connected proteins (Liu et al., 2017) and equal transcription of both, ASC-1 and its cofactor.

#### **3.4.1.1 pCDH-CMV-MCS-EF1-puro-Asc-1-HA**

The sequence for *Asc-1* was in the pCDH- CMV-MCS-EF1-puro vector, but there were no restriction sites and parts of the untranslated region were inserted. For further cloning, *Asc-1* was flanked with the two restriction sites EcoRI and NotI, but without stop-codon at the end by PCR and cloned into the empty pCDH-CMV-MCS-EF1-puro plasmid. Sequencing revealed two point mutations after the PCR, which both were removed using the lightning site mutagenesis kit (Agilent). Using the same kit, next the sequence for the HA-tag and a stop-codon was inserted before the 3' end. Another round of sequencing revealed, that the construct was correct. The insert of the empty pCDH- CMV-MCS-EF1-puro vector was EcoRI-*Asc-1*-HA-Stop-BamHI-NotI (see full vector map in the supplements).

**Table 7: Primers for cloning and sequencing pCDH-Asc-1-HA**

Gene	Sequence 5'-3'
<b>PCR primers</b>	
EcoRI-Asc-1-no stop-BamHI-NotI fwd	taaacgaattcatgagggcgggacagcgacat
EcoRI-Asc-1-no stop-BamHI-NotI rev	atntagcggccgcggatccttgtgtcttcaagggctgtc
<b>Mutagenesis primers</b>	
Pointmutation C to T fwd	gaacctacctcgtgccatcttcatttccatcccac
Pointmutation C to T rev	gtgggatggaaatgaagatggcacgaggtagggtc
Pointmutation A to G fwd	ctccaactatgtgcttcagcctgtctttccaact
Pointmutation A to G rev	agttgggaaagacaggctgaagcacatagtggag
HA-TGA insertion fwd	agccctgaagacacaatacccatacagatgttccagattacgctt gaggatccgcgcc
HA-TGA insertion rev	Ggccgcggatcctcaagcgtaatctggaacatcgatgggtatt gtgtctcaagggct
<b>Sequencing primers</b>	
Asc-1 5' cloning site fwd	tgcggggcccacagcggta
Asc-1 3' cloning site rev	gctgaagcacatagttggag
Asc-1 Exon 3 fwd	gtgcttcagcctgtcttcc
Asc-1 Exon 4 fwd	tcactgttggttgcag
Asc-1 Exon 4 rev	gtacgctggagctgtcacc
Asc-1 Exon 6 fwd	caggagtgtctgcctcca
Asc-1 Exon 6 rev	accagtgggatggaaatgaa
Asc-1 Exon 7 rev	gtagccattgatccctcaa
Asc-1 Exon 8 fwd	gggacacttaccagcttcc
Asc-1 Exon 9 fwd	actatcctgggcctgtgt
Asc-1 Exon 10 fwd	actggggtcccattctt

**3.4.1.2 pCDH-CMV-MCS-EF1-puro-Asc-1-HA-2a-4F2hc**

The sequence for 4F2hc (Slc3a2) was in the plasmid pYX-Asc. Via PCR, the DNA for 4F2hc was flanked 5' NheI and 3' NotI and EcoRI with the restriction enzyme sites. Via NheI and EcoRI, it was cloned into the plasmid pULTRA-P2rx5, behind a T2A-element. From there, a PCR was performed to create a sequence for BamHI-2a-NheI-4F2hc-NotI construct which was cloned into the vector created above (pCDH-CMV-MCS-EF1-puro-EcoRI-Asc-1-no stop-BamHI-NotI) using BamHI and NotI restriction sites. Via the mutagenesis kit, an HA Tag was added between Asc-1 and BamHI. As in the PCR occurred many point mutations in the sequence of 4F2hc, a PCR from the original plasmid was performed adding the restriction sites NheI 3 and NotI 5' and first cloned into the TOPO vector (TOPO™ TA Cloning™ Kit, Thermo Fischer Scientific 450641) for sequencing. Parallel, the correct NheI-EcoRI-Asc-1-HA-BamHI-2a-NheI insert was cut out via the restriction enzyme NheI and cloned into an empty pCDH- CMV-MCS-EF1-puro with XbaI and NheI, destroying the 3' XbaI/NheI site. After checking for right orientation, the correct 4F2hc sequence was cloned via NheI and NotI behind the Asc-1 construct, creating the pCDH-CMV-MCS-

EF1-puro-NheI-EcoRI-Asc-1-HA-BamHI-2a-NheI.4F2hc-Stop-NotI plasmid (see full vector map in the supplements).

**Table 8: Primers for cloning and sequencing pCDH-Asc-1-HA-2a-4f2hc**

Primer	Sequence 5'-3'
<b>PCR primers</b>	
NheI-4F2hc-Stop-NotI-EcoRI fwd	atttgagaattcgcgccgctcaggccacaaaggggaact
NheI-4F2hc-Stop-NotI-EcoRI rev	Atttgagaattcgcgccgctcaggccacaaaggggaact
BamHI-T2A-4F2hc-NotI fwd	taaacggatccggctccggcgag
BamHI-T2A-4F2hc-NotI rev	atttagcggccgctcaaggccaca
<b>Mutagenesis primers</b>	
HA-insertion fwd	Gccctgaagacacaatacccatacgatgttccagattacgctggatc cggtccg
HA-insertion rev	Cggagccggatccagcgtaatctggaacatcgatgggtattgtgtctt caagggc
<b>Sequencing primers</b>	
4F2hc fwd 1	gagtactgagcacctg
4F2hc fwd 2	tataccggaccatcttctc
4F2hc rev	ctacaatgacgcctgag

### 3.4.2 Transformation of Escherichia coli

For cloning, plasmids were transformed into competent Escherichia coli (E.coli) bacteria. To create competent bacteria, a pre-culture was incubated in 5 ml LB medium over night (Infors HT Multirton) and transferred into 100 ml LB medium the next day. Bacteria were cultured until  $OD_{550} = 0.5-0.6$  (NanoDrop 2000c, Thermo Scientific) and incubated on ice for 10 minutes. Bacteria were centrifuged down and pellet was re-suspended in 10 ml TSS-medium (1 % Trypton, 0.5 % Yeast Extract, 0.5 % NaCl, 10 % PEG (MW 3000), 5 % DMSO, 5 % 1 M  $MgCl_2$ ). 2.5 ml Glycerin was added and solution was aliquoted and frozen at  $-80\text{ }^{\circ}\text{C}$ . For transformation of DNA into competent bacteria, DNA and bacteria were mixed and incubated on ice for 30 min. Afterwards, a heat shock of  $42\text{ }^{\circ}\text{C}$  for 45 seconds was performed in a water bath and bacteria were incubated on ice for 2 min. 500  $\mu\text{l}$  of LB medium was added and bacteria were incubated 1 h at  $37\text{ }^{\circ}\text{C}$  and 300 rpm (ThermoMixer C, Eppendorf). Bacteria were centrifuged down 5 min at 11.000 xg and supernatant was decanted. Pellet was re-suspended in the rest of supernatant and plated on LB plates with the antibiotics according to the plasmids resistance to select positive clones.

For cloning plasmids into the TOPO vector, the TOPO cloning kit (TOPO™ TA Cloning™ Kit, Thermo Fischer Scientific 450641) was used according to the manufacturer's protocol. After transformation into ultracompetent E.coli (XL10-Gold Competent Cells; Agilent 200315), bacteria were plated on agar plates containing X-GAL and IPTG for selection of positive clones.

### **3.4.2.1 Isolation of plasmids**

To isolate plasmids from transformed bacteria, single clones were picked from an agar plate and cultured in liquid 2 ml LB medium with the appropriate antibiotics overnight at 37 °C and 300 rpm. On the next day, bacteria were centrifuged down 1 min 13.000 xg and DNA was extracted from the pellet using the Plasmid Mini Kit (Qiagen). For higher amounts of DNA, 2 ml of LB medium was incubated during the day and transferred into 100 ml LB medium for overnight culture. For isolating the DNA, the Plasmid Midi Kit (Quiagen) was used according to the manufacturer's protocol.

## **3.5 Cell culture**

### **3.5.1 Isolation and immortalization of stromal vascular fraction**

Murine subcutaneous or brown adipose tissue was dissected and digested for 30 minutes at 37 °C in DMEM (Dulbecco's Modified Eagle Medium, DMEM + GlutaMAX + high glucose) containing 1 mg/ml collagenase type IV and 1 % BSA (Albumin fraction V). The digestion was stopped by washing with PBS containing 1 % BSA. The cell suspension was filtered through a 100 µm strainer to remove undigested tissue pieces. Cells were centrifuged for 5 min at 800 xg and washed with growth medium (DMEM) containing 10 % fetal bovine serum and 1 % penicillin/streptomycin. After a second centrifugation step, the cells were re-suspended in growth medium and seeded on 6-well plates. The cells were immortalized using an ecotropic SV40 large T retrovirus produced in HEK 293T cells and transferred several passages to select successful immortalized cells.

### **3.5.2 Cell line maintenance**

Immortalized cells were seeded on 6-well plates and infected with a lentivirus containing a pLKO.1 vector with a scrambled (scr) or an anti-Asc-1 short hairpin RNA (shRNA), or a pCDH-CMV-MCS-EF1-puro vector with an ASC-1-HA-2a-4F2HC or GFP overexpression. After 24 hours, cells were selected with growth medium containing 2.5 µg/ml puromycin. This medium also was used for all cell culture experiments. All cell lines were kept at 37 °C and 5 % CO<sub>2</sub> (HERAcell 240 I; Thermo Scientific). Every two days, cells were passaged or medium was changed.

### **3.5.3 Differentiation**

Subcutaneous preadipocytes were grown in cell culture plates up to 100 % confluence and the differentiation was induced with 0.5 mM 3-Isobutyl-1-methylxanthin (IBMX), 1  $\mu$ M dexamethasone, and 170 nM insulin in the growth medium. After two days, the medium was changed to continuum medium containing only 170 nM insulin. Differentiation of brown preadipocytes was induced with 0.5 mM IBMX, 5  $\mu$ M dexamethasone, 0.125 mM indomethacine, 1 nM triiodothyronine (T3) and 100 nM insulin. After two days, the medium was changed to continuum medium containing only 100 nM insulin and 1 nM T3. The medium was changed every 2 days until completed differentiation at day 8. In addition, some cells were supplemented with 1  $\mu$ M rosiglitazone during the first 2 days of differentiation or with 10  $\mu$ M of the ASC-1-Inhibitor BMS-466442 from the day of seeding or differentiation start to end of the differentiation phase. Medium containing BMS-466442 was sterile filtered through a 0.2  $\mu$ m PVDF filter. For the differentiations in amino acid depleted medium, amino acid free medium was supplemented with 10 % FBS, 1 % penicillin/streptomycin and amino acids in the same concentration as the DMEM used for the other cell culture experiments.

### **3.5.4 Seahorse measurements**

Cells were seeded in a 96 well Seahorse plate and induced for differentiation with rosiglitazone according to the protocol above. After fulfilled differentiation, the oxygen consumption rate (OCR) was measured with a XF96 Extracellular Flux analyzer (Seahorse). Cells were equilibrated at 37 °C in XF Assay Medium Modified DMEM supplemented with 25 mM glucose and 5 mM sodium pyruvate one hour prior measurement. All compounds were diluted in assay medium and loaded in the equilibrated cartridge ports: A) 20  $\mu$ g/ml oligomycin, B) 20  $\mu$ M FCCP, C) 50  $\mu$ M rotenone and 20  $\mu$ M antimycin A, D) 1 M 2-Deoxy-D-glucose. Each cycle comprised 3 minutes mixing, 1 minute waiting and 2 minutes measuring. For the analysis, the mean of cycle 4 and 5 presents basal respiration (OCR) and the mean of cycle 7 and 8 refers to proton leakage (OCR).



## 3.6 Transcriptional and protein analysis

### 3.6.1 RNA isolation

RNA from cells was isolated using the RNeasy mini kit (Qiagen). Tissue was lysed in 1 ml Qiazol with a tissue lyzer. 200 µl Chloroform was added and samples were shaken for 15 seconds. After incubation for 5 minutes at room temperature, samples were centrifuged at 12.000 xg for 15 minutes at 4 °C. Aqueous phase was transferred into a new tube and the same volume of 70 % ethanol was added. After mixing, samples were transferred to RNeasy columns of the RNeasy mini kit and protocol was followed according to the manufacturer's instructions. RNA concentration was measured using a nanodrop (NanoDrop 2000; Thermo Scientific).

#### 3.6.1.1 cDNA synthesis

For cDNA synthesis, 0.5-1 µg total RNA was used and transcribed to cDNA with the High Capacity cDNA Reverse Transcription Kit (Applied Biosystems).

#### 3.6.1.2 qPCR

qPCR was performed in a C1000 Touch Thermal Cycler (Bio Rad), using 300 nM forward and reverse primers and iTaq Universal SYBR Green supermix (BioRad). The target gene expression was normalized on TATA box binding protein (TBP) expression.

**Table 9: qPCR primers**

gene	Fwd sequence 5'-3'	Rev sequence 5'-3'
<i>aP2</i>	gatgcctttgtggaacct	ctgtcgtctgcggtgattt
<i>Asc-1</i>	agtgttccaggacacccttg	gggtggcactcaagaaagag
<i>CD68</i>	tcacctgacctgctctctc	aggccaatgatgagaggcag
<i>Dao</i>	ctgcctccattctccaaacg	agggtccggaacttcatctc
<i>Kim1</i>	agtggctctgtattgttgcgag	aggacgtgtgggaatctctg
<i>Mac-1</i>	tgacctggcttagaccctg	acctctgagcatccatagcc
<i>P2rx5</i>	ctgcagctcacccatcctgt	cactctgcaggaagtgtca
<i>Pat2</i>	gtccaagaagctgcagag	tgttgccttgaccagatga
<i>Pepck</i>	ctgcataacggctctggacttc	cagcaactgcccgtactcc
<i>Pgc1α</i>	agccgtgaccactgacaacgag	gctgcatggttctgagtctaag
<i>Ppary</i>	ccctggcaaagcatttgtat	gaaactggcacccttgaaaa
<i>Prdm16</i>	ccgctgtgatgagtgtgatg	ggacgatcatgtgtgctcc
<i>Shmt1</i>	ctcagtgctggggtgtcaat	cagggtccaagcccattgattc
<i>Srr</i>	cattgcttgaatacctggc	tgagcagttcattctcccc
<i>Tbp</i>	accctcaccaatgactcctatg	tgactgcagcaaatcgcttgg
<i>Tfam</i>	caggaggcaaaggatgattc	ccaagacttcatttcattgtcg
<i>Tnfa</i>	cccacgtcgtagcaaacca	gtctttgagatccatgccgttg
<i>Ucp1</i>	ctgccaggacagtaccaag	tcagctgttcaaagcacaca

### 3.6.2 Protein isolation from cells or tissue

Cells were washed with PBS and homogenized in IP lysis buffer containing 0.1 % SDS, 1 % protease-inhibitor, 1 % phosphatase-inhibitor cocktail II and 1 % phosphatase-inhibitor cocktail III with syringes. Tissue was homogenized in a tissue lyzer in the same IP buffer, but SDS was added after homogenization to avoid foam formation. Samples were incubated on ice for 10 min and centrifuged 10 min at 14.000 xg at 4 °C. The supernatant was collected and protein concentration was determined using the Pierce BCA protein assay kit (Thermo Fischer Scientific).

#### 3.6.2.1 SDS Page and Western Blot

SDS gels were prepared according to following protocol:

<u>10 % Resolving gel (10 ml):</u>		<u>4 % Stacking gel (5 ml)</u>	
3.3 ml	30 % Acrylamide	0.75 ml	30 % Acrylamide
2.6 ml	1.5 M TrisHCl pH 8.8	1.3 ml	0.5 M TrisHCl pH 6.8
4.1 ml	H <sub>2</sub> O	3 ml	H <sub>2</sub> O
100 µl	10 % SDS	50 µl	10 % SDS
50 µl	10 % APS	25 µl	10 % APS
15 µl	Temed	10 µl	Temed

Protein samples were mixed with 4x sample buffer containing 1:40 β-mercaptoethanol, boiled for 10 min at 70 °C and loaded on a SDS gel. Electrophoresis (Mini-PROTEAN® Tetra System, Bio-Rad) was performed in SDS running buffer (1x buffer: 3 g Tris, 14.4 g Glycin, 1 ml 10 % SDS in 1l MQ-H<sub>2</sub>O) at 100 V (PowerPac HC; Bio-Rad) for 10 minutes followed by 120 V until the phenolblue was running out. Proteins were transferred on a PVDF membrane in Western Blot running buffer (1x buffer: 3 g Tris, 14.4 g Glycin, 100 ml MeOH in 1l MQ-H<sub>2</sub>O) for 1 h at 100 V. Membranes were blocked in 5 % BSA/TBST for 1 h and incubated in primary antibody over night at 4 °C. After washing 3 times in TBST for 10 minutes, secondary antibodies were incubated for 1 h at RT. The HRP-linked primary antibodies were incubated 1 h at RT instead of overnight. After a second wash, ECL was added to the membranes and the signal was detected with films in a dark room.

### **3.6.3 Immunoprecipitation**

1 mg total protein was incubated with anti-ASC-1 (FabGennix) in an over-head shaker (ELMI Intelli-Mixer RM-2M) at 4 °C over night. On the next day, 50 µl of agarose bead suspension (Protein A/G PLUS-Agarose; Santa Cruz Biotechnology sc-2003) was added and incubated 1 h at 4 °C. Samples were centrifuged down 3 min 3000 xg and washed 3 times with lysis buffer containing protease and phosphatase inhibitors. After the last centrifugation, beads were re-suspended in 2x sample buffer containing β-mercaptoethanol and boiled 10 min at 70 °C before loading on an SDS gel.

## **3.7 Amino acid analysis (Collaboration)**

Amino acid analysis was performed by Alexander Braun, Marina Spona-Friedl and Martin Elsner (Institute of Groundwater Ecology, Helmholtz Center Munich 85764 Neuherberg, Germany).

### **3.7.1 D-serine quantification**

Tissues were homogenized in 1 ml 100 % methanol using a Polytron, dried at 60 °C under a stream of N<sub>2</sub>. Dried residues were reconstituted in 50 µl milliQ water. Separation of the serine enantiomers was performed with chemical derivatization using Marfey's reagent (N<sub>α</sub>-(2,4-dinitro-5-fluorophenyl)-l-alaninamide; Sigma-Aldrich), generating dinitrophenyl-5-l-alanine-d/l-serine diastereomers (DNPA-D/L-serine), which can be separated by reverse-phase chromatography (Berna and Ackermann, 2007). To this end, 100 µl methanol, 50 µl 0.125 M sodium tetraborate (Sigma-Aldrich) buffer and 50 µl 1 % Marfey's reagent in acetone (Sigma-Aldrich) were added to the reconstituted sample and heated to 50 °C for 60 min. Derivatization was then stopped by addition of 20 µl 2N HCl (Sigma-Aldrich). For standard curve calibration, D- and L- serine (Sigma-Aldrich) standards were prepared at 166, 55, 18, 6, 2, 0.7, 0.2, 0.07, and 0.02 mg/l by serial dilution of a 500 mg/l stock solution and derivatized as described above.

Chromatographic separation of DNPA-D- and DNPA-L-Serine was accomplished on an Agilent HP 1200 HPLC system using a Synergi Hydro-RP (C18) 150 mm×2.1 mm I.D., 4 µm 80 °A particles column (Phenomenex) at 25 °C. Mobile phase A was LC-MS grade water with 0.1 % acetic acid (Fluka) and mobile phase B was acetonitrile

(Thermo Scientific), which was delivered according to the following gradient profile (min/% mobile phase B): 0.0/5, 1.9/5, 12/20, 20/20, 24/90, 30/90. The flow rate was 0.2 ml/min and the injection volume was 10  $\mu$ l.

The HPLC system was coupled to a Q-Trap MS/MS system (Applied Biosystems). Ionization was accomplished by electrospray ionization in the negative ion mode. Mass spectrometry was carried out in the multiple reaction monitoring mode. To determine the MS/MS fragment pattern with the highest intensity, a single analyte standard containing DNPA-D/L-serine was dissolved in a mixture of water and methanol 50:50 (v/v) at a concentration of 1 mg/l. The standard was infused at a flow rate of 200  $\mu$ l/min for tuning the compound-dependent MS parameters. The infusion experiment was performed using a syringe pump directly connected to the interface. Optimal detection was provided by scanning for the mass pair 356/356. Declustering potential, collision energy, collision cell exit potential, and entrance potential were optimized to -45, -12, -3, and -6 V. The optimized values for the parameters ion spray voltage, nebulizer gas, auxiliary gas, curtain gas, collision gas and auxiliary gas temperatures were -4500, 40, 35, 20, 3, and 400  $^{\circ}$ C, respectively. The curtain, collision, turbo, and nebulizer gas was nitrogen generated from pressurized air in a nitrogen generator. To obtain adequate selectivity and sensitivity, the mass spectrometer was set to unit resolution, and the dwell time was 150 ms.

Calibration curves were obtained by plotting the peak area of D/L-serine against their concentration. Peak integration was automatically accomplished via Analyst software (version 1.4.2, AB/MDS Sciex). A least squares regression analysis was used to obtain a linear equation over the range of the calibration. The assay finally produced a standard curve that was linear over a range of 0.02-166 mg/l. Samples were measured in triplicates.

### **3.7.2 Measurement of free amino acids**

Cells were homogenized in 1 ml 100 % methanol using a Polytron and placed on a column of Dowex 50Wx8 ( $H^+$  form, 200–400 mesh, 5 x 10 mm). The column was washed twice with 750 ml of water and was developed with 1 ml of 2 M ammonium hydroxide. An aliquot of the eluate was dried under a stream of nitrogen, and the residue was dissolved in 50 ml of dry acetonitrile. A total of 50 ml of N-(tert-butyl)dimethylsilyl)-N-methyl-trifluoroacetamide containing 1 % tert-butyl)dimethylsilylchlorid (Sigma-Aldrich) was added. The mixture was kept at 70  $^{\circ}$ C for 30 min. The resulting mixture of tert-butyl-dimethylsilyl derivatives (TBDMS) of amino acids was used for GC/MS analysis without further work-up. Gas

chromatography/mass spectrometry analysis was performed on a GC-17A Gas Chromatograph (Shimadzu, Duisburg, Germany) equipped with a fused silica capillary column (Equity TM-5; 30 m x 0.25 mm, 0.25 mm film thickness; SUPELCO, Bellefonte, PA) and a QP-5000 mass selective detector (Shimadzu, Duisburg, Germany) working with electron impact ionization at 70 eV. An aliquot (1  $\mu$ l) of a solution containing TBDMS amino acids was injected in 1:5 split mode at an interface temperature of 260 °C and a helium inlet pressure of 70 kPa. The column was developed at 150 °C for 3 min and then with a temperature gradient of 10 °C min<sup>-1</sup> to a final temperature of 260 °C that was held for 3 min. Data were collected using the Class 5000 software (Shimadzu, Duisburg, Germany). Samples were analyzed three times.

### **3.8 Statistics**

Data are presented as mean  $\pm$  standard error of the mean (SEM) unless stated differently in the figure legend. Statistical significance was determined by unpaired Student's t-test or, for multiple comparisons, using One- or Two-Way ANOVA, followed by Tukey's Multiple Comparison's Test, or as stated in the respective figure legend. Differences reached statistical significance with  $p < 0.05$ . For NMR spectroscopy, multivariate statistics, i.e. orthogonal partial least-squares discriminant analysis (OPLS-DA), were carried out in order to discriminate liver samples from mice under different serine supplementation. Here, OPLS loading plots show metabolites across the whole non-targeted metabolite analysis that differ between the treatment groups. These metabolites were then quantified and univariate statistical analysis carried out.

# 4 Results

## 4.1 Depletion of ASC-1 remodels genetic predisposition and enables beige over white adipocyte differentiation

To address the function of ASC-1 in white adipocytes, immortalized subcutaneous preadipocytes were infected with a lentivirus containing a shAsc-1 expressing plasmid, leading to a stable knockdown of ASC-1. As control, a lentivirus containing a non-targeting shScr expressing plasmid was used.

### 4.1.1 Loss of ASC-1 induces beige adipocyte differentiation *in vitro*

In preadipocytes as well as after differentiation with or without the PPAR $\gamma$  agonist

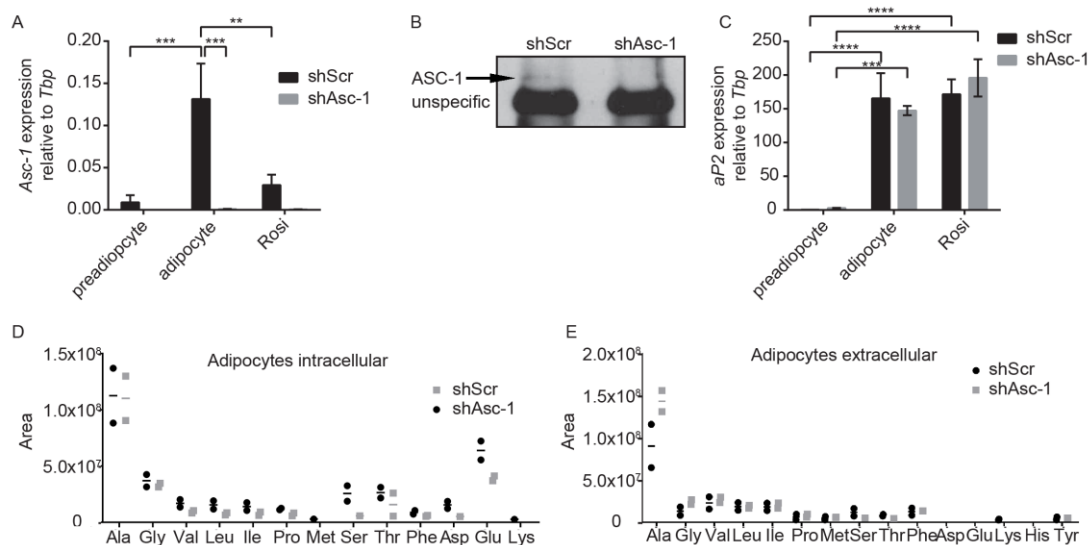


**Figure 5: Loss of ASC-1 changes the intra- and extracellular amino acid profiles.** ASC-1 underexpressing (shAsc-1) and scrambled (shScr) control subcutaneous preadipocytes were grown to 100 % confluence and RNA or protein was taken from the day of differentiation start (preadipocyte) and after 8 days of differentiation with (Rosi) or without rosiglitazone (adipocyte). **(A)** Relative gene expression of *Asc-1* (n=5-6). **(B)** Immunoprecipitation of ASC-1 in differentiated adipocytes (45kDa). **(C)** Relative gene expression of *aP2* (n=5-6). **(D)** Intracellular free amino acids of differentiated adipocytes (n=2). **(E)** Extracellular free amino acids of differentiated adipocytes (technical n=2, biological n=2). Data are represented as mean (for amino acids) or as mean  $\pm$  SEM. Statistics were calculated using ordinary two-way ANOVA with Tukey's multiple comparison post-hoc test (\*\*\*\*P<0.0001, \*\*\* P<0.001, \*\* P<0.01).

rosiglitazone, *Asc-1* was reduced on RNA level in shAsc-1 cells, confirming the knockdown (**Figure 5A**). Compared to shScr adipocytes, shScr preadipocytes expressed only low levels of *Asc-1*. Interestingly, when cells were differentiated with rosiglitazone, *Asc-1* expression was significantly reduced in shScr control cells. On protein level, shScr control adipocytes expressed only low ASC-1 levels that were not detectable in immunostainings or Western Blot (data not shown). After immunoprecipitation (IP), a weak protein band at the size of ASC-1 was observed in the shScr compared to the IP of shAsc-1 lysate (**Figure 5B**). A knockdown of the amino acid transporter ASC-1 did not impair the differentiation capacity as indicated by the adipocyte marker *aP2* (**Figure 5C**), but resulted in changes in intra- (**Figure 5D**) and extracellular (**Figure 5E**) free amino acids. Intracellular, serine was reduced, while alanine and glycine concentrations were not altered in the cells, but increased in the medium. This indicates a defect in amino acid in- and efflux that results in an altered amino acid profile due to the existing amino acid balance. Therefore, valine, leucine, isoleucine, proline, phenylalanine, aspartate and glutamate, not being transported by ASC-1, were reduced. The branched-chain amino acids valine, leucine and isoleucine are known to activate

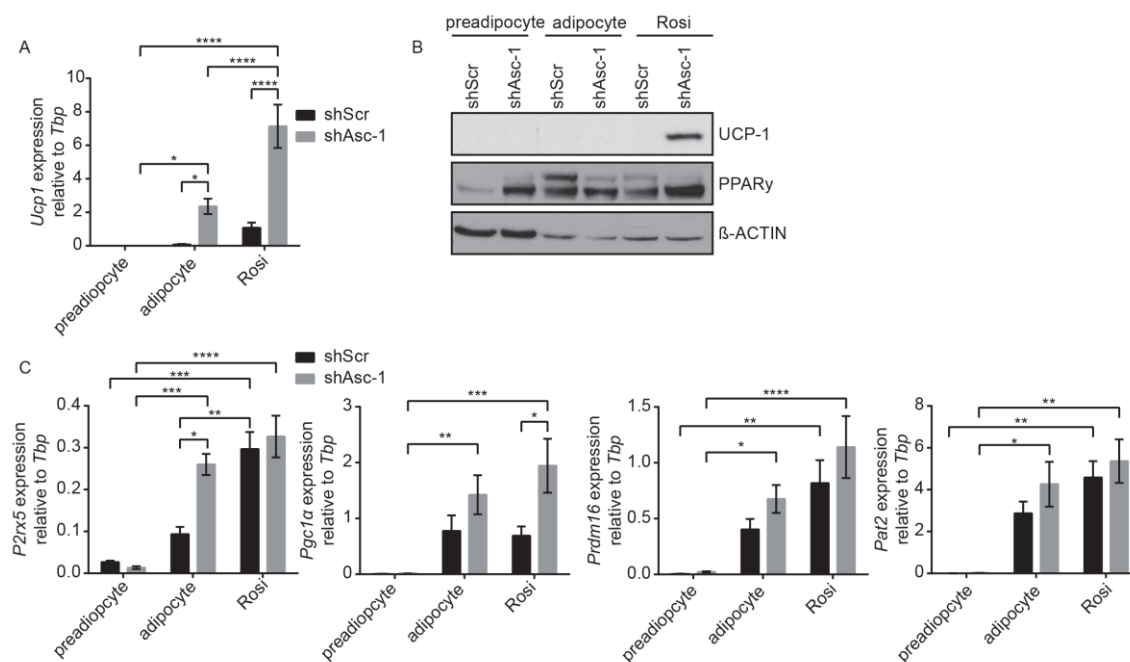


**Figure 6: Loss of ASC-1 increases brown adipocyte marker gene expression.** ShAsc-1 and shScr control preadipocytes were grown to 100 % confluence and RNA or protein was taken from the day of differentiation start (preadipocyte) and after 8 days of differentiation with (Rosi) or without rosiglitazone (adipocyte). (A) Relative gene expression of *Ucp1* (n=9-10). (B) Western blot of UCP1 (33 kDa), PPAR $\gamma$  (PPAR $\gamma$ 1 53 kDa, PPAR $\gamma$ 2 57 kDa) and  $\beta$ -ACTIN (42 kDa). (C) Relative gene expression of *P2rx5* (n=3), *Pgc1 $\alpha$*  (n=9), *Prdm16* (n=9) and *Pat2* (n=3). Data are represented as mean  $\pm$  SEM. Statistics were calculated using ordinary two-way ANOVA with Tukey's multiple comparison post-hoc test (\*\*\*\*P<0.0001, \*\*\* P<0.001, \*\* P<0.01, \* P<0.05).

mTOR (mammalian target of rapamycin), which can regulate differentiation, lipogenesis and function of white and brown adipocytes (Blomstrand et al., 2006; Liu et al., 2016). Regarding the drastic changes in the intracellular amino acid profile, it was investigated whether loss of ASC-1 affects beige adipocyte gene expression. In shScr cells, *Ucp1* was low expressed after differentiation, while shScr cells treated with rosiglitazone had increased *Ucp1* expression (**Figure 6A**). In contrast, shAsc-1 adipocytes expressed significantly higher *Ucp1* levels compared to shScr cells, especially when differentiated with rosiglitazone. On protein level, rosiglitazone treated shAsc-1 cells had a strong UCP1 signal which was not detectable in shScr control cells (**Figure 6B**). In addition to *Ucp1*, also *P2rx5* was significantly increased in differentiated shAsc-1 cells but did not further increase upon rosiglitazone treatment (**Figure 6C**). The beige adipocyte marker *Pgc1α* was not altered in normal differentiated, but significantly increased in rosiglitazone differentiated shAsc-1 compared to shScr cells. *Prdm16* as well as *Pat2*

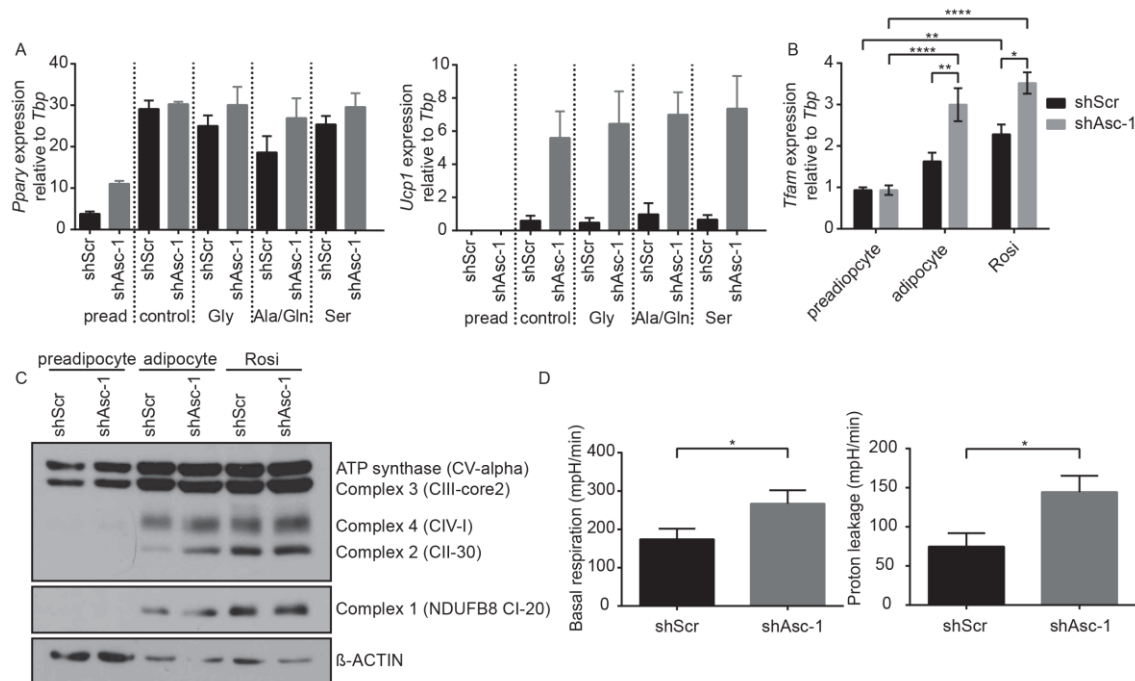


**Figure 7: Beige ASC-1 knockdown cells are functional beige adipocytes. (A)** ShAsc-1 and shScr control subcutaneous preadipocytes were grown to 100 % confluence and differentiation was induced with or without amino acids as indicated. RNA was taken from the day of differentiation start (pread) and after 8 days of differentiation. Relative gene expression of *Pparγ* and *Ucp1* (n=3). **(B)** Relative gene expression of *Tfam* after differentiation with (Rosi) or without rosiglitazone (adipocyte) (n=6). **(C)** Western blot of Oxphos mix (CV alpha (53 kDa), CIII-core 2 (47 kDa), CIV-I (39 kDa), CII-30 (30 kDa), NDUFB8 (20 kDa)), β-ACTIN (42 kDa). **(D)** Basal respiration and proton leakage calculated from the OCR measured by a Seahorse flux analyzer after differentiation with rosiglitazone (n=3). Data are represented as mean ± SEM. Statistics were calculated using t-test or ordinary two-way ANOVA with Tukey's multiple comparison post-hoc test (\*\*\*\*P<0.0001, \*\* P<0.01, \* P<0.05).



were slightly but not significantly increased in shAsc-1 compared to shScr cells. To further examine whether the changes in intra- and extracellular amino acids profiles were responsible for the beige phenotype of ASC-1 knockdown cells, preadipocytes were differentiated with or without the amino acids transported by ASC-1. A lack of cysteine in the medium resulted in apoptosis instead of differentiation (data not shown) due to a lack of the cysteine producing enzyme cystathionine beta synthase in preadipocytes. In contrast, depletion of glycine, alanine or serine did not alter the phenotype of shAsc-1 cells (**Figure 7A**), indicating that the effects on beiging are not caused by changes in the extracellular amino acid concentrations. In line with the increased expression of brown adipocyte genes, the mitochondrial marker *Tfam* was significantly increased in shAsc-1 compared to shScr adipocytes (**Figure 7B**) indicating an increase in mitochondrial mass. Western blot revealed elevated expression of complex 2 of the mitochondrial respiratory chain (**Figure 7C**) in differentiated shAsc-1 cells. Therefore, the functionality of beige shAsc-1 adipocytes was investigated using Seahorse measurements. Compared to shScr cells, shAsc-1 cells had a significantly higher mitochondrial basal respiration and proton leakage (**Figure 7D**), indicating that a loss of ASC-1 and its resulting changes in intracellular amino acid profile enhances beige over white adipocyte differentiation.

#### **4.1.2 Overexpression of ASC-1 reduces brown adipocyte gene expression in brown adipocytes**

A knockdown of ASC-1 in white preadipocytes resulted in beiging of the cells, suggesting that ASC-1 could be important in maintaining white adipocyte identity. To further test this hypothesis, it was investigated whether the system could be reversed. Therefore, it was examined whether a stable overexpression of ASC-1 in brown preadipocytes reduces brown adipocyte specific gene expression.

Immortalized brown preadipocytes were stable co-overexpressed with an HA-tagged ASC-1 and its co-receptor 4F2HC (**Figures 8A and B**). Control brown preadipocytes were overexpressed with GFP. Immunostainings of brown preadipocytes revealed that ASC-1-HA localized in undefined non- $\beta$ -actin containing membrane domains (**Figure 8C**). In mature adipocytes, ASC-1-HA was expressed on the cell surface. Similar to the knockdown of ASC-1 in subcutaneous white adipocytes, the overexpression of ASC-1 in brown preadipocytes had no effect on the differentiation, when cells were treated with rosiglitazone (**Figure 8D**). Though differentiation without

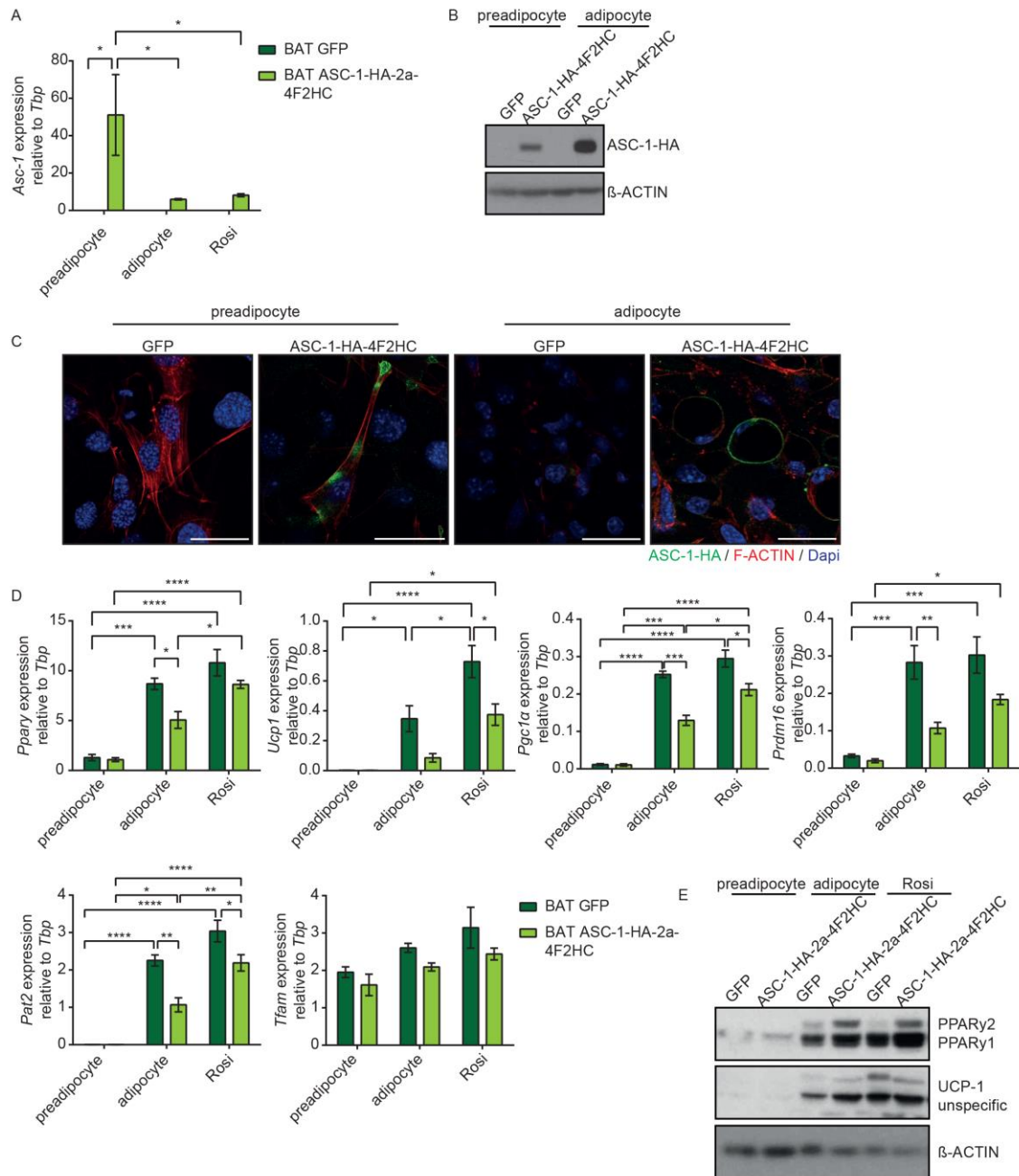


**Figure 8: Overexpression of ASC-1 in brown preadipocytes reduces brown adipocyte specific gene expression.** ASC-1-HA-2a-4F2HC or GFP overexpressing brown preadipocytes were grown to 100 % confluence and RNA or protein was taken from the day of differentiation start (preadipocyte) and after 8 days of differentiation with (Rosi) or without rosiglitazone (adipocyte). **(A)** Relative gene expression of *Asc-1* (n=3). **(B)** Western Blot of ASC-1-HA (45 kDa) and  $\beta$ -ACTIN (42 kDa). **(C)** Immunofluorescence staining before and after differentiation. Green: ASC-1-HA. Red: F-ACTIN. Blue: Dapi. Size bar represents 30  $\mu$ m. **(D)** Relative gene expression of *Ppar*, *Ucp1*, *Pgc1a*, *Prdm16*, *Pat2* and *Tfam* (n=3). **(E)** Western blot of PPARy (PPARy1 53 kDa, PPARy2 57 kDa), UCP1 (33 kDa), and  $\beta$ -ACTIN (42 kDa). Data are represented as mean  $\pm$  SEM. Statistics were calculated using ordinary two-way ANOVA with Tukey's or Sidak's (for *Pgc1a*) multiple comparison post-hoc test (\*\*\*\*P<0.0001, \*\*\* P<0.001, \*\* P<0.01, \* P<0.05). Figures B and C were already published as Bachelor's Thesis (Christina Lindner, Characterization of ASC-1 in brown adipocytes, 2017).

rosiglitazone lead to a significant reduction of *Pparγ* expression on RNA level, PPAR $\gamma$  protein was not impaired (**Figure 8E**). Interestingly, overexpression of ASC-1 increased PPAR $\gamma$ 2 expression compared to GFP control adipocytes, while PPAR $\gamma$ 1 was not altered. In contrast to the phenotype observed in subcutaneous ASC-1 knockdown cells, ASC-1 overexpression in brown preadipocytes significantly reduced gene expression of *Ucp1*, *Pgc1 $\alpha$* , *Prdm16* and *Pat2*, while *Tfam* was slightly but not significantly reduced compared to GFP control cells (**Figure 8D**). Thus, loss or gain of ASC-1 can affect white or brown adipocyte identity.

#### 4.1.3 Depletion of ASC-1 re-programs preadipocytes resulting in spontaneous differentiation into beige adipocytes

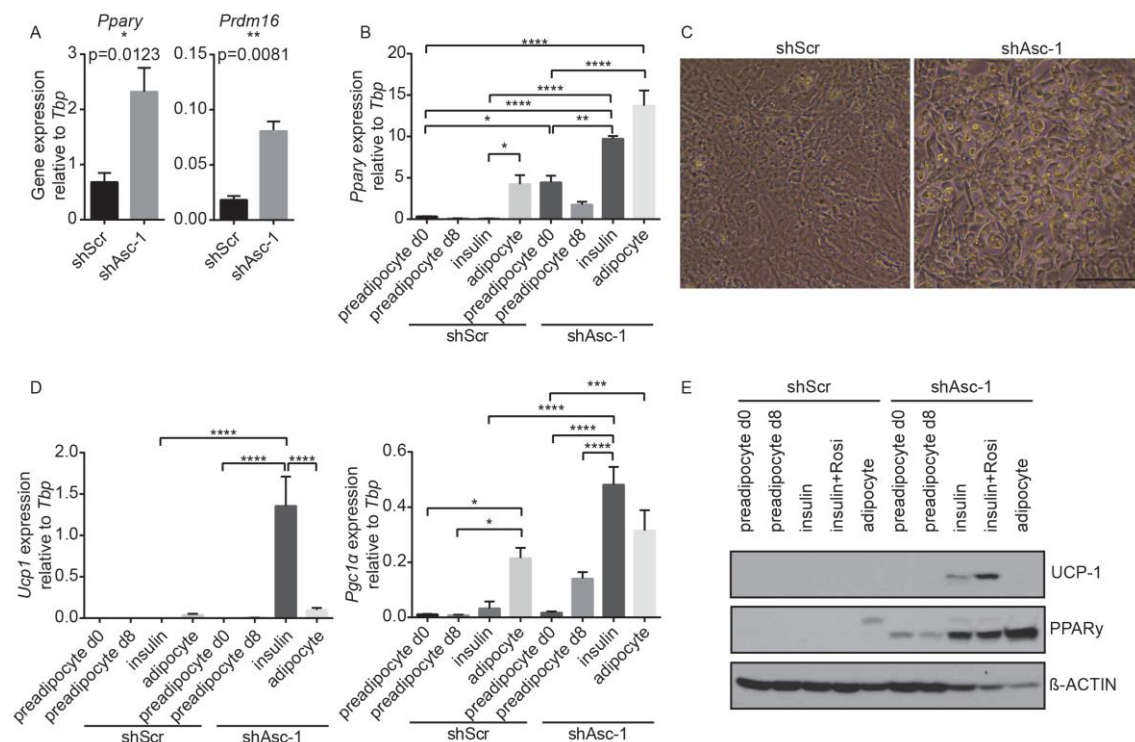


**Figure 9: Knockdown of ASC-1 results in spontaneous differentiation.** (A) Relative gene expression of *Pparγ* and *Prdm16* of proliferating ASC-1 underexpressing and scrambled control subcutaneous preadipocytes (n=4). (B, D) Preadipocytes were grown to 100 % confluence and differentiation was induced. RNA or protein was taken from the day of differentiation start (preadipocyte d0) and after 8 days (preadipocyte d8) as well as after 8 days of insulin treatment (insulin), insulin and rosiglitazone treatment (insulin+rosi) or differentiation (adipocyte). Relative gene expression of *Pparγ* (n=3), *Ucp1* (n=3-6), *Pgc1 $\alpha$*  (n=4-6) and *Prdm16* (n=4-6). (C) Preadipocytes were seeded with insulin and after 3 days, images were taken. Size bar represents 100  $\mu$ m. (E) Western Blot of UCP1 (33 kDa), PPAR $\gamma$  (PPAR $\gamma$ 1 53 kDa, PPAR $\gamma$ 2 57 kDa) and  $\beta$ -ACTIN (42 kDa). Data are represented as mean  $\pm$  SEM. Statistics were calculated using t-test or ordinary two-way ANOVA with Tukey's multiple comparison post-hoc test (\*\*\*\*P<0.0001, \*\*\* P<0.001, \*\* P<0.01, \* P<0.05).

As already seen in figure 5B, confluent shAsc-1 preadipocytes had higher PPAR $\gamma$  protein expression than shScr control cells. In addition, proliferating non-confluent shAsc-1 preadipocytes had significant higher RNA levels of *Ppar $\gamma$*  and *Prdm16* (Figure 9A). As PPAR $\gamma$  is a key regulator of adipocyte differentiation and together with PRDM16 induces browning (Ohno et al., 2012), it was tested whether shAsc-1 preadipocytes can differentiate spontaneously into mature adipocytes. Therefore, cells were grown to confluence and incubated for 8 additional days with either normal growth medium, with growth medium containing insulin, or with a differentiation induction mix containing IBMX, dexamethasone and insulin. As expected, shScr control cells only expressed *Ppar $\gamma$*  after induction with the whole differentiation mix (Figure 9B and E). In contrast, shAsc-1 preadipocytes expressed similar amounts of *Ppar $\gamma$*  than the differentiated shScr control adipocytes and *Ppar $\gamma$*  expression significantly increased after the addition of insulin. With the differentiation cocktail, *Ppar $\gamma$*  expression further increased, but was not significantly different to the insulin treated adipocytes. The spontaneous differentiation and accumulation of lipid droplets in the shAsc-1 cells was also visible by eye after 3 days of insulin treatment (**Figure 9C**). In line with the previous findings, *Ucp1* expression was low in shScr adipocytes, and not significantly altered in normal differentiated shAsc-1 cells (**Figure 9D and E**). When shAsc-1 preadipocytes were incubated only with insulin, *Ucp1* expression was significantly higher than in normal differentiated cells. On protein level, UCP1 expression was further increased with the addition of rosiglitazone to the insulin containing medium. According to this observation, insulin was sufficient to significantly increase *Pgc1 $\alpha$*  (**Figure 9D**) and *Prdm16* expression (data not shown). This demonstrates that a knockdown of ASC-1 alters the characteristics of preadipocytes, leading to increased expression of adipocyte markers and spontaneous differentiation.

#### **4.1.4 Being of ASC-1 knockdown cells could be caused by accumulation of intracellular D-serine**

To investigate whether the effects on being are directly mediated by the loss of ASC-1 rather than by off-target effects induced by the shRNA, preadipocytes were differentiated with 10  $\mu$ M of the ASC-1 inhibitor BMS-466442 (Brown et al., 2014) from the day of differentiation start until the fulfilled differentiation after 8 days. Cells differentiated normally to mature adipocytes, as indicated by expression of *Ppar $\gamma$*  (**Figure 10A**). However, neither *Ucp1*, nor *Prdm16* or *Pgc1 $\alpha$*  were altered after differentiation with the inhibitor. When cells were treated with the ASC-1 inhibitor 2

days before reaching confluency and throughout the differentiation phase, again no differences in the differentiation capacity were observed (**Figure 10B**). After differentiation, *Ucp1* was slightly but not significantly elevated in inhibitor treated cells whereas there was a significant increase in the expression of *Prdm16* and *Pgc1 $\alpha$*  in inhibitor treated cells compared to DMSO controls. In contrast, there were no differences in gene expression of *Ppar $\gamma$* , *Ucp1*, *Prdm16* or *Pgc1 $\alpha$*  in confluent preadipocytes after 2 days of ASC-1 inhibitor treatment (**Figure 10B; preadipocytes**). These findings reveal that early inhibition of ASC-1 has no impact on preadipocyte gene expression itself but may re-program the proliferating preadipocyte to become a beige adipocyte, and that this re-programming occurs before reaching confluency.

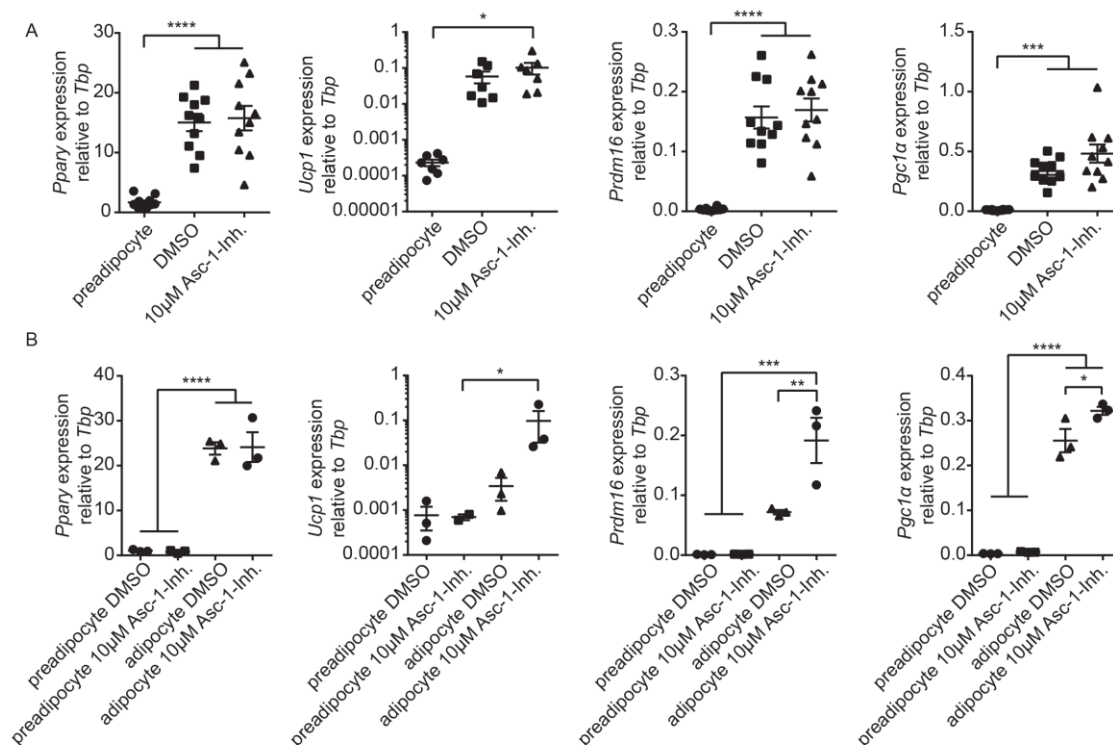


**Figure 10: Early chemical inhibition of ASC-1 induces beige adipocyte differentiation.** Scrambled control subcutaneous preadipocytes were seeded without (A) or with (B) 10  $\mu$ M ASC-1-Inhibitor (BMS-466442) or DMSO as control. After 2 days, when cells reached 100% confluency, differentiation was induced with ASC-1 inhibitor or DMSO. (A) Relative gene expression of *Ppar $\gamma$*  (n=10), *Ucp1* (n=7), *Prdm16* (n=10) and *Pgc1 $\alpha$*  (n=10). (B) Relative gene expression of *Ppar $\gamma$* , *Ucp1*, *Prdm16* and *Pgc1 $\alpha$*  (n=3). Data are represented as mean  $\pm$  SEM. Statistics were calculated using ordinary two-way ANOVA with Tukey's multiple comparison post-hoc test (\*\*\*\*P<0.0001, \*\*\* P<0.001, \*\* P<0.01, \* P<0.05).

To address the question why ASC-1 predominantly acts in preadipocytes, where it only is expressed at low levels, single cell clones of immortalized subcutaneous preadipocytes were picked and investigated regarding their expression of *Asc-1*. At

the same time, the expression of *Pparg* was examined, as previous experiments showed a reciprocal correlation between *Asc-1* and *Pparg* in preadipocytes. Upon 52 examined single cell clones, there were 3 clones with very high *Asc-1* and low *Pparg*

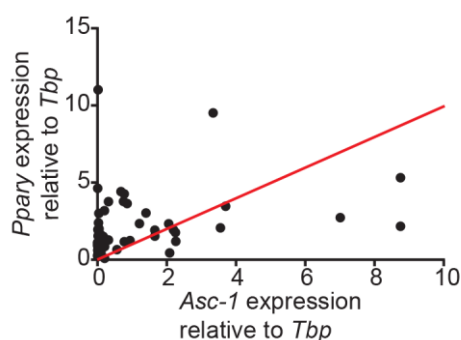


**Figure 11: *Asc-1* is differently expressed in subcutaneous single cell clones.** Correlation between expression of *Pparg* and *Asc-1* of undifferentiated subcutaneous single cell clones.

expression (**Figure 11**). These findings show that the stromal vascular fraction of SCF is heterogeneous and consists of several different adipocyte precursor cells.

As shown before, amino acids were altered in mature shAsc-1 cells. Therefore, next the amino acid profile of preadipocytes was investigated, hypothesizing that intracellular amino acid changes could be responsible for the beige phenotype and the spontaneous differentiation of shAsc-1 cells. In confluent preadipocytes, the intracellular amino acid profile was altered (**Figure 12A**). In addition to alanine, glycine and serine, which can be transported by ASC-1, also intracellular levels of proline, threonine and aspartate were reduced. In the medium, no changes were observed (**Figure 12A**). In cells, various amino acid transporters exist, which makes the results difficult to interpret. Therefore, the focus was set on D-serine, which only can be transported by ASC-1 with high affinity. Intra- and extracellular D-serine levels were measured in proliferating, subconfluent as well as in confluent preadipocytes. Intracellular D-serine concentrations were drastically increased in subconfluent shAsc-1 compared to shScr preadipocytes (**Figure 12B**). After becoming confluent, D-serine levels were reduced to normal. In the medium, D-serine levels were reduced both, in subconfluent and confluent shAsc-1 cells due to reduced secretion of D-serine by ASC-1. Interestingly, the D-serine producing enzyme *Srr* was reduced in both cell lines after reaching confluency, but no difference was observed between shAsc-1 and shScr cells (**Figure 12C**). In contrast, the D-serine degrading enzyme *Dao* was not significantly but slightly increased in confluent shAsc-1 compared to control preadipocytes.

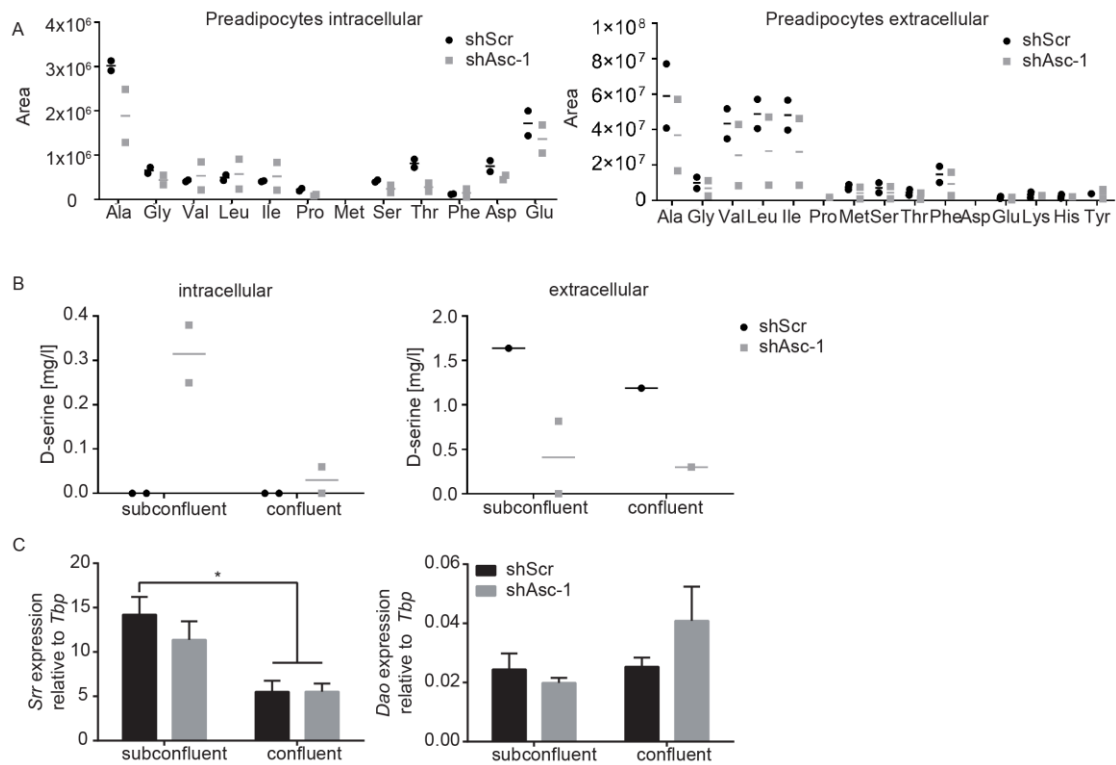


**Figure 12: Knockdown of ASC-1 alters intracellular amino acid profile of preadipocytes.** (A) Intra- and extracellular free amino acids of confluent preadipocytes (n=2). (B) Intra- and extracellular D-serine levels of subconfluent and confluent preadipocytes (n=1-2). (C) Expression of *Srr* (n=3-4) and *Dao* (n=3-4) in subconfluent and confluent preadipocytes. Data are represented as mean or as mean ± SEM (for *Srr* and *Dao*). Statistics were calculated using ordinary two-way ANOVA with Tukey's or Sidak's (for *Dao*) multiple comparison post-hoc test (\* P<0.05).

To further test whether accumulating D-serine is responsible for the beige phenotype of subcutaneous ASC-1 knockdown cells, brown ASC-1 overexpressing preadipocytes were differentiated with different concentrations of D-serine from the day of differentiation start (08) or two days before the start of differentiation (-28) (**Figure 13**). D-serine had no effect on the differentiation capacity or the expression of its transporter *Asc-1*. In addition, treatment with D-serine was not able to normalize *Ucp1* expression in the ASC-1 overexpressing cells.

In conclusion, these *in vitro* findings suggest that a loss of ASC-1 re-programs proliferating preadipocytes before reaching confluency. This could be caused either by changes of intracellular amino acids like D-serine that only can be transported by ASC-1, or by changes in the whole amino acid profile due to an imbalance of amino acids transported by ASC-1.

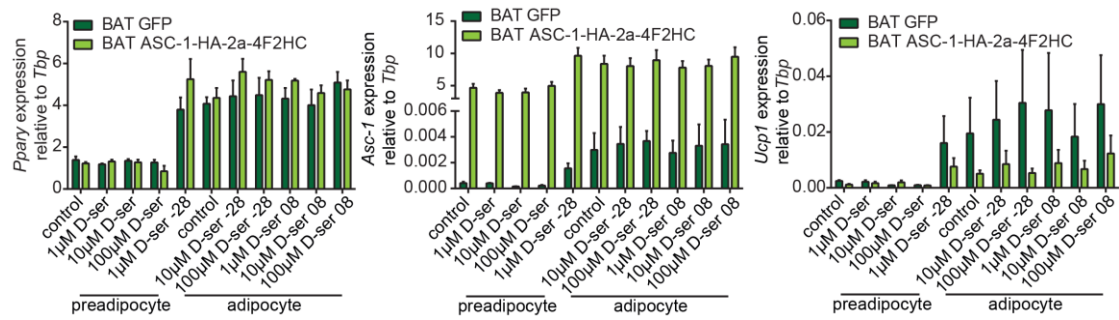


**Figure 13: Extracellular D-serine does not alter brown adipocyte identity.** Relative gene expression of *Pparγ*, *Asc-1* and *Ucp1* of ASC-1-HA-2a-4F2HC or GFP overexpressing brown adipocytes differentiated with or without 1, 10 or 100  $\mu$ M D-serine 2 days before or from the day of differentiation on (n=3). Data are represented as mean  $\pm$  SEM.

#### 4.1.5 Whole body loss of ASC-1 results in hepatosteatosis and reduced UCP1 expression in BAT

ASC-1 whole body knockout mice die 3 weeks after birth due to severe effects in the brain (Xie et al., 2005). Hence, two week old ASC-1 knockout mice were studied to validate the *in vitro* findings. As published before (Rutter et al., 2007), a whole body

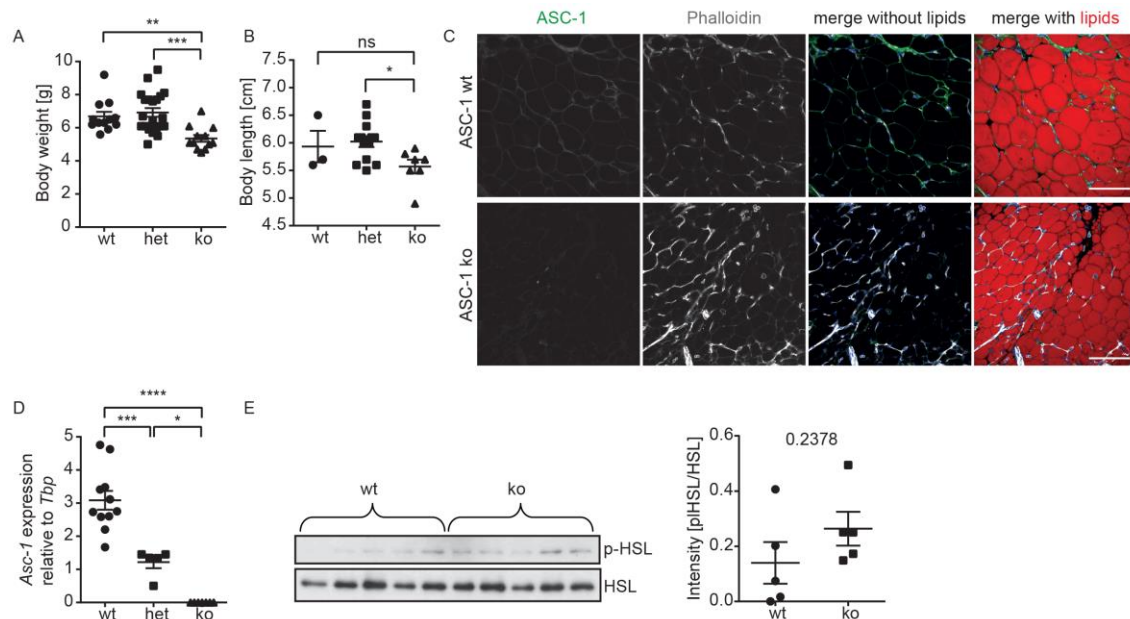


**Figure 14: Whole body ASC-1 knockout mice have smaller adipocytes in SCF.** (A) Body weight of 2 week old ASC-1 wt, het and ko mice (n=12-21). (B) Body length of 2 week old ASC-1 wt, het and ko mice (n=3-13). (C) Immunofluorescence staining of ASC-1 in SCF of 2 week old ASC-1 wt and ko mice. Size bar represents 100  $\mu$ m. (D) *Asc-1* expression in subcutaneous adipose tissue of 2 week old ASC-1 wt, het and ko mice (n=5-11). (E) Western Blot and quantification of SCF 1 week old ASC-1 wt and ko mice on p-HSL (82 kDa) and total HSL (82 kDa). Data are represented as mean  $\pm$  SEM. Statistics were calculated using ordinary one-way ANOVA with Tukey's multiple comparison post-hoc test (\*\*\*\*P<0.0001, \*\*\*P<0.001, \*\*P<0.01, \*P<0.05).



knockout of ASC-1 resulted in reduced body weight (**Figure 14A**) due to smaller body size (**Figure 14B**). In the subcutaneous adipose tissue, ASC-1 mRNA and protein was diminished in 2 weeks old mice (**Figure 14C and D**), confirming the knockout. In the SCF of ASC-1 knockout mice, adipocyte size and lipid droplets appeared smaller than in wildtype littermates. Therefore, phosphorylation of the lipolysis inducing protein HSL was investigated, but no changes were observed in SCF (**Figure 14E**). H&E stainings confirmed that adipocytes in SCF were smaller in ko compared to wt animals, mainly due to accumulation of beige adipocytes as shown in the UCP1 staining (**Figure 15A**). The smaller cell size matched the reduced SCF tissue mass (**Figure 15B**). Investigation of RNA levels in SCF revealed that *Ppar $\gamma$*  expression was not altered (**Figure 15C**) and, against expectancy, UCP1 expression in SCF was not increased in ASC-1 ko mice. Also *Pgc1 $\alpha$* , *Prdm16*, *Pat2*, *P2rx5* and *Tfam* were expressed at the same level in ASC-1 wt, het and ko mice (**Figure 15C**). In contrast to SCF, BAT morphology was comparable between ASC-1wt and ko mice (**Figure 15A**) and BAT weight was not altered in ASC-1 ko mice (**Figure 15B**). Interestingly, UCP1 expression was decreased in BAT on protein (**Figure 15A**) and RNA (**Figure 15C**) level in ASC-1 ko compared to wt animals. While *Ppar $\gamma$* , *Pgc1 $\alpha$* , *Prdm16*, *Pat2* and *P2rx5* were not altered, *Tfam* was reduced in BAT of ASC-1 ko animals (**Figure 15C**). In line with reduced *Tfam* and *Ucp1* expression in brown adipose tissue of ASC-1 ko animals, also rectal body temperature was significantly reduced, suggesting a severe effect on BAT function in ASC-1 ko mice (**Figure 15D**). Although body weight was reduced, liver weight remained the same in ASC-1 ko compared to wt mice, which was due to a significant increase in liver triglycerides (**Figure 15A, B and E**). In addition, ASC-1 ko animals had reduced levels of blood glucose (**Figure 15F**), which could be explained by muscle contractions caused by seizures and tremors (Xie et al., 2005). Due to those severe effects on whole body metabolism, it is difficult to evaluate data concerning the role of ASC-1 in adipose tissue. Therefore, 8 week old wt and het animals were challenged with chow (CD) or a 58 % high fat diet (HFD) for 13 weeks. Though ASC-1 het animals fed a HFD gained more weight than wt animals, the differences were not significant (**Figure 16A**). According to this, fat depot and liver weight of male mice were only significant different between CD and HFD fed animals, but not between genotypes (**Figure 16B**). Liver triglyceride content was significantly increased after HFD feeding, but not altered between genotypes (**Figure 16C**), indicating that liver steatosis of young ASC-1 ko mice was a result of problems in

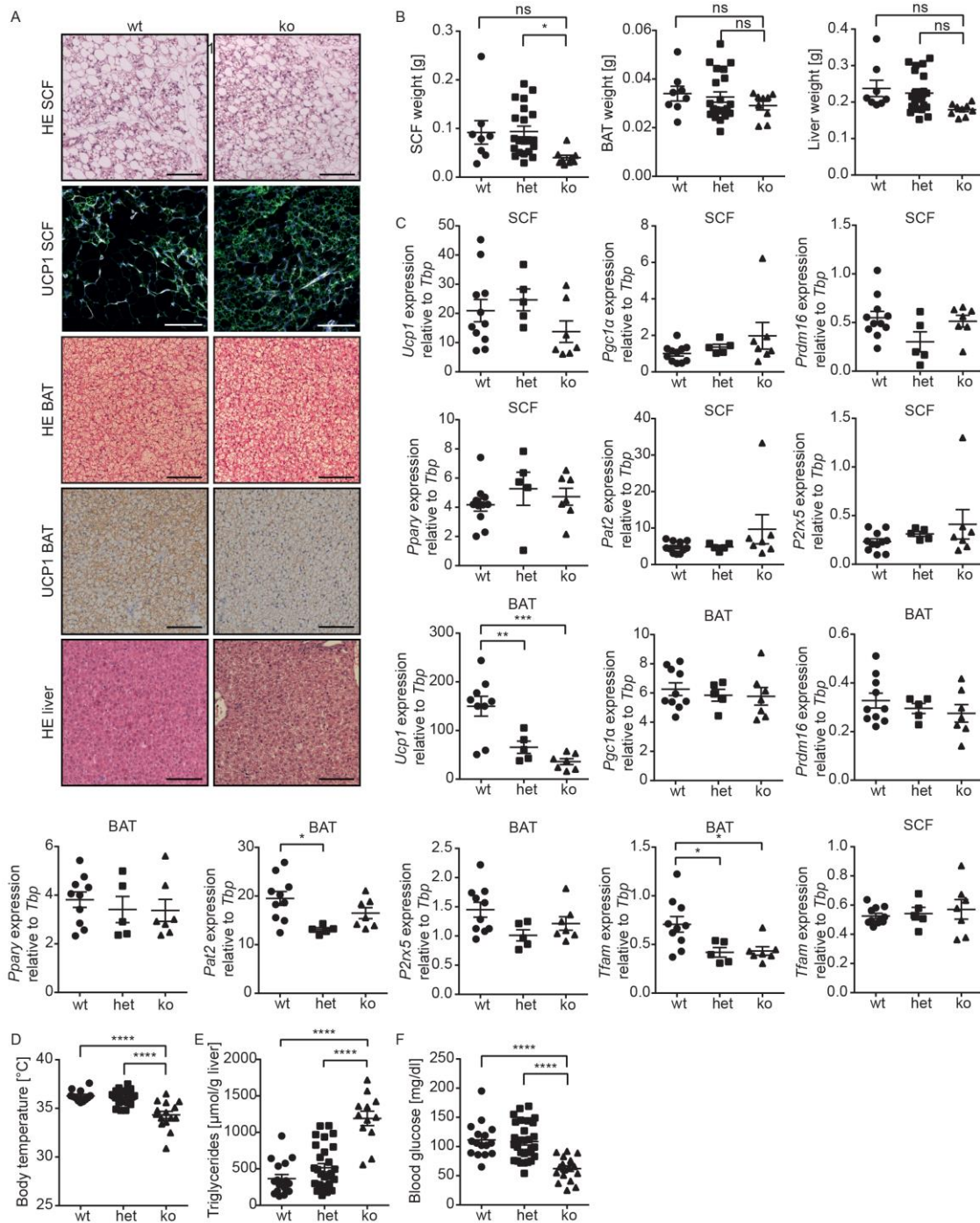


**Figure 15: Global loss of ASC-1 induces hepatosteatosis and reduces UCP1 in BAT. (A)** Histology of SCF, BAT and liver of 2 week old ASC-1 wt and ko mice. Immunostaining for UCP1 in SCF: green: UCP1, white: F-ACTIN, blue: DAPI. Size bars represent 100 μm. **(B)** Tissue weight of 2 week old ASC-1 wt, het and ko mice (n=8-21). **(C)** *Ucp1*, *Pgc1α*, *Prdm16*, *Pparγ*, *Pat2*, *P2rx5* and *Tfam* expression in SCF and BAT of 2 week old ASC-1 wt, het and ko mice (n=5-11). **(D)** Rectal body temperature (n=12-30), **(E)** liver triglyceride content (n=12-28) and **(F)** blood glucose of 2 week old ASC-1 wt, het and ko mice (n=16-29). Data are represented as mean ± SEM. Statistics were calculated using ordinary one-way ANOVA with Tukey's multiple comparison post-hoc test (\*\*\*\*P<0.0001, \*\*\* P<0.001, \*\* P<0.01, \* P<0.05).

whole body metabolism. On HFD, rectal body temperature was unaltered in both genders (**Figure 16D**) and on both diets. *Ucp1* was expressed equally in BAT and SCF (**Figure 16E**). Neither random fed blood glucose nor plasma insulin levels were altered in ASC-1 het mice (**Figure 16F and G**). After 11 weeks of HFD feeding, ASC-1 het and wt mice were glucose intolerant compared to CD fed mice, but no changes between genotypes were observed (**Figure 16H**). According to this, insulin tolerance was not altered in het mice (**Figure 16I**). In summary, ASC-1 het mice did not differ from wt animals independent of the diet. This suggests that ASC-1 het animals can compensate the loss of *Asc-1* in one allele.

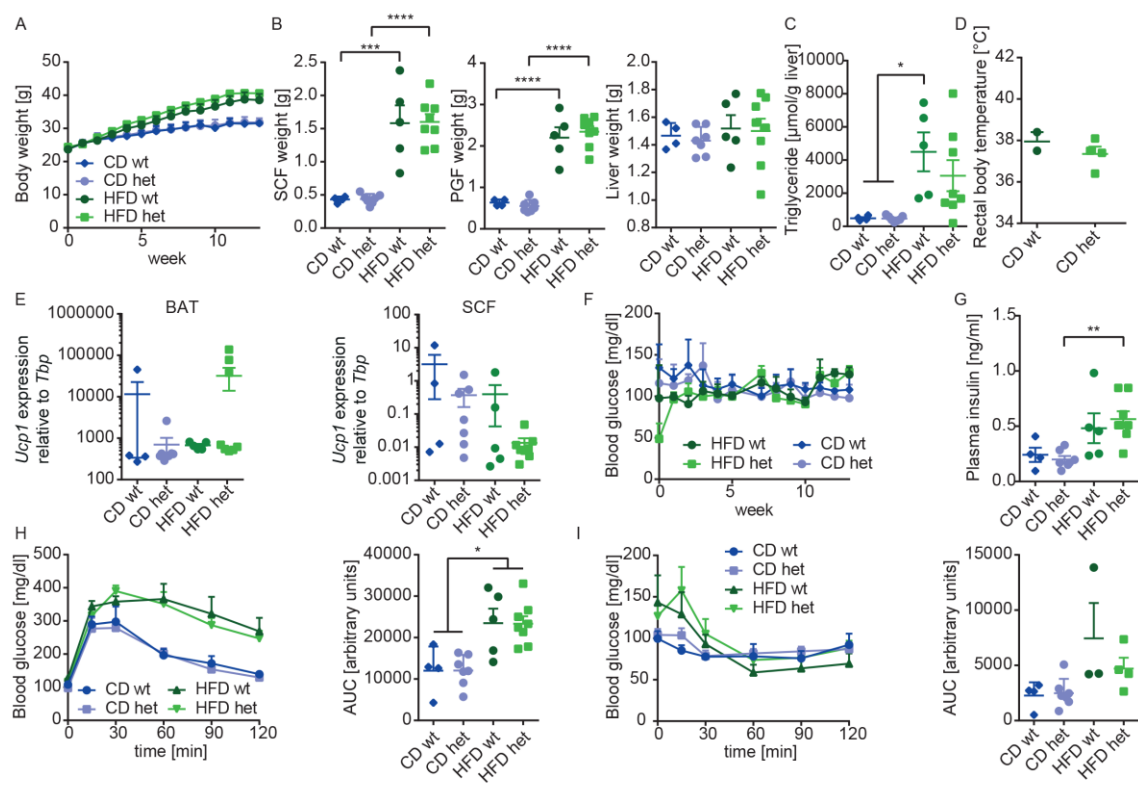


**Figure 16: Heterozygous ASC-1 ko mice develop normal upon CD and HFD feeding.** Male het and wt ASC-1 ko mice were fed a CD or HFD for 13 weeks from an age of 8 weeks on. **(A)** Body weight of 21 week old ASC-1 wt and het mice during CD or HFD feeding (n=4-8). **(B)** SCF, PGF and liver weight of male ASC-1 wt and het mice (n=4-8). **(C)** Liver triglyceride content after 13 weeks of CD or HFD feeding (n=4-8). **(D)** Rectal body temperature of 9 week old ASC-1 wt and het mice (n=2-4). **(E)** Relative *Ucp1* expression in BAT and SCF after 13 weeks of CD or HFD feeding (n=4-8). **(F)** Random fed blood glucose during 13 weeks of CD or HFD feeding (n=4-8). **(G)** Plasma insulin level after 13 weeks of CD or HFD feeding (n=4-8). **(H)** GTT of ASC-1 wt and het mice after 12 weeks of CD or HFD feeding (n=4-8). **(I)** ITT of ASC-1 wt and het mice after 12 weeks of CD or HFD feeding (n=4-8). Data are represented as mean  $\pm$  SEM. Statistics were calculated using ordinary one- or two-way ANOVA with Tukey's multiple comparison post-hoc test (\*\*\*\*P<0.0001, \*\*\* P<0.001, \*\* P<0.01, \* P<0.05).

## **4.2 D-serine regulates insulin secretion and weight gain**

Another aim of this part was to investigate the effects of D-serine supplementation on whole body metabolism, which so far is unknown even though it is used in clinical trials to treat the symptoms of schizophrenia. It further was investigated whether D-serine has an impact on WAT being *in vivo*. Parts of this chapter already were published recently (Suwandhi et al., 2018).

### **4.2.1 D-serine supplementation ameliorates diet induced obesity and preference to HFD**

To investigate the distribution of oral supplemented D-serine, eight week old mice were gavaged with D-serine and sacrificed after 15, 30, 60, 120, 240 and 360 minutes. D-serine levels were assessed in serum, liver, kidney, brain, and perigonadal adipose tissue (PGF) (**Figure 17A**). D-serine rapidly appeared in plasma with peak concentrations 15 minutes after gavage. Highest tissue levels of D-serine were found in kidneys, peaking within 30 minutes and supporting previous data demonstrating preferential clearance of D-serine via the kidneys (Rais et al., 2012). Moreover, Matrix-assisted laser desorption/ionization Fourier-transform ion cyclotron resonance mass spectrometry imaging (MALDI FT-ICR MSI) revealed that <sup>13</sup>C-labeled D-serine accumulated in the proximal tubules one hour after gavage (**Figure 17B**). Rapid uptake of D-serine was also observed within 15 minutes, albeit with much lower amplitude, in PGF and within 60 minutes in the liver (**Figure 17A**). In contrast, D-serine was detectable in brain homogenates at baseline, but its levels did not significantly increase upon exogenous administration, indicating a slow uptake into or a quick clearance in the brain. Tissue concentrations of D-serine returned to baseline within six hours. To investigate the long-term metabolic effects of D-serine supplementation, four week old male C57BL/6 mice were either fed a regular chow diet (CD) or a high fat diet (HFD; 58% calories from fat) with or without supplementation of 1 % D-serine in the drinking water for eight weeks. After six weeks, food-intake was similar between the groups with a tendency of reduced food intake in HFD + D-serine animals compared to HFD control mice during night (**Figure 17C**). In line with that, water intake was not altered between D-serine and control animals. Though, as HFD fed animals consumed less amount of food in gram, those animals had reduced water intake and in turn also a reduced D-serine exposure

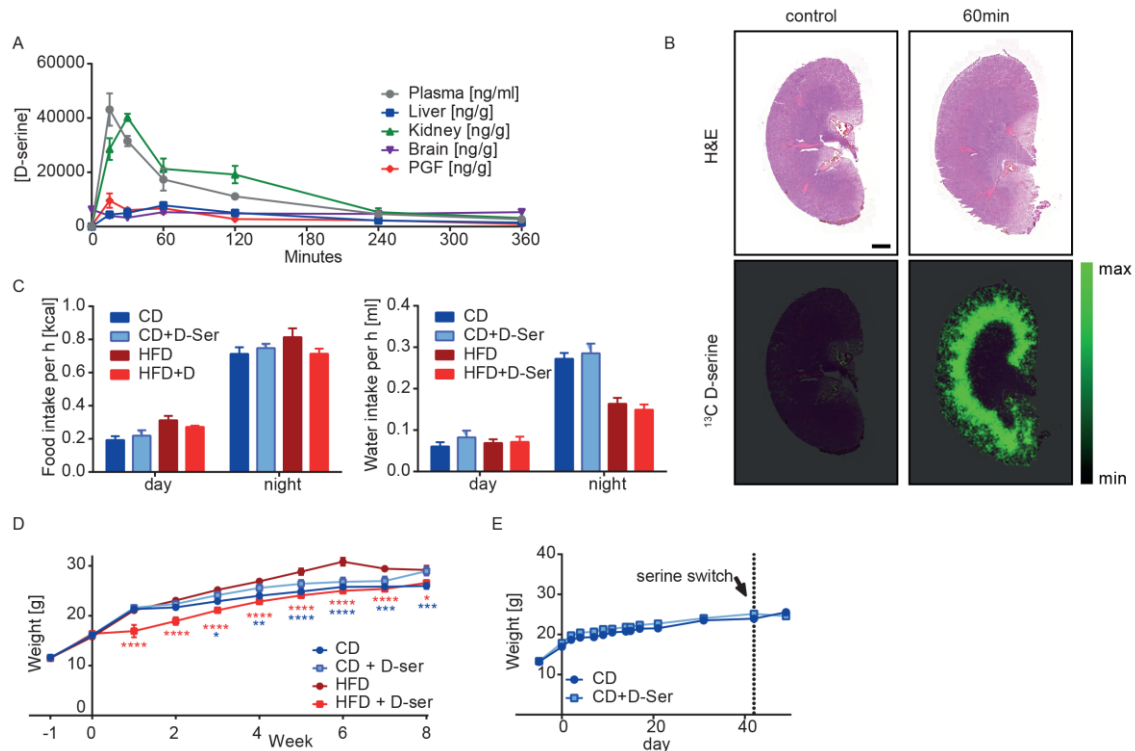


**Figure 17: Oral administered D-serine is taken up by various organs.** (A) 8 week old C57BL/6 mice were gavaged with 100 mg/kg body weight D-serine or saline as controls. Groups of four mice were sacrificed 15, 30, 60, 120, 240, and 360 minutes after administration and D-serine concentrations were measured by mass spectrometry. Mice gavaged with saline were used as controls and shown as time 0. (B) 4 week old C57BL/6 mice were gavaged with 10 mg/kg  $^{13}\text{C}$ -labeled D-serine ( $m/z$  105.037 [M-H]) and sacrificed after 60 minutes. Kidneys were prepared for MALDI FT-ICR MSI and stained with H&E. As negative control, animals were gavaged with water. Size bar represents 1mm. (C) 4 week old C57BL/6 mice were fed a CD or HFD, and drinking water was supplemented with or without 10 g/l D-serine. Food and water intake per hour after 6 weeks of D-serine supplementation. (D) Body weight curves over 8 weeks of serine supplementation ( $n=7-8$ ). (E) Body weight before and after serine switch ( $n=5$ ). Data are represented as mean  $\pm$  SEM. Statistics were calculated using ordinary one-way ANOVA with Tukey's or Sidak's (for water intake and serine switch) multiple comparison post-hoc test (\*\*\*\* $P<0.0001$ , \*\*\*  $P<0.001$ , \*\*  $P<0.01$ , \*  $P<0.05$ ).

compared to CD fed animals. In CD fed mice, D-serine supplementation did not result in statistically significant alterations in body weight gain (**Figure 17D**) although a continuous trend to higher body weight was observed in D-serine supplemented mice. This trend was reversed by changing the water supplementation of the groups (**Figure 17E**), indicating a small but biologically significant effect of D-serine on weight gain upon CD feeding. In contrast, mice fed HFD + D-serine showed a strongly reduced weight gain during the first week of supplementation. Afterwards, weight gain paralleled HFD fed mice, but HFD + D-serine mice did not catch up weight and after 8 weeks on diet, HFD + D-serine fed mice had the same weight as CD control animals (**Figure 17D**). Assessment of body composition after two and

eight weeks of treatment revealed that the reduced body weight of HFD + D-serine fed mice was primarily due to decreased fat mass (**Figure 18A**), which was also reflected by reduced SCF, PGF, and BAT mass (**Figure 18B**). HFD + D-serine fed mice also showed a small but significant decrease in lean mass compared to controls (**Figure 18A**), albeit body length was the same in all D-serine supplemented mice compared to controls at the end of the study (**Figure 18C**). Nevertheless, HFD control animals had a significant increased body length compared to CD animals.

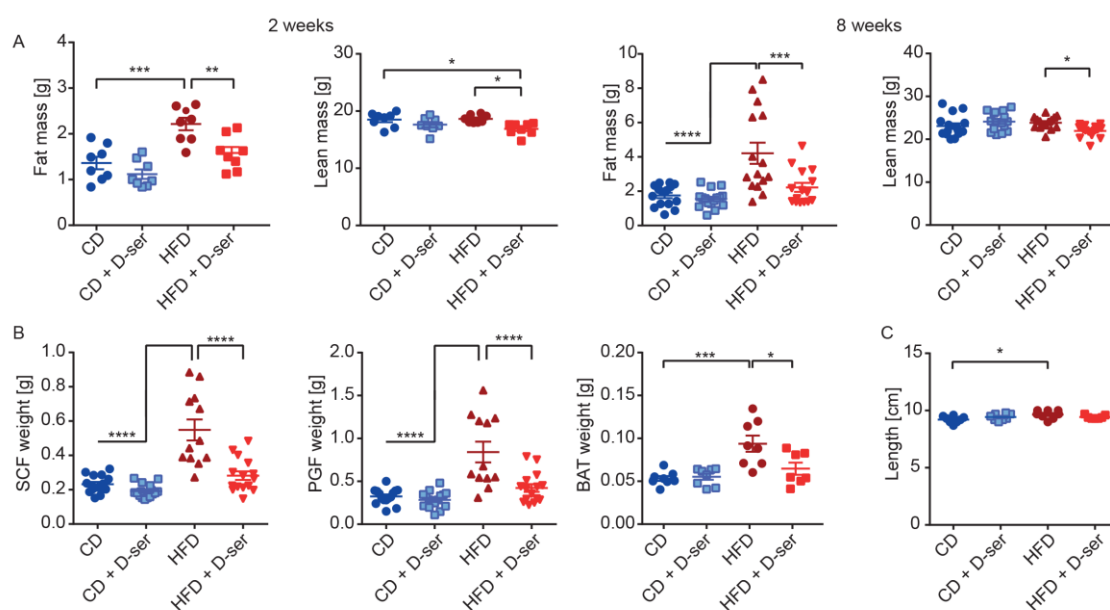


**Figure 18: D-serine prevents from diet induced obesity.** (A) Body composition after 2 and 8 weeks of serine supplementation. (B) Fat pad weight after 8 weeks of D-serine supplementation. (C) Body length of 12 week old C57BL/6 mice after feeding a CD or HFD and supplementation with 10 g/l D-serine in drinking water for 8 weeks. Data are shown as mean  $\pm$  SEM. Statistics were calculated using ordinary one- or two-way ANOVA with Tukey's multiple comparison post-hoc test (\*\*\*\* $P < 0.0001$ , \*\*\*  $P < 0.001$ , \*\*  $P < 0.01$ , \*  $P < 0.05$ ).

After six weeks of D-serine supplementation, neither substrate utilization (RER) nor energy expenditure were altered in HFD + D-serine compared to control animals (**Figure 19A**). On CD, animals had increased energy expenditure during the night. Moreover, nocturnal activity was reduced in both diet groups supplemented with D-serine after six weeks on treatment. Therefore, the observed reduction in body weight of HFD + D-serine animals most likely resulted from reduced food consumption during the first week (**Figure 19B**) and a continued trend throughout the whole study (**Figure 17C**). To test if age or a history of HFD feeding have an impact on the effects of D-serine, six week old mice were fed a HFD diet for eight weeks prior to supplementation with D-serine. After the establishment of diet induced obesity, D-serine was added to the drinking water of one group (**Figure 19C-D**). D-serine supplementation reduced food intake (**Figure 19C**) and weight gain (**Figure**

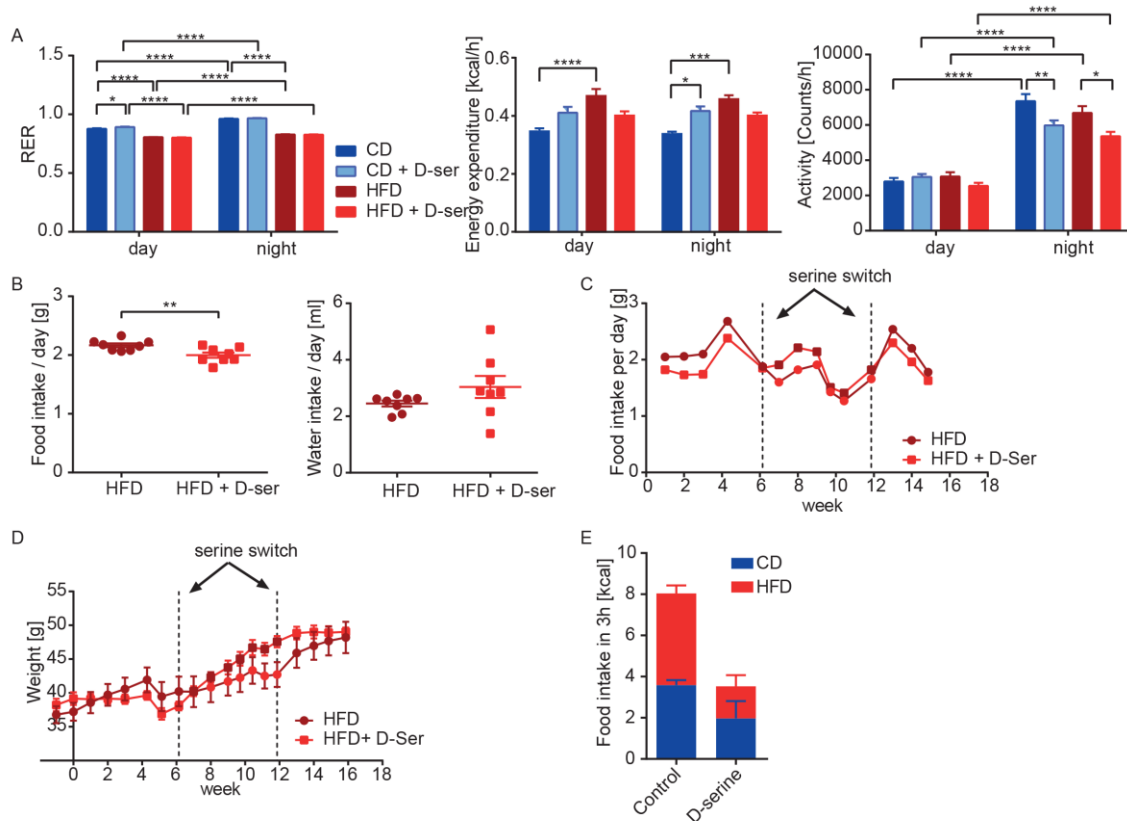


**Figure 19: D-serine reduces high fat diet food intake.** (A) Metabolic activity of 10 week old C57BL/6 mice after D-serine supplementation for 6 weeks (n= 5-6). (B) Food and water intake per day during the first week of serine supplementation upon HFD feeding. (C) Daily food intake and (D) weight gain of obese mice during 15 weeks of serine supplementation on HFD (n=4). After 6 and 12 weeks, the water bottles were switched. (E) Food preference test after 4 weeks of D-serine supplementation. Mice were fasted over-night and refed with CD and HFD for 3 hours. Data are shown as mean  $\pm$  SEM. Statistics were calculated using t-test or ordinary two-way ANOVA with Tukey's or Sidak's (for locomotor activity) multiple comparison post-hoc test (\*\*\*\* $P < 0.0001$ , \*\*\* $P < 0.001$ , \*\* $P < 0.01$ , \* $P < 0.05$ ).

**19D).** Moreover, switching D-serine supplementation between control and D-serine supplemented mice rapidly reversed weight gain and food intake repeatedly (**Figure 19C-D**). Therefore, aversion to HFD was tested in a food preference test of overnight fasted CD fed mice supplemented for four weeks with D-serine. Control mice consumed similar amounts of calories from CD and HFD, whereas mice treated with D-serine consumed ~50% less total calories with a marked reduction in the consumption of HFD (**Figure 19E**). Thus, D-serine is rapidly taken up into the circulation and various peripheral organs but appears to regulate food preference and thereby HFD induced body weight gain through direct or indirect actions in the CNS.

## 4.2.2 D-serine induced changes in gut microbiota do not mediate reduced weight gain on HFD

Changes in gut microbiota can modulate feeding behavior (Hamilton and Raybould, 2016) and the development of obesity (Ussar et al., 2015). D-serine can be produced and utilized by microbiota, potentially affecting overall community structure and activity (Connolly et al., 2015) but also alter D-serine levels in the host (Sasaki et al., 2016; Silbernagl et al., 1999). Thus, D-serine induced changes in gut microbiota could contribute to the reduced weight gain in HFD + D-serine treated mice.

Histological analyses of the small intestine following three weeks of D-serine supplementation did not reveal morphological differences between D-serine treated and control CD and HFD fed mice (**Figure 20A**). Analysis of fecal gut microbiota at days 0, 2, 7, and 14 in four week old male mice fed either CD or HFD with or without D-serine revealed a rapid reconfiguration of gut microbiota within two days of HFD

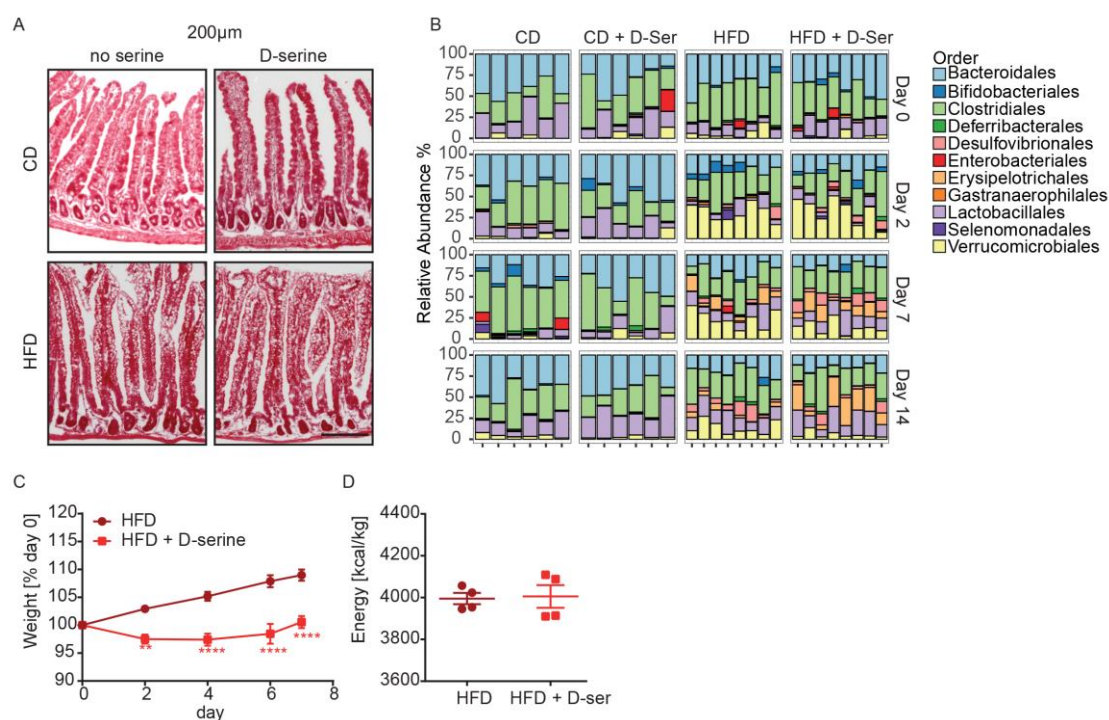


**Figure 20: D-serine alters gut microbiota composition.** (A) Histological analyses of the small intestine after three weeks of 1 % D-serine supplementation in drinking water. Size bar represents 200 μm. (B) Microbiome relative abundance at Order level. The barplot is displayed by treatment and day of intervention. (C) Weight gain in germfree C57BL/6 mice fed with HFD with or without D-serine supplementation. (D) Fecal caloric content of germfree C57BL/6 mice after one week of treatment. Data are shown as mean ± SEM. Statistics were calculated using t-test or ordinary two-way ANOVA with Sidak's multiple comparison post-hoc test (\*\*\*\*P < 0.0001, \*\* P < 0.01).



feeding, with additional changes observed at later time points in the HFD fed groups (**Figure 20B**), which was previously reported (Ussar et al., 2015). Focusing on the analysis of the microbiota on day 14 after the diet change, an increase of members of the family *Erysipelotrichaceae* in HFD + D-serine mice could be observed compared to HFD control mice. This suggests that D-serine modulates the microbiota composition. To further test if those changes are the cause for the metabolic changes, germfree C57BL/6 mice were fed a HFD with or without D-serine supplementation. Similar to what was observed in conventionally raised mice, D-serine supplementation blunted weight gain in germfree mice (**Figure 20C**) with no differences in fecal caloric content (**Figure 20D**), further strengthening the conclusion that gut microbiota do not directly contribute to D-serine mediated alterations in food preference and HFD induced weight gain.

#### **4.2.3 D-serine accumulates in metabolically important organs without inducing tissue inflammation**

After eight weeks of supplementation, D-serine accumulated in SCF, BAT and in the liver (**Figure 21A**). As the D-serine producing enzyme serine racemase (*Srr*) was not altered in those tissues in D-serine fed animals (**Figure 21B**), the accumulation of D-serine in the organs was due uptake of supplemented D-serine rather than biosynthesis. In contrast, in BAT of CD + D-serine animals, *Srr* was reduced compared to CD control animals, indicating a compensatory effect and reduced endogenous D-serine production. In all 4 tissues, no changes in the expression of *Dao* were observed (**Figure 21B**). Though D-serine was accumulating in white adipose tissue, no changes in fibrosis (**Figure 21C**) or the expression of inflammation markers *Tnfa* and *Mac1* (**Figure 21D**) were observed. Also *Mac1* and *Cd68* as markers for hepatic inflammation were not altered after 8 weeks of D-serine supplementation (**Figure 21D**).

Histological analysis of SCF, PGF, and BAT did not reveal differences in CD + D-serine mice compared to controls, whereas average adipocyte size in PGF and SCF was reduced in HFD + D-serine mice (**Figure 22A-B**). Histology of BAT showed lower lipid content in HFD + D-serine mice (**Figure 22A**), but this was not associated with significant changes in the expression of UCP1 (**Figure 22C**). Similarly, the reduced adipocyte size in white adipose tissues was not indicative for increased presence of beige adipocytes in SCF, PGF, or PRF (**Figure 22C**). According to

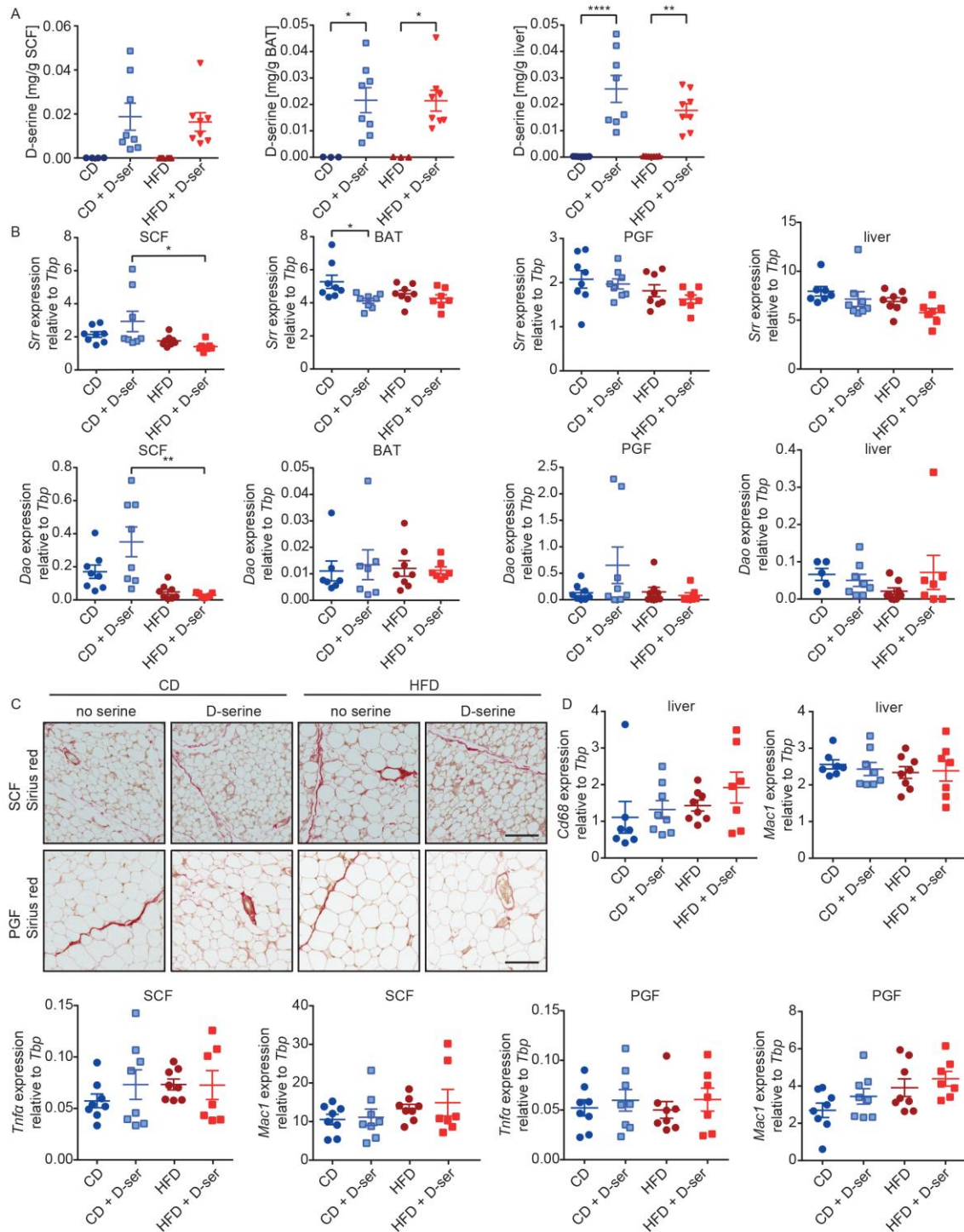


**Figure 21: D-serine accumulates in organs but does not induce inflammation.** Mice were supplemented with 1 % D-serine in drinking water for 8 weeks. **(A)** D-serine levels in SCF, BAT and liver. **(B)** Relative expression of *Srr* and *Dao* in SCF, BAT, PGF and liver. **(C)** Sirius red staining of subcutaneous (SCF) and perigonadal (PGF) fat tissue. Size bars represent 100 $\mu$ m. **(D)** Relative gene expression of *Tnfa* and *Mac1* in SCF and PGF and *Cd68* and *Mac1* in liver. Data are shown as mean  $\pm$  SEM. Statistics were calculated using ordinary one-way ANOVA with Tukey's multiple comparison post-hoc test. (\*\*\*\* $P < 0.0001$ , \*\*  $P < 0.01$ , \*  $P < 0.05$ ).

reduced adipocyte size, liver weight (**Figure 22D**) and liver triglyceride content (**Figure 22E**) were significantly reduced in HFD + D-serine fed compared to HFD control mice after eight weeks on diet. These changes also were observed in histological analysis (**Figure 22A**). As demonstrated in figure 17A, D-serine was cleared through the kidneys, which was shown to induce kidney damage in rats (Rais et al., 2012). Histologically, kidneys did not show any differences in D-serine

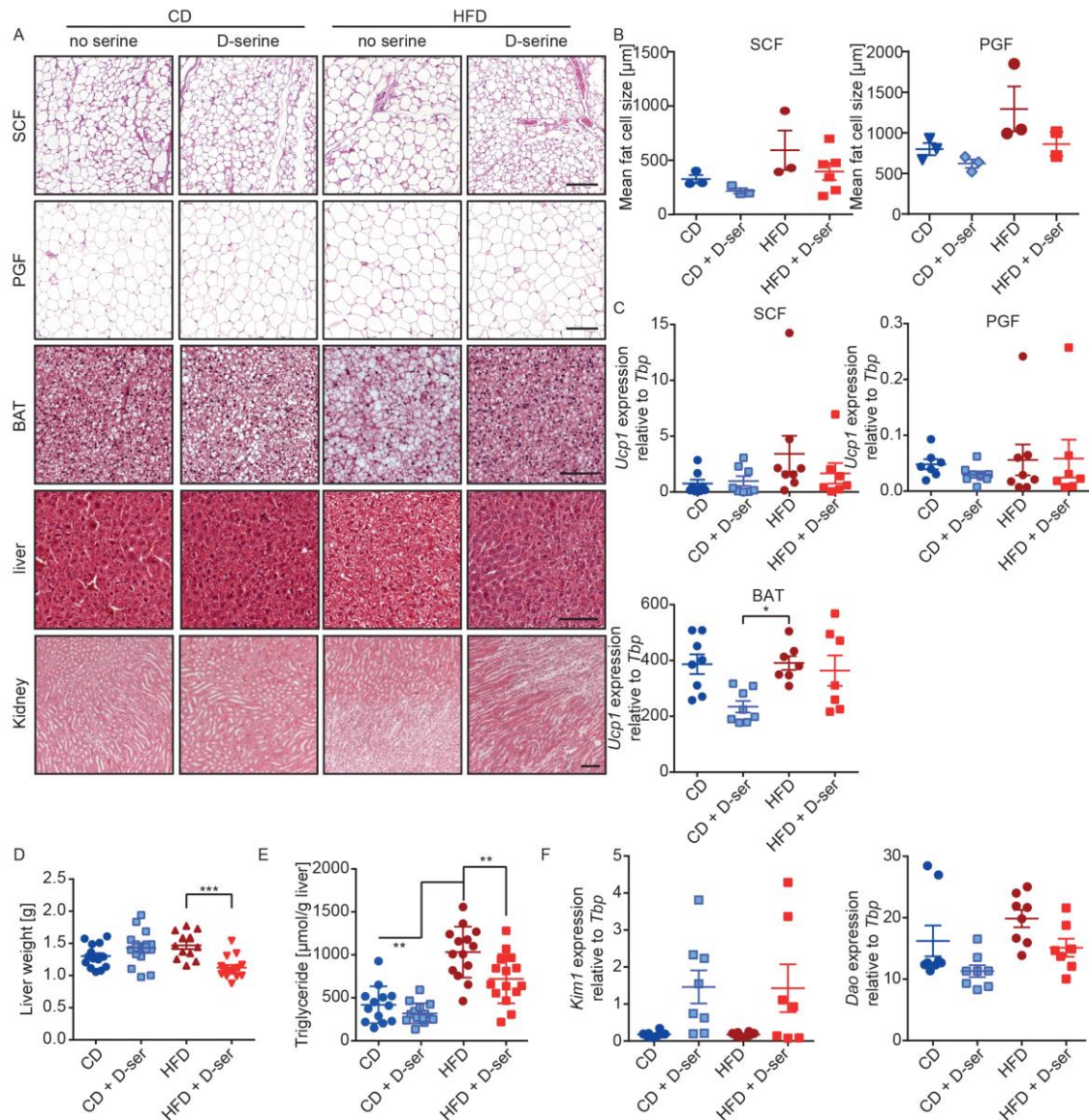


**Figure 22: D-serine reduces adipocyte cell size and prevents from hepatosteatosis upon HFD feeding.** (A) Representative H&E stainings of subcutaneous (SCF), perigonadal (PGF), brown fat (BAT), liver and kidney after 8 weeks of treatment. Size bars represent 100 µm. (B) Quantification of mean fat cell size in PGF and SCF. (C) Relative *Ucp1* expression in SCF, PGF and BAT after 8 weeks of D-serine supplementation. (D) Liver weight after 8 weeks of D-serine supplementation (n=8). (E) Liver triglyceride content after 8 weeks of D-serine supplementation (F) Relative expression of *Kim1* and *Dao* in kidneys after 8 weeks of D-serine supplementation. Data are shown as mean ± SEM. Statistics were calculated using ordinary one-way ANOVA with Tukey's multiple comparison post-hoc test (\*\*\*)  $P < 0.001$ , \*\*  $P < 0.01$ , \*  $P < 0.05$ ).

compared to control animals after 8 weeks of D-serine supplementation (**Figure 22A**). Expression of the kidney injury molecule 1 (*Kim1*) was increased in both D-serine groups, but changes were not significant (**Figure 22F**). Though, some mice seemed to have first signs of kidney damage. The D-serine degrading enzyme *Dao* was not altered in the kidneys, indicating that D-serine was excreted rather than degraded by the kidneys (**Figure 22F**).

#### **4.2.4 D-serine administration induces diet independent glucose intolerance but not insulin resistance**

D-serine supplementation blunted HFD diet induced weight gain and hepatosteatosis. Reduced fat accumulation is associated with improved glucose homeostasis. Therefore, CD and HFD diet fed animals supplemented with D-serine were subjected to an intraperitoneal glucose tolerance test (GTT) after six weeks on diet. Both CD and HFD mice supplemented with D-serine were hyperglycemic at baseline and severely glucose intolerant (**Figure 23A**). Measurement of random fed blood glucose after three and eight weeks revealed elevated glucose levels in mice receiving D-serine (**Figure 23B**). However, random fed insulin levels were not changed in CD + D-serine animals and reduced to CD levels in HFD + D-serine mice after three weeks of diet (**Figure 23C**). After eight weeks of treatment, insulin (**Figure 23C**) and c-peptide (**Figure 23D**) levels were not different within diet groups. Intraperitoneal insulin tolerance test (ITT) did not reveal differences in insulin sensitivity after three weeks of D-serine supplementation in CD fed animals (**Figure 23E**). Therefore, the observed D-serine associated hyperglycemia is independent from impaired insulin tolerance. Thus it was tested if increased hepatic gluconeogenesis contributes to hyperglycemia in D-serine treated mice. *Pepck* expression was not altered in the liver after eight weeks of D-serine treatment (**Figure 23F**). According to this, a pyruvate tolerance test (PTT) after 5 weeks of D-serine supplementation did not show a statistically significant increase in gluconeogenesis in D-serine treated CD fed animals (**Figure 23G**). Similar to the effects of weight gain (**Figure 19D**), hyperglycemia and glucose intolerance could be induced in mice with established diet induced obesity and reversed within one week of switching D-serine with water (**Figure 23H-K**).

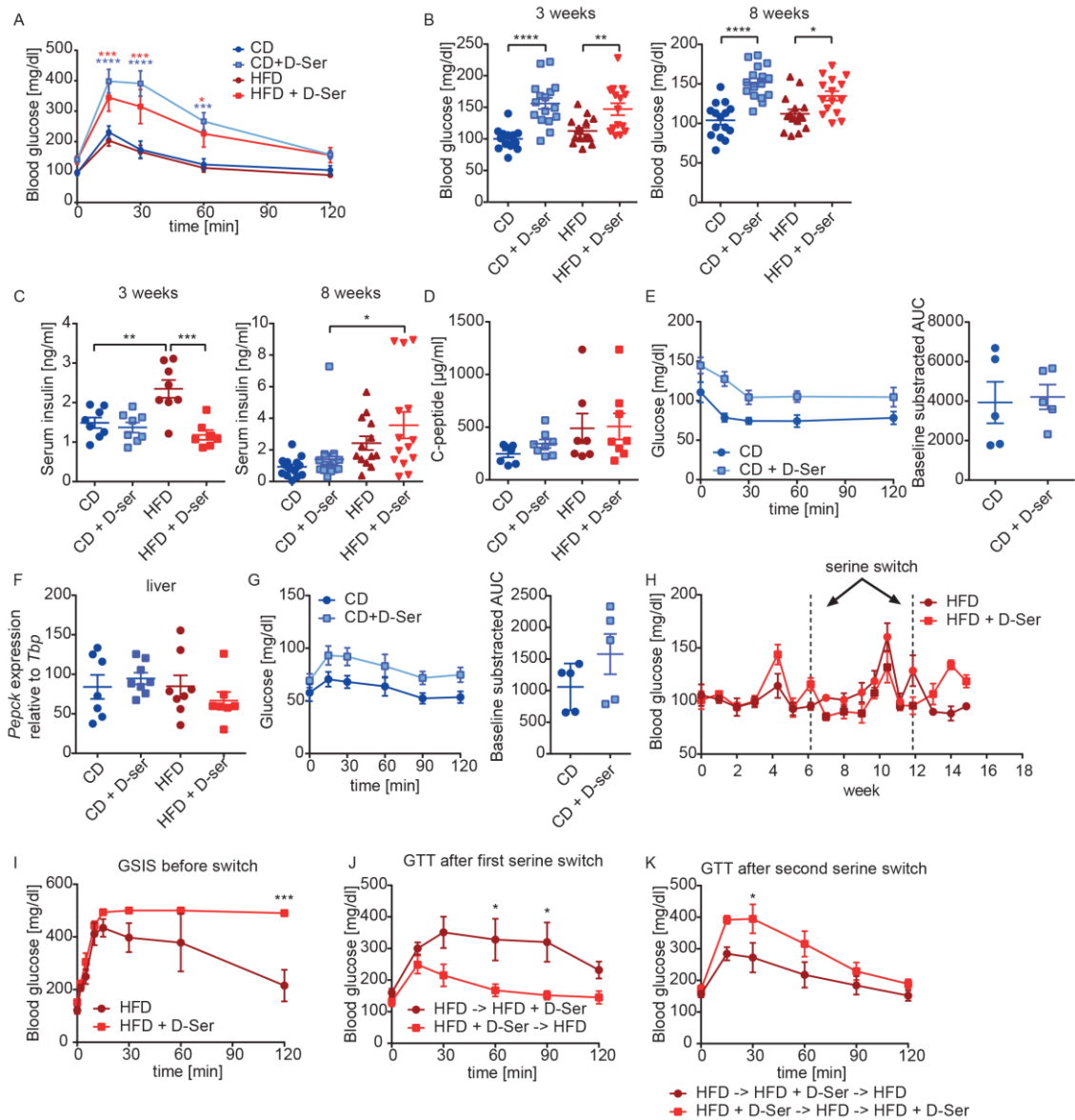


**Figure 23: D-serine impairs glucose tolerance.** (A) GTT after 6 weeks of D-serine supplementation (n=7-8). (B) Blood glucose and (C) serum insulin levels after 3 (random fed) and 8 (4h fasted) weeks of serine supplementation. (D) Serum C-peptide levels after 8 weeks of serine supplementation. (E) ITT after 3 weeks of D-serine supplementation (n=5). (F) Relative gene expression of *Pepck* in liver after 8 weeks of D-serine supplementation. (G) PTT after 5 weeks of D-serine supplementation (n=5). (H) Random fed blood glucose levels during 15 weeks of serine supplementation on HFD (n=4). Before D-serine supplementation, mice were fed a HFD for 8 weeks. 6 and 12 weeks after the D-serine supplementation, the water bottles were switched. (I) Glucose tolerance after 5 weeks of D-serine supplementation, (J) 6 weeks after the first serine switch and (K) 3 weeks after the second serine switch. Data are shown as mean  $\pm$  SEM. Statistics were calculated using t-test or ordinary one- or two-way ANOVA with Tukey's (A, B, C, D, F) or Sidak's multiple comparison post-hoc test (\*\*\*\* $P$ <0.0001, \*\*\*  $P$ <0.001, \*\*  $P$ <0.01, \*  $P$ <0.05).

#### 4.2.5 D-serine supplementation alters hepatic one-carbon metabolism but not gluconeogenesis

To identify potential alternative pathways for hepatic gluconeogenesis altered by D-serine, NMR based metabolomics was used. Metabolites from various metabolic pathways including glycolysis/gluconeogenesis, amino acids, nucleosides, choline, osmolytes, small acids and amines were identified. Total serine levels were elevated in D-serine treated animals (**Figure 24A**), most likely due to accumulation of D-serine (**Figure 22A**). Conversely, glycine and the reduced form of glutathione were lowered (**Figure 24A**). Serine is metabolized to glycine through SHMT1 and further to glutathione. *Shmt1* expression was reduced in both diet groups of D-serine supplementation (**Figure 24B**). No other statistically significant metabolite differences, despite a decrease of phosphorylcholine in HFD + D-serine treated animals, were observed (**Figure 24A**). This also included  $\beta$ -hydroxybutyrate, which can serve as an intermediate metabolite in the conversion from D-serine to glucose (**Figure 24A**). Liver glycogen content was not different between groups (**Figure 24C**). Thus, D-serine accumulates in liver and alters hepatic one carbon metabolism but does not alter hepatic glucose metabolism

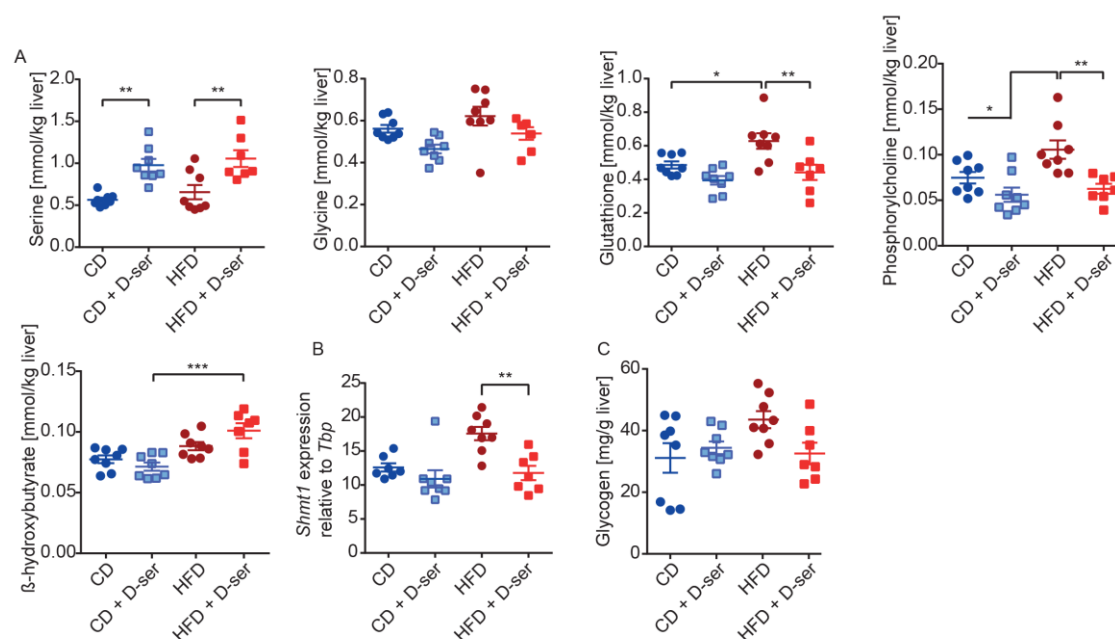


**Figure 24: D-serine alters hepatic one-carbon metabolism.** (A) Liver serine, glycine, glutathione, phosphorylcholine and  $\beta$ -hydroxybutyrate content after 8 weeks of D-serine supplementation, as quantified by NMR metabolomics. (B) Relative liver *Shmt1* expression after 8 weeks of D-serine supplementation. (C) Liver glycogen content after 8 weeks of D-serine supplementation. Data are shown as mean  $\pm$  SEM. Statistics were calculated using ordinary two-way ANOVA with Tukey's multiple comparison post-hoc test (\*\*\*)  $P < 0.001$ , \*\*  $P < 0.01$ , \*  $P < 0.05$ ).

#### 4.2.6 D-serine impairs insulin secretion from pancreatic beta cells

MALDI imaging of  $^{13}\text{C}$ -D-serine showed uptake into islets of Langerhans and the exocrine pancreas but not peripancreatic lymph nodes (Figure 25A). D-serine supplementation did not affect islet size (Figure 25B), islet size distribution (Figure 25C), or morphology (Figure 25D). However, D-serine supplementation blunted first and second phase insulin secretion in CD fed animals resulting in hyperglycemia (Figure 25E).

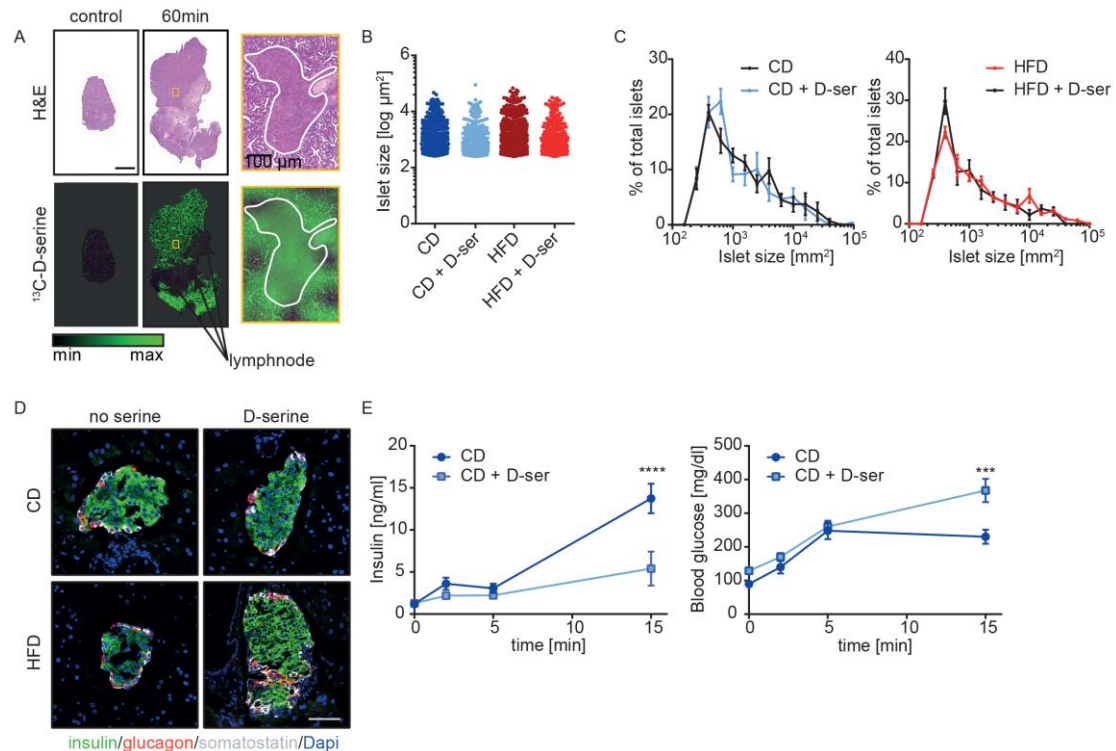


**Figure 25: D-serine impairs insulin secretion from pancreatic beta cells.** (A) 4 week old C57BL/6 mice were gavaged with 10 mg/kg  $^{13}\text{C}$ -labeled D-serine and sacrificed after 60 minutes. Pancreata were prepared for MALDI FT-ICR MSI and stained with H&E staining. As negative control, animals were gavaged with water. Size bar represents 2mm. (B) Quantification of islet size and (C) islet size distribution (n=4 per group) after 8 weeks of D-serine supplementation. (D) Triple staining of pancreatic islets after 3 weeks of serine supplementation. White: somatostatin. Red: glucagon. Green: insulin. Blue: Dapi. Size bar represents 50  $\mu\text{m}$ . (E) Glucose stimulated insulin secretion after 4 weeks of serine supplementation (n=5). Data are shown as mean  $\pm$  SEM, ordinary two-way ANOVA with Tukey's multiple comparison post-hoc test. Data are shown as mean  $\pm$  SEM. Statistics were calculated using ordinary two-way ANOVA with Sidak's multiple comparison post-hoc test (\*\*\*\*P<0.0001, \*\*\* P<0.001).

Pancreatic  $\beta$ -cells express NMDA receptors (Hogan-Cann and Anderson, 2016), and Marquard and colleagues (Marquard et al., 2015) showed that inhibition of pancreatic NMDA receptors by dextromethorphan (DXM) or its product dextrorphan (DXO) increases insulin secretion *in vitro* and *in vivo*. To test if inhibition of NMDA receptors

using DXM can reverse the effects of D-serine on insulin secretion, mice were fed a HFD and drinking water supplemented with D-serine, 0.3 % DXM or a combination thereof. DXM supplementation prevented D-serine induced hyperglycemia (**Figure 26A**). However, DXM as well as D-serine and DXM + D-serine treated mice were less glucose tolerant than HFD fed control mice after one week of supplementation (**Figure 26B**). Importantly, DXM treated mice had reduced energy expenditure (**Figure 26C**) but a trend to increased food intake (**Figure 26C**). Most importantly, however, DXM supplemented mice had significantly lower water intake (**Figure 26C**) and therefore also reduced D-serine uptake in the co-administrated mice. Thus, the observed normalization of blood glucose could result from reduced D-serine exposure.

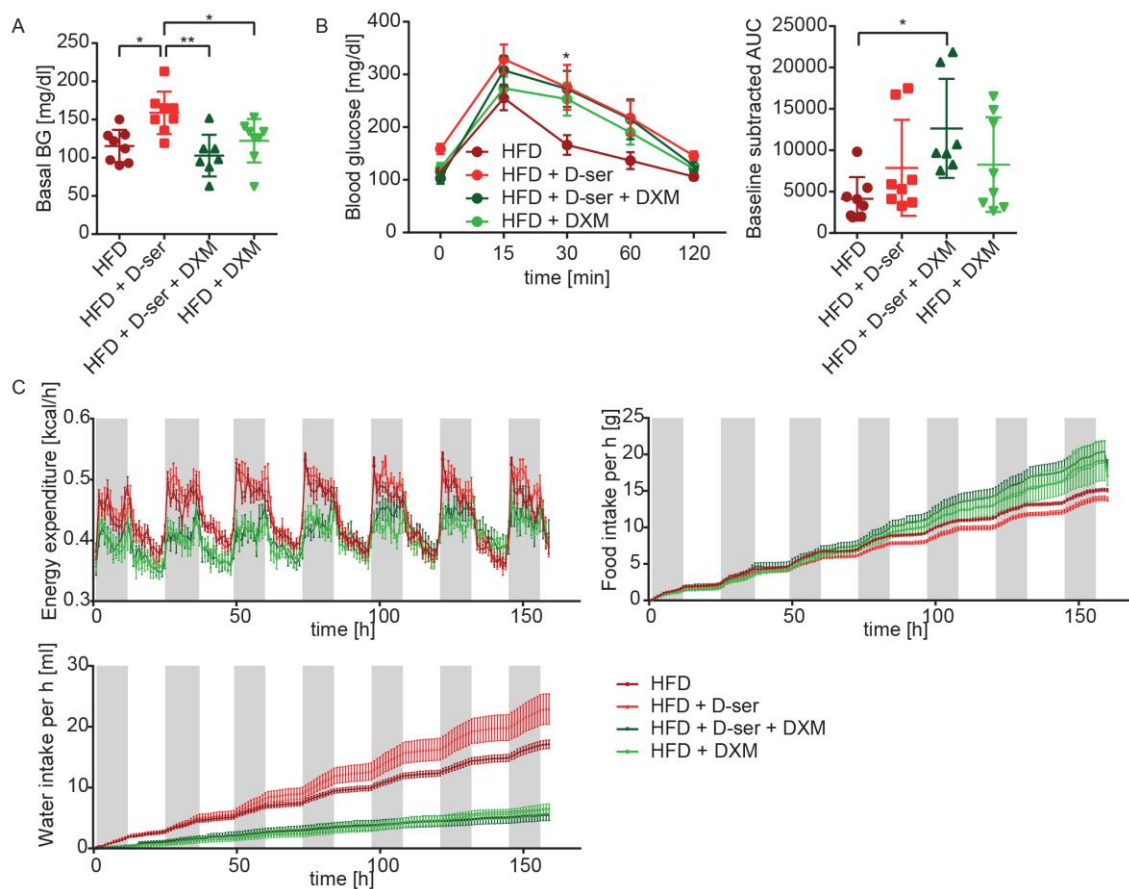


**Figure 26: DXM supplementation reduces water intake. (A)** 4 h fasted blood glucose after one week on HFD +/- 1 % D-serine and 0.3 % dexamethorphan (DXM) in the drinking water. **(B)** Intraperitoneal GTT after 1 week of 1 % D-serine +/- 0.3 % DXM in the drinking water. **(C)** Metabolic activity of 4 week old C57BL/6 mice supplemented with 1 % D-serine +/- 0.3 % DXM in the drinking water for 1 week. Data are shown as mean  $\pm$  SEM. Statistics were calculated using t-test, ordinary one- or two-way ANOVA with Tukey's multiple comparison post-hoc test (\*\*  $P < 0.01$ , \*  $P < 0.05$ ).



To overcome this limitation, the effects of D-serine and NMDA receptor inhibition on GSIS were tested in isolated islets. DXO supplementation, as previously shown, increased glucose stimulated insulin secretion while D-serine did not alter insulin secretion (**Figure 27A**). The combination of D-serine and DXO did not show any differences compared to DXO treated islets. Measurements of islet membrane potential corroborated these findings as no changes after addition of D-serine could be observed at high (16.7 mM) glucose concentrations (**Figure 27B**). However, DXO caused partial membrane depolarization in the presence of D-serine (**Figure 27B**), consistent with a non-significant tendency to augment insulin secretion (**Figure 27A**).

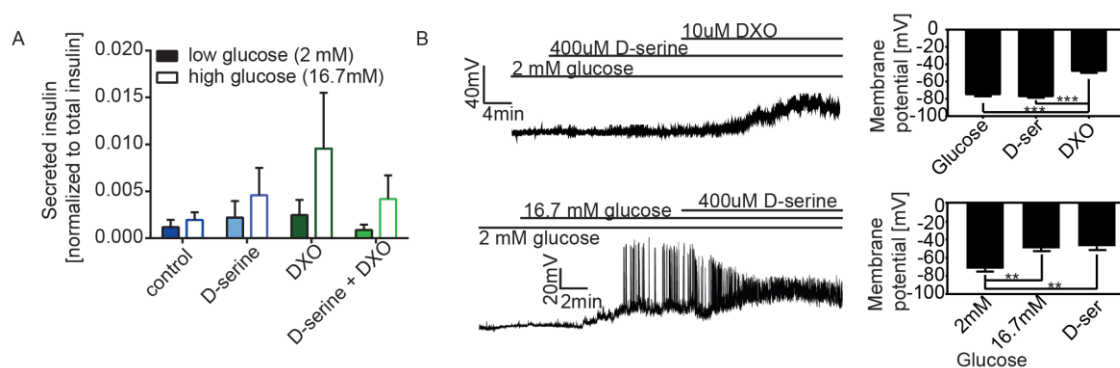


**Figure 27: D-serine does not directly impair insulin secretion *in vitro*.** (A) Insulin secretion test of isolated pancreatic islets pretreated with either 400  $\mu$ M D-serine, 10  $\mu$ M Dextrorphan tartrate (DXO) or a combination thereof for 1 hour. (B) Representative current-clamp trace of a mouse pancreatic  $\beta$ -cell displaying the electrical response to 400  $\mu$ M D-serine and 10  $\mu$ M DXO, in the presence of 2 or 16.7 mM glucose. The graph on the right shows mean membrane potential ( $n= 3-5$ ). Data are shown as mean  $\pm$  SEM. Statistics were calculated using ordinary one-way ANOVA with Tukey's multiple comparison post-hoc test (\*\* $P < 0.01$ , \*\*\*  $P < 0.001$ ).

#### 4.2.7 D-serine regulates insulin secretion via the sympathetic nervous system

Thus, D-serine does not appear to regulate insulin secretion via direct action on pancreatic  $\beta$ -cells. Conversely, D-serine action is best described in the CNS. Indeed, D-serine levels were significantly elevated in the hypothalamus following eight weeks of D-serine supplementation (**Figure 28A**) and  $^{13}\text{C}$ -D-serine was rapidly taken up into the hypothalamus following oral gavage (**Figure 28B**). Interestingly, chronic D-serine supplementation reduced c-Fos expression in various hypothalamic regions, suggesting a role of hypothalamic NMDARs in long term depression (**Figure 28C-D**).

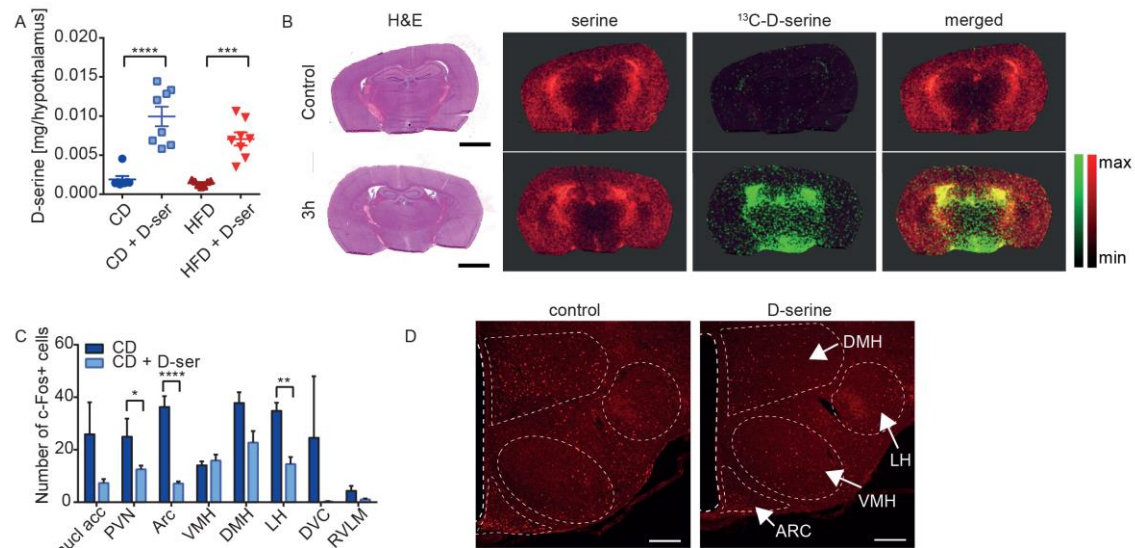


**Figure 28: D-serine accumulates in the hypothalamus and alters c-Fos expression.** (A) Hypothalamic D-serine levels after 8 weeks chronic D-serine supplementation. (B) 4 week old C57BL/6 mice were gavaged with 10 mg/kg  $^{13}\text{C}$ -labeled D-serine and sacrificed after 3 hours. Brains were prepared for MALDI FT-ICR MSI and stained with H&E staining. As negative control, animals were gavaged with water. Size bar represents 2 mm. (C) c-Fos expression in different brain regions after 6 weeks of D-serine supplementation (n=1-3). (D) Representative pictures for (C). Data are shown as mean  $\pm$  SEM. Statistics were calculated using t-test or ordinary one-way ANOVA with Tukey's multiple comparison post-hoc test (\*\*\*\*P<0.0001, \*\*\*P<0.001, \*\*P<0.01, \*P<0.05).

Thus, it was tested if D-serine regulates insulin secretion through the sympathetic nervous system. D-serine supplemented animals were injected with the  $\alpha$ 2-adrenergic receptor inhibitor BRL44408 (Ito et al., 2017; Kiss et al., 1995) prior to assessment of glucose tolerance and insulin secretion. Injection of BRL44408 normalized D-serine induced hyperglycemia within 30 minutes and completely restored glucose tolerance in these mice. BRL44408 had no significant effects in CD fed animals compared to controls (**Figure 29A**). This was accompanied by a substantial increase in insulin secretion (**Figure 29B**). A GTT performed one week after the single injection of BRL44408 did not reveal a significant improvement of overall glucose tolerance of BRL44408 + D-serine mice, but basal glucose levels remained significantly improved (**Figure 29C**). In contrast to the effects of high dose D-serine supplementation, supplementation with 0.1 % D-serine showed the opposite effect resulting in improved glucose tolerance compared to control animals after 11 and 23 days (**Figure 29D and F**), which was due to increased insulin secretion (**Figure 29E**). In line with that, acute injection of 4 g D-serine/kg body weight also revealed improved glucose tolerance (**Figure 29G**).

In summary, it here was shown that D-serine reduced HFD induced weight gain, but independent of the diet impacts glucose stimulated insulin secretion via indirect action through the sympathetic nervous system.

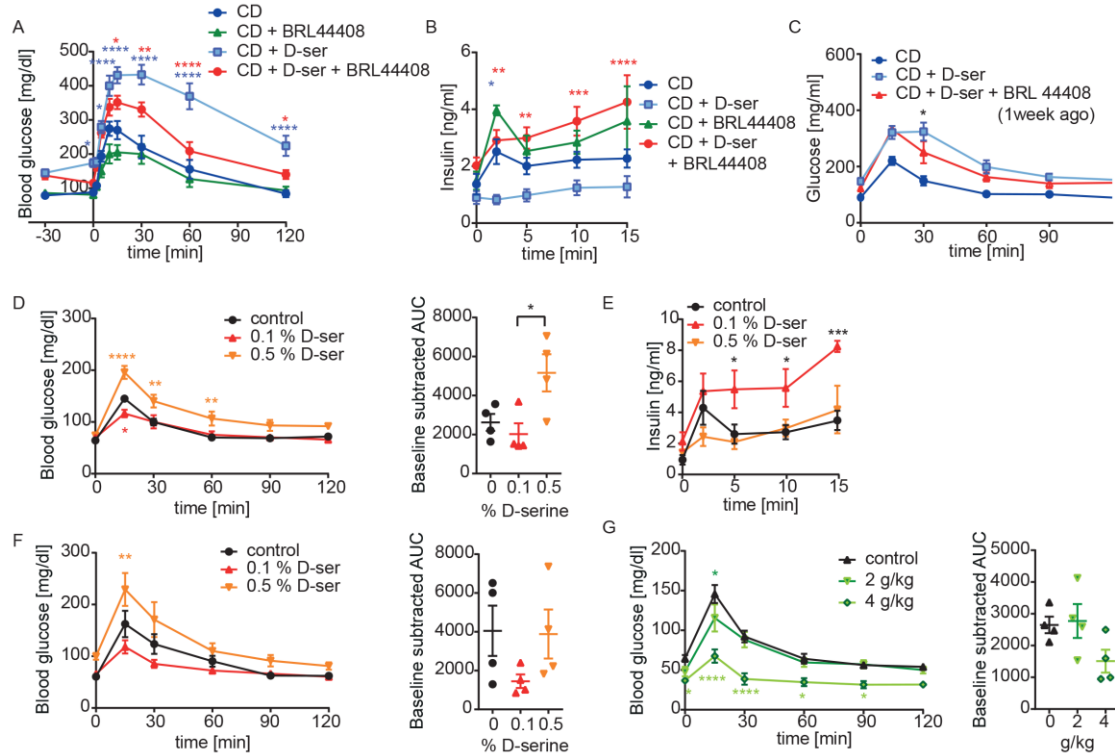


**Figure 29: Inhibition of  $\alpha$ 2-adrenergic receptors normalizes glucose tolerance of D-serine supplemented mice.** (A) Glucose and (B) insulin levels during a GSIS after 2 weeks of D-serine supplementation +/- treatment with the  $\alpha$ -adrenergic receptor inhibitor BRL44408 (5 mg/kg) 30 min prior to glucose administration (n=5). (C) GTT after 3 weeks of D-serine supplementation and one week after a single injection of BRL44408 (5 mg/kg) (n=5). (D) GTT after 11 days of 0.1 or 0.5 % D-serine supplementation (n=4). (E-F) GSIS after 4 weeks of D-serine supplementation (n=4). (G) GTT 2 hours after i.p. injection of D-serine (n=4). Data are shown as mean  $\pm$  SEM. Statistics were calculated using t-test, ordinary one- or two-way ANOVA with Tukey's multiple comparison post-hoc test (\*\*\*\*P<0.0001, \*\*\* P<0.001, \*\* P<0.01, \* P<0.05).

### 4.3 L-serine remodels hepatic metabolism

To proof whether the effects of D-serine on food intake and insulin secretion are caused by D-serine and not by its proteogenic enantiomer L-serine, mice were supplemented with 1 % L-serine in drinking water and fed with either CD or HFD for 8 weeks.

#### 4.3.1 L-serine supplementation has no effect on body weight or adipose tissue morphology

Interestingly, water intake of CD, but not HFD fed animals was increased when they were supplemented with L-serine (**Figure 30A**). At the same time, L-serine had no effect on food intake (**Figure 30A**). According to this, there was no difference in body weight throughout 8 weeks of treatment (**Figure 30B**). After feeding a HFD, animals were significant longer than control animals, but L-serine had no effect on body length (**Figure 30C**). Eight weeks after L-serine supplementation, mice on HFD had a significantly increased fat mass compared to CD fed animals (**Figure 30D**).

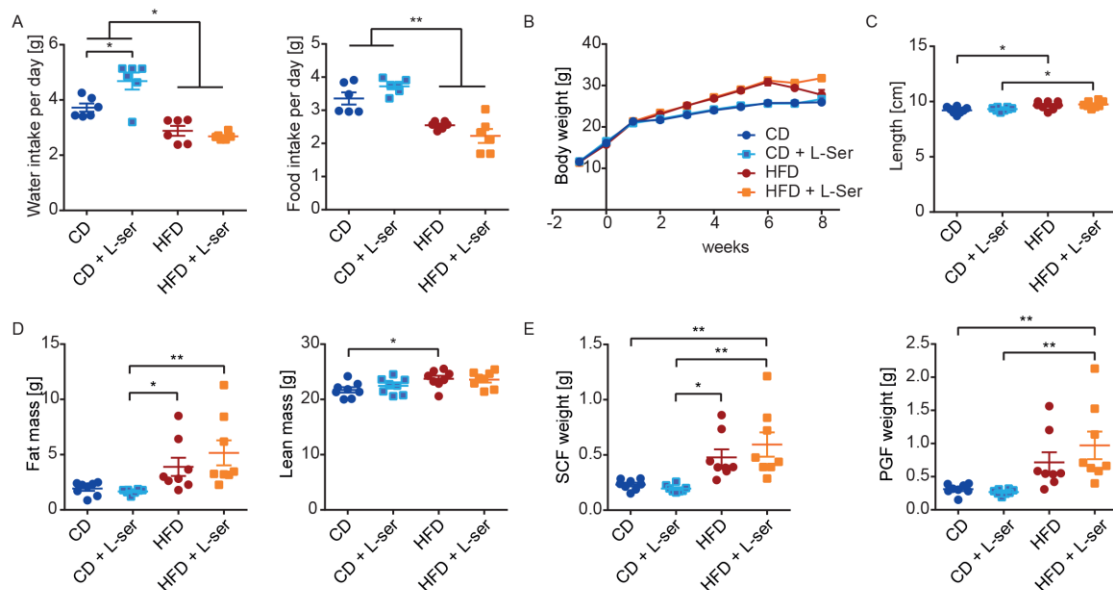


**Figure 30: L-serine has no effect on body weight gain.** 4 week old C57BL/6 mice were fed a CD or HFD, and drinking water was supplemented with or without 10 g/l L-serine. **(A)** Water and food intake per day after 6 weeks of L-serine supplementation (n=6). **(B)** Body weight during 8 weeks of L-serine supplementation (n=8). **(C)** Body length after 8 weeks of L-serine supplementation (n=8). **(D)** Body composition after 8 weeks of L-serine supplementation (n=8). **(E)** Fat pad weight after 8 weeks of L-serine supplementation (n=8). Data for CD and HFD control animals are partly same as in the D-serine part. Data are shown as mean  $\pm$  SEM. Statistics were calculated using ordinary one- or two-way ANOVA with Tukey's multiple comparison post-hoc test (\*\* P<0.01, \* P<0.05).

In control animals, lean mass was significantly increased after HFD, which could be explained by increased body size. Though, L-serine supplemented mice showed no differences in lean mass after receiving HFD. According to elevated body fat mass after eight weeks of HFD feeding, all HFD groups had an increased SCF and PGF weight, but no differences between control and L-serine fed animals were observed (**Figure 30E**). Histological analysis did not show any differences in morphology or adipocyte size in SCF and PGF (**Figure 31A-B**). In line with that, *Ucp1* expression was not altered in L-serine treated compared to control animals, indicating no

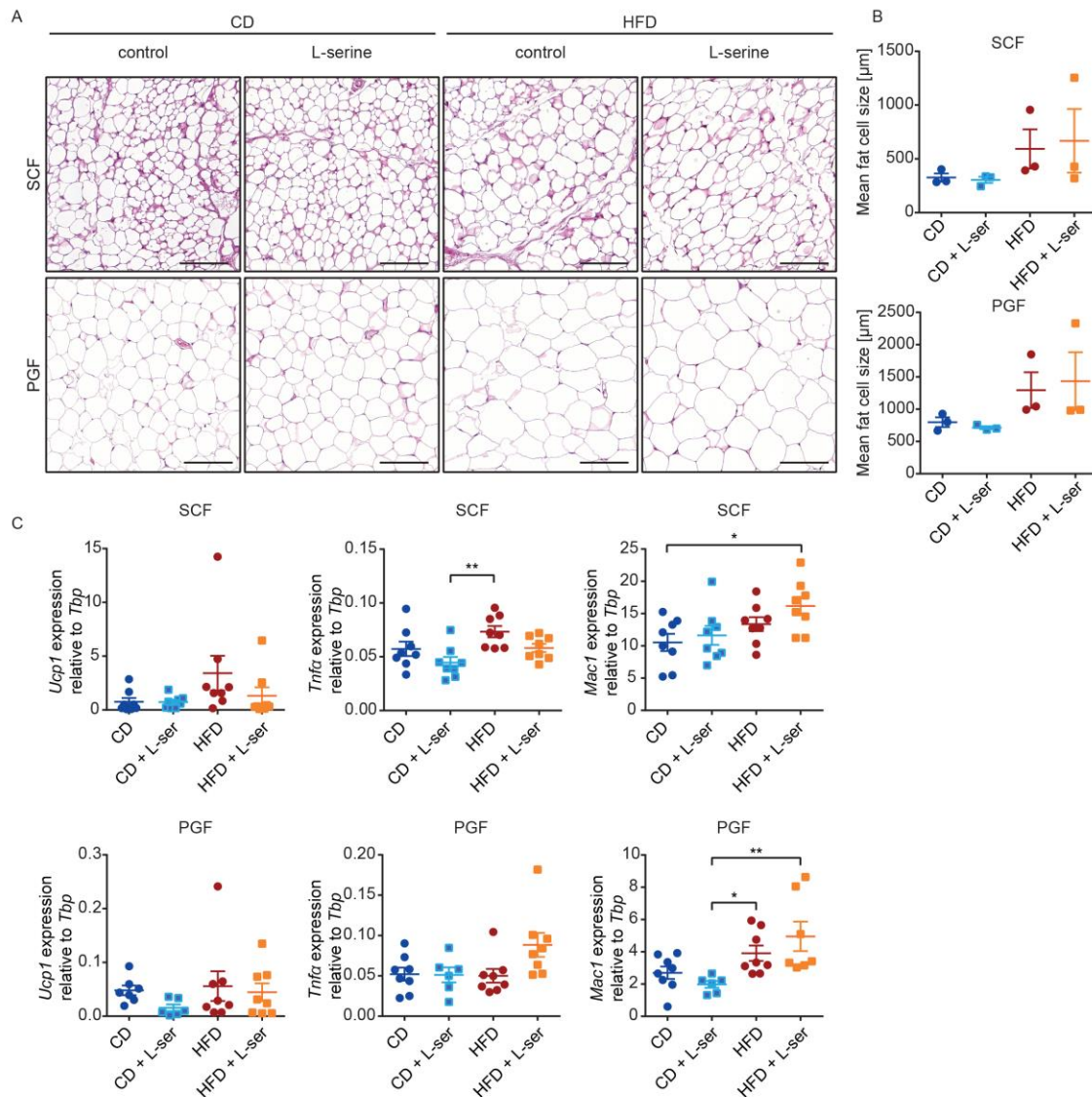


**Figure 31: L-serine does not alter white adipose tissue morphology.** (A) Representative H&E stainings of the SCF and PGF after 8 weeks of treatment (n=3). Size bar represents 100 µm. (B) Quantification of mean fat cell size in PGF and SCF after measuring every cell in one stained layer. (C) Relative gene expression of *Ucp1*, *Tnfa* and *Mac1* in SCF (n=8) and PGF (n=6-8). Data for CD and HFD control animals are partly same as in the D-serine part. Data are shown as mean ± SEM. Statistics were calculated using ordinary one-way ANOVA with Tukey's multiple comparison post-hoc test (\*\* P<0.01, \* P<0.05).

changes in being of white adipose tissue (**Figure 31C**). In SCF, *Tnfa* and *Mac1* were not altered, but in PGF, there was a tendency of increased expression in both inflammation markers in HFD treated animals (**Figure 31C**).

BAT tissue weight was increased after HFD feeding, but no changes in L-serine compared to controls were observed (**Figure 32A**). Morphologically, there were no differences in BAT after L-serine treatment (**Figure 32B**), but *Ucp1* expression was increased in HFD + L-serine compared to CD + L-serine fed mice (**Figure 32C**). Interestingly, *Srr* and *Shmt1* were reduced in CD + L-serine compared to CD control animals (**Figure 32C**).

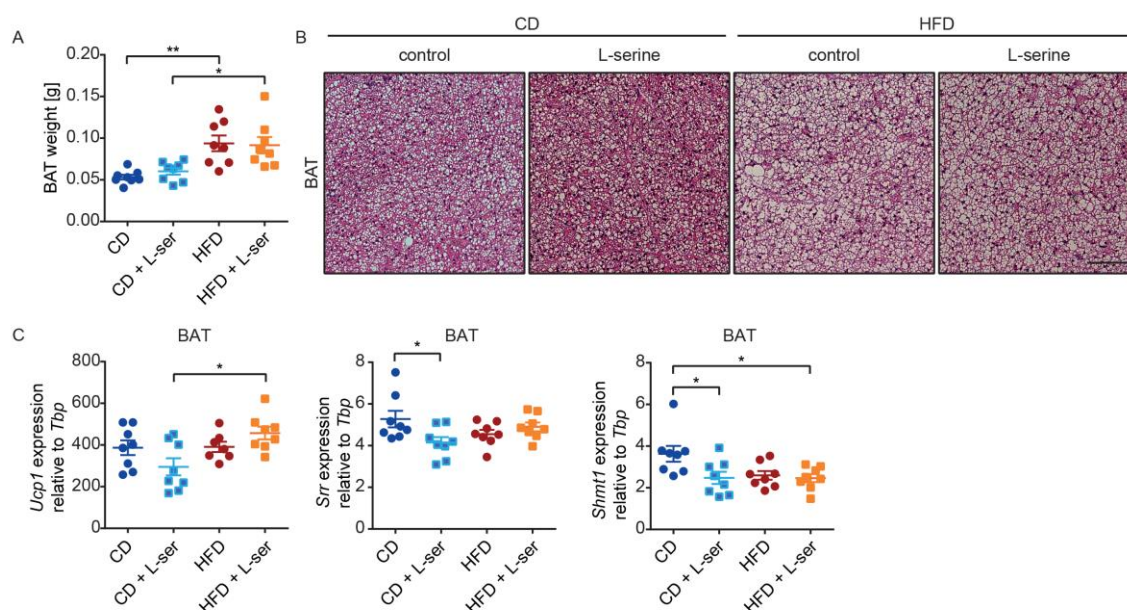


**Figure 32: L-serine alters *Shmt1* expression in BAT.** Mice were supplemented with 1 % L-serine in drinking water for 8 weeks. (A) Tissue weight (n=8) and (B) representative H&E stainings of BAT. Size bar represents 100  $\mu$ m. (C) Relative BAT gene expression of *Ucp1*, *Srr* and *Shmt1* (n=8). Data for CD and HFD control animals are partly same as in the D-serine part. Data are shown as mean  $\pm$  SEM. Statistics were calculated using ordinary one-way ANOVA with Tukey's multiple comparison post-hoc test (\*\*  $P < 0.01$ , \*  $P < 0.05$ ).

#### 4.3.2 L-serine increases hepatic PEPCK but has no effect on glucose tolerance

To investigate whether L-serine supplementation alters glucose metabolism, a GTT was performed after six weeks of treatment. Glucose tolerance was unchanged in all groups (**Figure 33A**) and random fed blood glucose also was not changed after eight weeks of diet (**Figure 33B**). Though glucose tolerance was not altered, random fed insulin levels were increased in HFD control compared to CD fed mice (**Figure 33C**). Insulin levels of mice supplemented with L-serine were not different to CD controls.

Interestingly, hepatic *Pepck* expression was significantly increased in CD + L-serine, but not in HFD + L-serine supplemented mice compared to controls, indicating increased hepatic gluconeogenesis in those mice (**Figure 33D**). In contrast to D-serine, L-serine supplementation had no effect on the constellation of gut microbiota (**Figure 33E**), which fits to the observed data that L-serine has no impact on food intake, weight gain or glucose homeostasis.

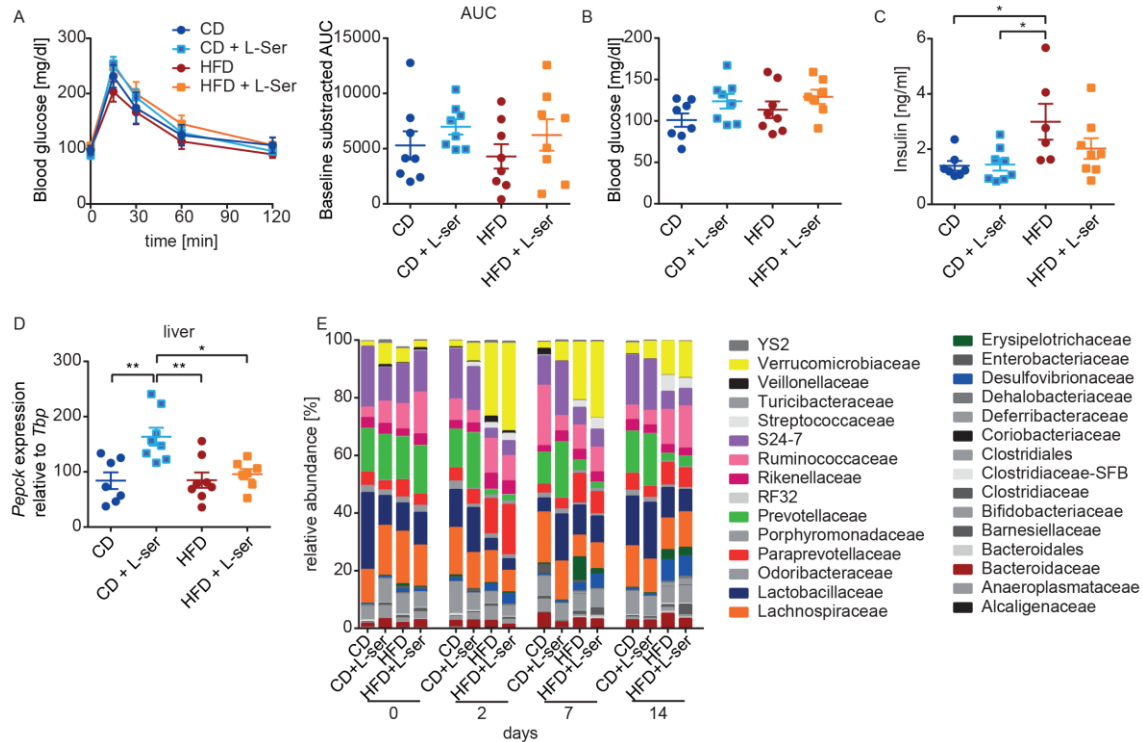


**Figure 33: L-serine has no impact on glucose tolerance or gut microbiota.** (A) GTT after 6 weeks of D-serine supplementation (n=8). (B) Blood glucose (n=7-8) and (C) insulin (n=6-8) levels after 8 weeks of L-serine supplementation. (D) Relative hepatic *Pepck* expression after 8 weeks of L-serine supplementation (n=7-8). (E) Microbiome relative abundance at Order level. The barplot is displayed by treatment and day of intervention. Data for CD and HFD control animals are partly same as in the D-serine part. Data are shown as mean  $\pm$  SEM. Statistics were calculated using ordinary one- or two-way ANOVA with Tukey's multiple comparison post-hoc test (\*  $P < 0.05$ ).

### 4.3.3 L-serine alters hepatic metabolism

After eight weeks on HFD, liver weight was significantly increased in control animals (**Figure 34A**). Interestingly, liver weight of HFD + L-serine treated animals was reduced to normal weight. Though, the reduced tissue weight was not caused by a reduction in triglyceride content (**Figure 3B-C**). In contrast to triglyceride content, liver glycogen content was significantly reduced in L-serine treated mice on both diets (**Figure 34D**). These changes were not caused by accumulation of serine (**Figure 34F**). Also, the expression of the serine-to-glycine-converting enzyme *Shmt1*

and liver glycine levels were not altered in L-serine treated animals (**Figure 34E-F**). NMR based metabolomics revealed a reduction in glutathione levels in L-serine supplemented mice on both diets (**Figure 34F**). At the same time, phosphorylcholine levels were decreased, whereas  $\beta$ -hydroxybutyrate was increased in in HFD + L-serine treated mice compared to HFD controls (**Figure 34C**), indicating tremendous changes in hepatic metabolism. In summary, L-serine supplementation here was shown to have a great impact on liver metabolism with so far unknown consequences.

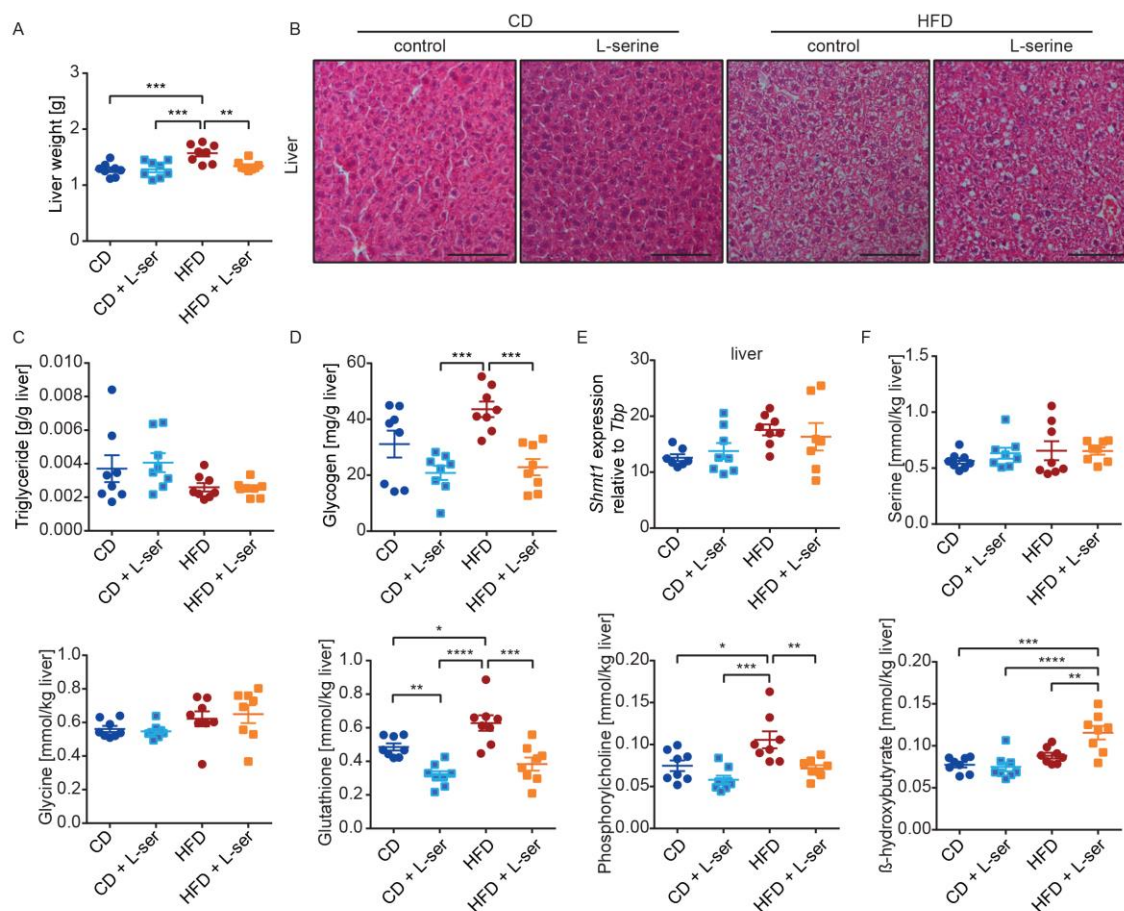


**Figure 34: L-serine alters hepatic metabolism.** Mice were supplemented with 1 % L-serine in drinking water for 8 weeks. **(A)** Tissue weight (n=8) and **(B)** representative H&E stainings of liver. Size bar represents 100  $\mu$ m. **(C)** Liver triglyceride and **(D)** glycogen content (n=8). **(E)** Relative liver *Shmt1* expression (n=7-8). **(F)** Liver serine, glycine glutathione, phosphorylcholine and  $\beta$ -hydroxybutyrate content, as quantified by NMR metabolomics (n=8). Data for CD and HFD control animals are partly same as in the D-serine part. Data are shown as mean  $\pm$  SEM. Statistics were calculated using ordinary one-way ANOVA with Tukey's multiple comparison post-hoc test (\*\*\*\*P<0.0001, \*\*\* P<0.001, \*\* P<0.01, \* P<0.05).



# 5 Discussion

## ***5.1 Depletion of ASC-1 remodels genetic predisposition and enables beige over white adipocyte differentiation***

The amino acid transporter ASC-1 transports small neutral amino acids in a bidirectional way (Fukasawa, 2000; Nakauchi et al., 2000). In the brain, it is the main transporter of the neurotransmitter D-serine. Hence, ASC-1 is very important for neuronal development and learning processes (Avellar et al., 2016; Basu et al., 2009). It recently was published that ASC-1 is expressed on the surface of white adipocytes (Ussar et al., 2014), but its function there has not been unraveled so far.

In this thesis it was shown that a knockdown or chemical inhibition of ASC-1 in subcutaneous white preadipocytes induces spontaneous differentiation into beige adipocytes *in vitro*. In contrast, overexpression of ASC-1 in brown preadipocytes resulted in reduced expression of brown adipocyte marker genes after differentiation. The beige phenotype of ASC-1 knockdown cells seemed to be driven by a subpopulation of preadipocytes, where ASC-1 is expressed. In contrast to those *in vitro* findings, a global loss of ASC-1 *in vivo* did not increase *Ucp1* expression in SCF, but reduced UCP1 expression in BAT.

### **5.1.1 ASC-1 as important regulator of adipocyte identity**

Knockdown of ASC-1 in subcutaneous preadipocytes via shRNA results in differentiation into beige adipocytes. This was shown by expression of *Ucp1*, *P2rx5*, *TFAM* and *Pgc1 $\alpha$* , which were increased in shAsc-1 compared to control adipocytes. While the expression of *Ucp1*, *TFAM* and *Pgc1 $\alpha$*  further increased when cells were differentiated with rosiglitazone, *P2rx5* did not further increase upon rosiglitazone treatment. This could be explained by an already maximal expression or a missing second stimulus in addition to rosiglitazone. In line with the elevated expression of those marker genes, shAsc-1 cells also had an increased basal mitochondrial respiration as well as proton leakage. Therefore, ASC-1 seems to be an important regulator of adipocyte identity. Besides ASC-1, several other proteins, transcription factors and hormones have been identified in regulating WAT beiging (Lo and Sun, 2013). Though, the mechanism of WAT beiging is unknown so far and research in

this field is ongoing. Thereby, more and more factors involved in WAT beiging are discovered, making the mechanism more complex (Martinez-Sanchez et al., 2017; Milet et al., 2017; Ng et al., 2017). In addition to that, cellular stress was shown to drive beiging of white adipose tissue (Jeanson et al., 2015). Therefore, many extra- or intracellular changes can result in beiging by secondary effects as for example by inducing cellular stress. In this thesis, the knockdown of ASC-1 was induced using an overexpression of a shRNA. Off-target effects are possible (Singh et al., 2011), but unlikely here, as chemical inhibition of ASC-1 led to similar effects. In addition, overexpression of ASC-1 in brown preadipocytes led to opposite effects to the knockdown in white preadipocytes. This finding at the same time excludes stress response caused beiging, but it remains unclear if ASC-1 directly or indirectly regulates adipocyte identity.

### **5.1.2 Depletion of ASC-1 re-programs preadipocytes resulting in changes of intracellular amino acids and spontaneous differentiation into beige adipocytes**

On one hand it could be that ASC-1 directly interacts with other proteins or transcription factors to regulate adipocyte gene expression. On the other hand it is possible that ASC-1 indirectly regulates adipocyte identity by its function as amino acid transporter.

To analyze the first option, cells were treated with the ASC-1 inhibitor BMS-466442 during differentiation. BMS-466442 is a non-competitive substrate inhibitor (Brown et al., 2014). Therefore, the inhibitor most likely is not transported into the cell and only can act extracellular which means, that it only inhibits amino acid transport but not potential intracellular protein-protein interactions. It was shown that chemical inhibition of ASC-1 induced beiging, which showed that the effect of ASC-1 on adipocyte identity is more likely to be mediated via amino acids.

Interestingly, the chemical inhibition of ASC-1 only lead to a beige phenotype when performed before cells reached confluency. This showed that the phenotype of ASC-1 knockdown cells is driven by an altered phenotype on preadipocytes. This is surprising, as ASC-1 is only low expressed in white preadipocytes. Though, overexpression of ASC-1-HA in brown preadipocytes revealed accumulation of ASC-1-HA in so far undefined non  $\beta$ -ACTIN containing membrane domains, indicating a function of ASC-1 in preadipocytes.

Subcutaneous adipose tissue is a heterogeneous organ that consists of a mixture of various different adipocyte precursors (Chau et al., 2014). Here it was shown that out of 52 single cell clones, 3 expressed *Asc-1* at very high levels compared to the rest. This brought up the hypothesis that *Asc-1* is expressed at higher levels in a subpopulation of adipocytes that could be beige preadipocytes and that it acts as a suppressor of beige adipocyte differentiation. In consequence of knocking down *ASC-1*, the suppressor of beige adipogenesis is removed. Interestingly, cells thereby started to differentiate spontaneously after reaching confluency, which could be driven by increased expression of the differentiation markers *Ppar $\gamma$*  and *Prdm16*. Both are known to be essential for the differentiation of preadipocytes (Harms et al., 2015). During differentiation, preadipocytes accumulate lipid droplets and therefore expand. In addition, it was observed that spontaneous differentiating sh*Asc-1* cells keep replicating. Hence, after 8 days of spontaneous differentiation, the majority of cells in the culture plate were spontaneously differentiated beige adipocytes, while only few preadipocytes remained. Therefore, spontaneously differentiated *ASC-1* knockdown cells expressed higher levels of brown marker genes compared to normal differentiated cells, where the whole population of preadipocytes was differentiated.

As the direct action of *ASC-1* on adipocyte identity was excluded using the inhibitor, the other option concerning its role as an amino acid transporter was investigated. It was shown that *ASC-1* knockdown preadipocytes and adipocytes had an altered extracellular and especially intracellular amino acid profile. In theory, a knockdown of *ASC-1* reduces the export or the uptake of alanine, serine, glycine and cysteine, depending on the preferred direction of transport. If uptake is reduced, those amino acids would have to be synthesized by the cells itself, resulting in a reduction of other intracellular amino acids that are used for their biosynthesis. Here, all significant intracellular changes were reductions of amino acids. Though, their impact on the phenotype is difficult to evaluate, as most of them can be transported by other amino acid transporters that are expressed in preadipocytes and adipocytes, making the system more complex.

D-serine has a very high affinity to *ASC-1* and, more important, is not, or with only low affinity, transported by other amino acid transporters expressed in white adipose tissue. Interestingly, D-serine accumulated in proliferating *ASC-1* knockdown preadipocytes, while its levels normalized after cells reached confluency. Hence, intracellular levels of D-serine could have an impact on the identity of adipocytes.

Though, differentiation of brown *ASC-1* overexpressing preadipocytes with D-serine did not normalize the expression of brown marker genes, which were reduced upon

ASC-1 overexpression. ASC-1 has a  $K_m$  of 22.8  $\mu\text{M}$  to D-serine (Nakauchi et al., 2000), which is in the range of tested D-serine concentrations during differentiation. Nevertheless, intracellular D-serine levels were not measured and it therefore is not known, whether D-serine was transported into the cells. Hence, further steps to unravel the role of D-serine in the mechanism of ASC-1 driven adipocyte identity need to be done.

### **5.1.3 Whole body loss of ASC-1 results in hepatosteatosis and reduced UCP1 expression in BAT**

A loss of ASC-1 in the brain is known to induce a severe phenotype that leads to early postnatal death (Rutter et al., 2007; Safory et al., 2015; Xie et al., 2005). Safory et al. could show that at least a part of the phenotype is caused by dysregulation of synaptic glycine levels (Safory et al., 2015), but many other studies showed that ASC-1 is the main transporter for D-serine (Rutter et al., 2007; Xie et al., 2005). Therefore, it could be the case that ASC-1 knockout mice suffer from several effects that are caused by either glycine or D-serine (Sason et al., 2016).

Due to the severe effects on central nervous system, pups with an age of 2 weeks were investigated in this thesis. It was shown that besides the brain, a knockout of ASC-1 has an impact on various other tissues. Especially surprising was the fact that 1-2 week old pups had a severe hepatosteatosis, indicating that those mice store energy instead of using it for growth, although their development already was behind their littermates (Xie et al., 2005). Pups are not able to undergo shivering thermogenesis (Chew and Spencer, 1967) and therefore maintain their body temperature through heat production by brown adipose tissue. ASC-1 ko mice had a reduced body temperature which was explained by decreased *Ucp1* RNA and protein levels. UCP1 expression in BAT primarily is regulated by adrenergic signaling from the brain (Galmozzi et al., 2014). Therefore, loss of ASC-1 could result in altered noradrenergic signaling and, as a side effect, reduce UCP1 expression in BAT. In contrast to reduced UCP1 expression in BAT, histological analysis revealed an increased abundance of beige adipocytes within SCF. This could be driven by a lack of ASC-1 in preadipocytes, as shown in *in vitro* experiments. Alternatively, WAT beiging could be caused by a chronic cold-stimulus due to reduced BAT activity. Nevertheless, total *Ucp1* expression in SCF remained comparable to wt littermates. This can be explained by the hypothesis, that UCP1 expression in beige adipocytes is reduced due to missing noradrenergic signaling. Therefore, a wildtype pup has few

beige adipocytes with normal UCP1 expression while a knockout pup has many beige adipocytes with low UCP1 expression. Total RNA extracts at the end reveal same *Ucp1* levels, though ko pups have more beige adipocytes.

This in turn could explain the accumulation of lipids in the liver. In BAT and beige SCF of ASC-1 ko pups, lipolysis instead of lipogenesis is active to burn fatty acids and produce heat. Due to missing UCP1, generated free fatty acids cannot be used as a substrate and are released into the plasma, where they next are transported to and stored by the liver. Hence, dysregulation of ASC-1 in the brain could reduce whole body UCP1 expression though SCF is prone to become beige, and result in hepatosteatosis although the pups would need the energy for maintaining body temperature.

The effects of loss of ASC-1 in the brain are complex and overlap each other. Therefore, it is complicated to rule out a mechanism for a specific investigation. Using het mice, it here was tried to circumvent the severe effects, but still investigate the role of ASC-1 in adipose tissue. However, het mice did not differ from wt mice regardless of the diet, indicating that one functional *Asc-1* allele is enough to compensate any effects.

## ***5.2 D-serine supplementation regulates insulin secretion and HFD induced weight gain***

D-serine is a known NMDA receptor co-agonist that is important in the central nervous system (Cheriyana et al., 2015). In schizophrenic patients, synaptic D-serine levels are reduced and treatment with D-serine was shown to improve cognitive and negative symptoms (Wolosker et al., 1999). Recently, its main transporter ASC-1 was found to be expressed in white adipose tissue (Ussar et al., 2014) and NMDA receptors are known to be expressed in liver, kidney, testis, muscle, and pancreas (Horio et al., 2011; Marquard et al., 2015; Nishimura et al., 2014). These results indicate that D-serine could have a role in peripheral tissues, but the specific function remains unclear.

The findings in this thesis show that chronic supplementation with the NMDA receptor co-agonist D-serine reduced HFD induced weight gain and thereby protected from the development of hepatosteatosis. In contrast, D-serine had no effect on food intake of CD fed animals. D-serine supplementation modified gut microbiota but changes occurred after reduction in food intake and therefore are not responsible for altered food preference. In addition, germ free mice fed HFD + D-serine displayed a reduced food intake and lost weight. After chronic supplementation, D-serine accumulated in various metabolically important organs as liver, adipose tissue, and kidney without causing tissue damage or inflammation. However, D-serine altered the one-carbon cycle in the liver.

Independent of the diet, D-serine induced hyperglycemia after 1 to 2 weeks of supplementation, due to an indirect reduction of insulin secretion from pancreatic beta cells. Injection of an  $\alpha 2$ -adrenergic receptor inhibitor normalized insulin secretion, indicating that D-serine regulates insulin secretion via the sympathetic nervous system.

### ***5.2.1 D-serine induced changes in food preference are independent of changes in gut microbiome***

Here, it was shown that D-serine reduces HFD but not CD intake and prevents from diet induced obesity. These data are in line with results from Sasaki et al. who described that D-serine suppresses intake of HFD and blunted weight gain (Sasaki et al., 2015). However, in contrast to this previous study, D-serine supplemented mice here resumed consuming HFD, albeit less than HFD control mice. Activation of

NMDARs located in the hindbrain reduce total food intake (Guard et al., 2009; Ritter, 2011), and NMDAR antagonists were reported to stimulate food intake through a reduction of corticosterone releasing hormone (CRH) release from hypothalamic CRH neurons (Tejas-Juarez et al., 2014). However, CRH is part of the leptin pathway to regulate food intake (Masaki et al., 2003), and Sasaki and colleagues showed a decrease in HFD food intake in D-serine treated *db/db* mice, arguing for a leptin independent regulation of food intake (Sasaki et al., 2015). Therefore, the underlying mechanism of D-serine on HFD intake and weight gain is complicated. Interestingly, in this thesis it was shown that D-serine supplementation reduces c-Fos expression in various regions of the hypothalamus, indicating that chronic co-agonism of D-serine on NMDARs in the hypothalamus promotes long term depression rather than long term potentiation. Thus, future experiments are needed to identify the neuronal populations and circuits regulating food preference in context of D-serine.

In addition to food intake, gut microbiota can have a strong impact on the development of obesity (Ussar et al., 2016; Ussar et al., 2015). Some classes of gut bacteria produce and take up D-serine and thereby restrict growth to certain bacterial classes (Connolly et al., 2016; Connolly et al., 2015; Li and Lu, 2016) and contribute to D-serine levels in the host (Sasaki et al., 2016; Silbernagl et al., 1999). Here, it was demonstrated that D-serine supplementation alters the composition of gut microbiota. Nevertheless, these changes did not appear to contribute to the altered weight gain as germfree mice also did not gain weight upon HFD + D-serine treatment. Interestingly, after 14 days of D-serine supplementation the obesogenic family *Erysipelotrichaceae* (Zietak et al., 2016) expanded in the intestines of HFD + D-serine fed animals. The increase occurred together with resuming weight gain in HFD + D-serine mice. Thus, D-serine mediated alterations in gut microbiota could play a role in increased weight gain and potentially explain differences to the study of Sasaki and colleagues, who did not observe the resumption of weight gain (Sasaki et al., 2015).

### **5.2.2 D-serine alters hepatic one-carbon cycle but does not induce tissue damage or inflammation**

This thesis demonstrated that orally administered D-serine rapidly enters the circulation, is taken up by and accumulates in liver, adipose tissue, kidney, and the hypothalamus. Degradation of D-serine by DAO results in the formation of hydrogen peroxide, which can result in tissue damage in the renal proximal tubules of rats (Montesinos Guevara and Mani, 2016; Rais et al., 2012). However, these findings

could not be replicated in mice, dogs or monkeys. In this thesis, nephrotoxicity was not detected, except a trend for increased KIM1 expression in some mice. Chronic supplementation of D-serine led to its accumulation in brain, liver and adipose tissue, but also in those tissues, no damage or signs of inflammation were detected. Though, accumulation of D-serine in the liver resulted in altered metabolite content, as glycine and the reduced form of glutathione were reduced in the livers of D-serine supplemented animals. In addition, the expression of serine to glycine converting enzyme SHMT1 was reduced in D-serine treated mice. SHMT1 activity is an important step in the one carbon cycle, as it transfers one carbon to THF that can be used in the synthesis of purines, mitochondrial tRNA methylation, thymidylate synthesis, and methionine re-methylation (Newman and Maddocks, 2017). Thus, D-serine could have positive effects on preventing the development of cancer, through limiting one-carbon units.

### **5.2.3 D-serine regulates insulin secretion and glucose homeostasis**

Most importantly, D-serine supplementation resulted in reversible hyperglycemia and glucose intolerance within one to two weeks of supplementation. The effects of D-serine on glucose tolerance were stronger in CD compared to HFD fed animals, which can be explained by the fact that animals on CD consume more water than on HFD. Glucose intolerance was caused by impaired insulin secretion from the pancreatic  $\beta$ -cells. Interestingly, variants in serine racemase (SRR), the enzyme catalyzing the conversion from L-serine to D-serine, are associated with T2D (Labrie et al., 2009; Tsai et al., 2010). Metabolic assessment of SRR ko mice revealed improved glucose tolerance (Lockridge et al., 2016). In contrast, knockdown of SRR in pancreatic  $\beta$ -cells blunted IBMX/ high glucose induced insulin secretion (Ndiaye et al., 2017), indicating tissue selective functions of SRR/D-serine in the regulation of glucose homeostasis. Marquard and colleagues described a role of NMDA receptors on  $\beta$ -cells in inhibiting insulin secretion *in vivo* and *in vitro* (Marquard et al., 2015). In contrast, no direct effect of D-serine on glucose stimulated insulin secretion from  $\beta$ -cells was observed here. The sympathetic nervous system has been established as an important regulator of insulin secretion (Osundiji and Evans, 2013; Osundiji et al., 2012) and  $\alpha$ 2-adrenergic receptor inhibition was previously described to reduce blood glucose levels in other contexts (Sim et al., 2014; Tang et al., 2014). Using an  $\alpha$ 2-adrenergic receptor inhibitor increased insulin secretion in D-serine supplemented mice and normalized blood glucose levels. Hence, it is assumed that D-serine impacts GSIS via activation of the sympathetic nervous system, rather than direct



action on  $\beta$ -cells. A single injection of the inhibitor was enough to normalize blood glucose levels for one week. This was surprising as the half-life time of BRL44406 is very short (Uhlen et al., 2016) and indicates that the inhibitor in some way resets the D-serine caused signal. Afterwards, hyperglycemia was re-established after more than one week which was comparable to the development of hyperglycemia in mice exposed to D-serine for the first time. However, D-serine seems to regulate only a subset of sympathetic nerves as it did not alter brown adipose tissue function of WAT being.

In contrast to those findings, supplementation with low D-serine concentrations improved insulin secretion and glucose tolerance. In addition, an acute injection of D-serine also reduced glucose tolerance. The reason behind remains unclear, but one could speculate that low D-serine concentrations are beneficial for glucose tolerance and insulin secretion. Chronic exposure to high D-serine concentrations could result in some form of D-serine resistance which also would explain the observation that the development of hyperglycemia takes 1 week.

#### **5.2.4 D-serine in the therapy of schizophrenia**

Schizophrenia is a psychotic disease with motor and cognitive defects affecting more than 21 million people worldwide (WHO, fact sheet on schizophrenia, April 2018; <http://www.who.int/en/news-room/fact-sheets/detail/schizophrenia>). Behavioral aspects of the disease lead to a sedentary lifestyle and poor food choices (Leitao-Azevedo et al., 2006), resulting in an above average rate of obesity in these patients. Moreover, many antipsychotic drugs used for the treatment of schizophrenia promote weight gain, contributing to the increased adiposity and a predisposition to develop the metabolic syndrome (Suvisaari et al., 2013). Together, this leads to a 2-5-fold higher risk in developing T2D, and complications of T2D are the number one cause of death in these patients (Foley et al., 2016; Suvisaari et al., 2013).

As D-serine is reduced in schizophrenic patients, clinical studies used it as monotherapy or in combination with antipsychotics and demonstrated improved total psychopathology, negative and cognitive symptoms (Avellar et al., 2016; Kantrowitz et al., 2015; Tsai et al., 1998). The serotonin and dopamine receptor antagonist clozapine, amongst other actions, raises peripheral and CNS D-serine levels (Tanahashi et al., 2012; Yamamori et al., 2014). At the same time, it has some of the strongest negative metabolic consequences such as increasing body weight and impairing glucose homeostasis (Hirsch et al., 2017; Rojo et al., 2015).

The results of this thesis together with a study by Sasaki et al. showed that D-serine reduced HFD food intake and weight gain upon HFD feeding (Sasaki et al., 2015). Thus, restoring D-serine levels and with that NMDAR function could be a new way to treat schizophrenia and the complications of those patients becoming obese. However, potential metabolic consequences of elevating D-serine levels were largely ignored until now. Here it was shown that chronic supplementation with high levels of D-serine has severe effects on glucose homeostasis which could be harmful for the treatment of schizophrenic patients. Though, it also was shown that an acute injection as well as low doses of D-serine in drinking water improved glucose tolerance. Clinical doses of D-serine are about 20-fold lower than the highest dose used in this study (Kantrowitz et al., 2016; Kantrowitz et al., 2015; Tsai et al., 1998). However, the effects of D-serine on glucose homeostasis most likely require accumulation of D-serine in the CNS. Thus, lower doses could simply take longer to reach the necessary threshold in humans. The same safety concerns also apply for the pharmacological inhibition of DAO, which is in clinical trials to increase D-serine levels (Hin et al., 2016; Lane et al., 2013; Rais et al., 2012). Nevertheless, it could be beneficial to acutely instead of chronically treat patients with D-serine to avoid accumulation of D-serine and the development of a D-serine resistance. Though, it is unclear whether this would be possible concerning the symptoms of schizophrenia.

Hence, the risk in the treatment of schizophrenia with D-serine or D-serine elevating drugs needs to be surveyed again. In general, medications may need to be adapted to the patients, as reduced D-serine levels can be caused by a lack of SRR or an elevated activity of DAO. Therefore, patients with reduced SRR activity could be more sensitive to D-serine supplementation and its side-effects compared to patients with elevated DAO activity, where the turnover of D-serine is much higher. Alternatively, a combinatorial treatment with glycine, the second NMDA receptor co-agonist, could be used as treatment, as glycine reduces hepatic gluconeogenesis (Yue et al., 2016) and could, in part, counteract the metabolic consequences of D-serine.

### **5.3 L-serine supplementation remodels hepatic metabolism**

L-serine is a conditional essential amino acid that can be produced by some but not all types of cells. L-serine can derive from three possible sources: dietary intake; biosynthesis from 3-phosphoglycerate or glycine; and by degradation of proteins and phospholipids (de Koning et al., 2003). It is one of the 20 proteinogenic amino acids and has an important role as phosphosite. Besides serine, also threonine and tyrosine can be phosphorylated, but over 95 % of protein phosphorylation occurs on serine residues (Metcalf et al., 2018). Phosphorylation of proteins is a fast and reversible process and regulates their conformation and activity. Thereby, phosphorylation is involved in the regulation of protein interactions, protein degradation, signal transduction, cell cycle, apoptosis and growth (Huttlin et al., 2010; Metcalf et al., 2018). Besides its important function in protein synthesis, L-serine serves as precursor for many other metabolites as for example one-carbon groups for the *de novo* synthesis of purine or pyrimidine nucleotides, other amino acids as cysteine and taurine, lipid messenger molecules, such as phosphatidylserine and ceramide, and the neuromodulators glycine and D-serine (de Koning et al., 2003; Metcalf et al., 2018).

Several diseases are associated with dysregulated L-serine levels and supplementation of L-serine was shown to be neuroprotective (Metcalf et al., 2018), to improve human sleep (Ito et al., 2014), to reduce mean arterial pressure (Mishra et al., 2008) and to improve symptoms caused by defects in L-serine biosynthetic pathway like seizures, spasticity, white matter volume, and myelination (El-Hattab, 2016; Tabatabaie et al., 2011). Therefore, its therapeutic potential in the treatment of progressive neurodegenerative diseases including amyotrophic lateral sclerosis and Alzheimer's disease is under investigation (Metcalf et al., 2018). Due to so far unknown negative side effects, L-serine was determined as "generally regarded as safe" by the FDA (Metcalf et al., 2018).

In line with this safety statement, this work showed that supplementation with 1 % L-serine in drinking water has no impact on body weight or lipid accumulation in fat depots after high fat diet feeding. Neither on CD, nor on HFD L-serine influenced glucose tolerance or insulin levels. However, hepatic *Pepck* expression was increased in CD + L-serine fed mice. Whereas hepatic triglyceride accumulation after HFD feeding was not altered, levels of glycogen were reduced. In addition, important metabolites in the liver were altered on both diets after L-serine supplementation.

### **5.3.1 L-serine supplementation alters serine catabolism in brown adipose tissue**

On CD, mice supplemented with L-serine consumed more water than controls, which could be explained by the sweet taste of L-serine (Schiffman and Engelhard, 1976). On HFD, water intake was similar between groups, maybe due to the satisfied demand for sweet taste from consuming the high sugar-containing HFD. Diets rich in protein or dietary amino acid supplementation were shown to alter gut microbiota (Bifari et al., 2017), but surprisingly supplementation with L-serine did not modify gut microbiota in this study. According to those findings, L-serine had no impact on food intake or weight gain.

Whereas L-serine supplementation had no effect on white adipose tissue, it reduced the enzymes responsible in serine catabolism in brown adipose tissue. Both, the L- to D-serine converting *Srr* and the serine-to-glycine-converting enzyme *Shmt1* were significantly reduced in CD + L-serine fed animals compared to controls. In BAT, serine is known to have an impact on glycolysis by activating the pyruvate producing enzyme pyruvate kinase isoform M2 (Chaneton et al., 2012; Lu et al., 2017). According to this, serine levels are increased upon cold-induced thermogenesis (Lopez-Soriano and Alemany, 1987). Mice in this study were kept at room temperature, which is a slight cold stimulus (van der Stelt et al., 2017). Mice on CD use glucose as substrate for non-shivering thermogenesis, but against expectations, *Shmt1* was upregulated in CD control compared to L-serine supplemented mice, leading to reduced serine biosynthesis. Some time ago it, was shown that the cytoplasmic form of SHMT, which is SHMT1, may convert glycine to serine instead the other way round (Garrow et al., 1993). If this is true in brown adipocytes, it could explain the observed upregulated *Shmt1* levels in CD control mice. Upon HFD feeding, mice use free fatty acids rather than glucose as substrate (see reduced RER in Figure 19A); therefore there is no demand for L-serine to defend body temperature.

### **5.3.2 L-serine does not impact glucose tolerance**

In chapter 4.2, D-serine was shown to reduce glucose tolerance by inhibition of insulin secretion. Opposed to that, L-serine had no effect on glucose tolerance or insulin levels. These data were in contrast to findings by Holm et al. who showed an increase in insulin levels after L-serine supplementation in female NOD mice, which are a model for type 1 diabetes (Holm et al., 2018). They found that L-serine reduced

beta cell inflammation, improved insulin levels and thereby normalized blood glucose levels. In addition, they showed improved glucose tolerance in mice supplemented with L-serine which could not be seen in this study on both diets. These differences could be due to the different mouse models, as in this study C57Bl/6 mice, a model for type 2 diabetes (Surwit et al., 1988), were used. In addition, Holm and colleagues used 9 fold higher concentrations of L-serine, which could explain the differences regarding insulin levels and glucose tolerance.

### **5.3.3 L-serine supplementation alters hepatic gluconeogenesis and metabolism**

In contrast to the results in glucose tolerance, mice fed a CD and supplemented with L-serine had a significantly elevated hepatic *Pepck* expression, indicating increased gluconeogenesis in the liver. In mammals, there exist two pathways of gluconeogenesis directly from L-serine (de Koning et al., 2003). One involves the formation of pyruvate and the other one the formation of hydroxypyruvate (de Koning et al., 2003). In addition, two of the products of L-serine metabolism, cysteine and glycine, are precursors for the synthesis of glutathione (de Koning et al., 2003). Depletion of glutathione is known to induce glycogenolysis in hepatocytes (Braun et al., 1996), which in turn can drive hepatic gluconeogenesis (Chung et al., 2015). Interestingly, glutathione levels were reduced in L-serine supplemented mice regardless of the diet, which could explain the observation that glycogen levels were reduced in L-serine supplemented animals. Therefore, supplementation of L-serine could upregulate hepatic gluconeogenesis via several pathways. At the same time, this observation could explain the fact that no changes in glucose tolerance were detected.

Interestingly, serine did not accumulate in the livers and neither *Shmt1*, nor its product glycine was altered after L-serine supplementation. This indicates either a fast turn-over of serine and glycine, the activation of alternative serine catabolism pathways (Yoshida and Kikuchi, 1970) or that the supplemented serine did not reach the liver and the observed effects are secondary effects due to changes in whole body metabolism.

## 6 Conclusion and Outlook

Overweight and obesity are a major health burden all over the world. Its comorbidities, above all cardiovascular diseases and T2D, increase the mortality of obese people. Though, the prevalence of obesity is increasing and much research is going on to study the causes and consequences of, and to find new ways to treat obesity. A novel approach is the tissue-targeted therapy that brings a drug specifically to the tissue of interest, reducing off-target and side effects. The first discovered surface protein specific for white adipose tissue was the amino acid transporter ASC-1. Bringing drugs to a specific protein always can interfere with its function. As ASC-1 is an amino acid transporter, inhibition could have negative side effects. Thus the aim of the thesis was to investigate the function of ASC-1 in white adipocytes. Here, it was shown that ASC-1 is an important regulator of white adipocyte identity. Inhibition or knockdown of ASC-1 in proliferating preadipocytes results in beiging of the cells during differentiation, while inhibition of mature adipocytes has no effect. Therefore, no negative effects would be expected in mature adipocytes, which are the majority of cells in white adipose tissue. In preadipocytes, inhibition by binding of a drug could cause beiging. That would be a positive side effect as it further would increase energy expenditure and reduce obesity. Therefore, ASC-1 would be a great molecule for tissue targeted therapy. Though, during drug development it needs to be kept in mind that ASC-1 also is expressed in various brain regions. All large-molecule products of biotechnology, such as monoclonal antibodies or recombinant proteins, do not cross the blood-brain barrier (Boss and Bergenheim, 2006; Pardridge, 2005). Though, obesity has been shown to disrupt the blood-brain barrier (Rhea et al., 2017), which enables the leakage of bigger molecules as antibodies into the brain (Preusser et al., 2017).

A combination of a drug and the Anti-ASC-1-antibody is relatively big which minimizes off-target effects in the brain. Though, eventual effects in the central nervous system are not completely excluded and need to be considered when developing the drug.

Nevertheless, the exact mechanism of ASC-1 in regulating adipocyte beiging remains unclear. Further experiments would be needed to test the hypothesis that ASC-1 is only expressed in beige precursor cells and suppresses differentiation into beige adipocytes. Therefore, single cell clones already were picked and it was shown, that some of them express *Asc-1* at higher levels than others. For future

experiments, it would be interesting whether those single cell clones differentiate into beige adipocytes when ASC-1 is inhibited. To further unravel the mechanism, it needs to be clarified whether this effect is caused indirectly by changes in intracellular amino acid signaling. Here, it already was shown that D-serine could play a role, but these experiments have only performed once and would needed to be repeated. Further, D-serine levels in ASC-1 overexpressing brown adipocytes would be interesting, as D-serine is supposed to have the opposite effect there. Overexpression of the D-serine degrading enzyme DAO in ASC-1 knockdown cells could unravel whether intracellular D-serine levels are responsible for the beige phenotype.

To prove those *in vitro* findings, it would be important to use fat-specific ASC-1 knockout mice. Here, this was not possible as the mouse line does not exist yet and whole body knockout mice were used instead. A loss of ASC-1 in the brain has severe effects and it hence is difficult to impossible to prove any mechanism.

After chronic D-serine supplementation in mice, it accumulated in SCF. The *in vitro* findings suggest that intracellular D-serine levels may impact on beiging in proliferating preadipocytes. In adipose tissue, most cells are mature adipocytes while only a lower amount of cells are preadipocytes. As shown by single cell analysis, ASC-1 is only expressed in 3 out of 52 cell clones. Therefore, accumulating D-serine could enter the different cells types in SCF, but would only affect those precursor cells that express high levels of ASC-1. Therefore, any occurring effect on beige adipogenesis simply could be overlapped by the high amount of unaffected white adipocytes. In conclusion, no effect on WAT beiging was expected and observed after chronic D-serine supplementation in mice.

More important, the main effects caused by D-serine supplementation were seen on HFD food intake and insulin secretion from pancreatic  $\beta$ -cells. The data suggest that D-serine acts via the sympathetic nervous system to regulate insulin secretion. Nevertheless, this has not been verified here and further experiments would be needed. For example, injections of D-serine directly into the brain followed by measuring glucose stimulated insulin secretion would be helpful to prove that D-serine acts via the central nervous system. In addition, genetic mouse models, as for example  $\beta$ -cell specific SRR knockout mice would be a good way to further investigate the role of D-serine on insulin secretion. All in all, the effects of chronic supplementation with D-serine on HFD food intake would be beneficial for the development of obesity, but its possible negative effect on insulin secretion are more

severe and need to be considered, when treating schizophrenic patients chronically with D-serine or drugs that increase levels of D-serine.

In addition to those findings, preliminary data show that L-serine supplementation alters hepatic metabolism with so far unknown consequences. The data especially suggest that hepatic gluconeogenesis is increased after L-serine supplementation, but this needs to be proved for example via a pyruvate tolerance test. In addition, the expression pattern of enzymes responsible for serine-based gluconeogenesis could be tested. An ITT would reveal if L-serine improves insulin tolerance as shown in the literature, and could also explain the unaltered GTT upon improved gluconeogenesis.

All in all, here it is shown that targeting the amino acid transporter ASC-1 could be a great approach for the treatment of obesity as it promotes white adipose tissue being and thereby increases energy expenditure. The mechanism behind may be driven by intracellular levels of the neurotransmitter D-serine.

Supplementation with D-serine did not alter WAT identity, but revealed a severe effect on HFD induced weight gain, as well as on glucose homeostasis. Hence, those metabolic side effects need to be considered and great caution needs to be taken when administrating D-serine chronically to schizophrenic patients. Independent of D-serine, L-serine supplementation results in altered liver metabolism. The consequences have not been investigated so far, but could have an impact on hepatic gluconeogenesis.

Therefore, the effects of ASC-1 are supposed to be dependent of D-serine, while the effects of D-/ or L-serine supplementation seem to be independent of their transporter ASC-1. Nevertheless, all three projects have a major impact on the treatment of schizophrenia, diabetes and/or obesity.



## VI References

- Andersson, D.P., Thorell, A., Lofgren, P., Wiren, M., Toft, E., Qvisth, V., Riserus, U., Berglund, L., Naslund, E., Bringman, S., *et al.* (2014). Omentectomy in addition to gastric bypass surgery and influence on insulin sensitivity: a randomized double blind controlled trial. *Clinical nutrition (Edinburgh, Scotland)* 33, 991-996.
- Arriza, J.L., Kavanaugh, M.P., Fairman, W.A., Wu, Y.N., Murdoch, G.H., North, R.A., and Amara, S.G. (1993). Cloning and expression of a human neutral amino acid transporter with structural similarity to the glutamate transporter gene family. *J Biol Chem* 268, 15329-15332.
- Austin, S., and St-Pierre, J. (2012). PGC1alpha and mitochondrial metabolism--emerging concepts and relevance in ageing and neurodegenerative disorders. *Journal of cell science* 125, 4963-4971.
- Avellar, M., Scoriels, L., Madeira, C., Vargas-Lopes, C., Marques, P., Dantas, C., Manhaes, A.C., Leite, H., and Panizzutti, R. (2016). The effect of D-serine administration on cognition and mood in older adults. *Oncotarget* 7, 11881-11888.
- Bacha, F., Lee, S., Gungor, N., and Arslanian, S.A. (2010). From pre-diabetes to type 2 diabetes in obese youth: pathophysiological characteristics along the spectrum of glucose dysregulation. *Diabetes care* 33, 2225-2231.
- Bartesaghi, S., Hallen, S., Huang, L., Svensson, P.A., Momo, R.A., Wallin, S., Carlsson, E.K., Forslow, A., Seale, P., and Peng, X.R. (2015). Thermogenic activity of UCP1 in human white fat-derived beige adipocytes. *Molecular endocrinology* 29, 130-139.
- Basu, A.C., Tsai, G.E., Ma, C.L., Ehmsen, J.T., Mustafa, A.K., Han, L., Jiang, Z.I., Benneyworth, M.A., Froimowitz, M.P., Lange, N., *et al.* (2009). Targeted disruption of serine racemase affects glutamatergic neurotransmission and behavior. *Molecular psychiatry* 14, 719-727.
- Bendikov, I., Nadri, C., Amar, S., Panizzutti, R., De Miranda, J., Wolosker, H., and Agam, G. (2007). A CSF and postmortem brain study of D-serine metabolic parameters in schizophrenia. *Schizophrenia research* 90, 41-51.
- Berna, M.J., and Ackermann, B.L. (2007). Quantification of serine enantiomers in rat brain microdialysate using Marfey's reagent and LC/MS/MS. *Journal of Chromatography B* 846, 359-363.
- Bifari, F., Ruocco, C., Decimo, I., Fumagalli, G., Valerio, A., and Nisoli, E. (2017). Amino acid supplements and metabolic health: a potential interplay between intestinal microbiota and systems control. *Genes & nutrition* 12, 27.
- Blomstrand, E., Eliasson, J., Karlsson, H.K., and Kohnke, R. (2006). Branched-chain amino acids activate key enzymes in protein synthesis after physical exercise. *The Journal of nutrition* 136, 269s-273s.
- Boss, O., and Bergenhem, N. (2006). Adipose targets for obesity drug development. *Expert opinion on therapeutic targets* 10, 119-134.
- Braun, L., Csala, M., Poussu, A., Garzo, T., Mandl, J., and Banhegyi, G. (1996). Glutathione depletion induces glycogenolysis dependent ascorbate synthesis in isolated murine hepatocytes. *FEBS letters* 388, 173-176.
- Broer, A., Brookes, N., Ganapathy, V., Dimmer, K.S., Wagner, C.A., Lang, F., and Broer, S. (1999). The astroglial ASCT2 amino acid transporter as a mediator of glutamine efflux. *Journal of neurochemistry* 73, 2184-2194.
- Brown, J.M., Hunihan, L., Prack, M.M., Harden, D.G., Bronson, J., Dzierba, C.D., Gentles, R.G., Hendricson, A., Krause, R., Macor, J.E., *et al.* (2014). In vitro Characterization of a small molecule inhibitor of the alanine serine cysteine transporter -1 (SLC7A10). *Journal of neurochemistry* 129, 275-283.
- Burnet, P.W., Hutchinson, L., von Hesling, M., Gilbert, E.J., Brandon, N.J., Rutter, A.R., Hutson, P.H., and Harrison, P.J. (2008). Expression of D-serine and glycine transporters in the prefrontal cortex and cerebellum in schizophrenia. *Schizophrenia research* 102, 283-294.

- Calenzani, G., Santos, F.F.D., Wittmer, V.L., Freitas, G.K.F., and Paro, F.M. (2017). Prevalence of musculoskeletal symptoms in obese patients candidates for bariatric surgery and its impact on health related quality of life. *Archives of endocrinology and metabolism* 61, 319-325.
- Calle, E.E., Rodriguez, C., Walker-Thurmond, K., and Thun, M.J. (2003). Overweight, obesity, and mortality from cancer in a prospectively studied cohort of U.S. adults. *The New England journal of medicine* 348, 1625-1638.
- Campfield, L.A., Smith, F.J., Guisez, Y., Devos, R., and Burn, P. (1995). Recombinant mouse OB protein: evidence for a peripheral signal linking adiposity and central neural networks. *Science (New York, NY)* 269, 546-549.
- Cannon, B., and Nedergaard, J. (2004). Brown adipose tissue: function and physiological significance. *Physiological reviews* 84, 277-359.
- Caporaso, J.G., Lauber, C.L., Walters, W.A., Berg-Lyons, D., Lozupone, C.A., Turnbaugh, P.J., Fierer, N., and Knight, R. (2011). Global patterns of 16S rRNA diversity at a depth of millions of sequences per sample. *Proceedings of the National Academy of Sciences of the United States of America* 108 Suppl 1, 4516-4522.
- Castillo, J.J., Hazlett, Z.S., Orlando, R.A., and Garver, W.S. (2017). A global evolutionary and metabolic analysis of human obesity gene risk variants. *Gene*.
- Chairoungdua, A., Kanai, Y., Matsuo, H., Inatomi, J., Kim, D.K., and Endou, H. (2001). Identification and characterization of a novel member of the heterodimeric amino acid transporter family presumed to be associated with an unknown heavy chain. *J Biol Chem* 276, 49390-49399.
- Chaneton, B., Hillmann, P., Zheng, L., Martin, A.C.L., Maddocks, O.D.K., Chokkathukalam, A., Coyle, J.E., Jankevics, A., Holding, F.P., Vousden, K.H., *et al.* (2012). Serine is a natural ligand and allosteric activator of pyruvate kinase M2. *Nature* 491, 458-462.
- Chau, Y.Y., Bandiera, R., Serrels, A., Martinez-Estrada, O.M., Qing, W., Lee, M., Slight, J., Thornburn, A., Berry, R., McHaffie, S., *et al.* (2014). Visceral and subcutaneous fat have different origins and evidence supports a mesothelial source. *Nat Cell Biol* 16, 367-375.
- Cheriyian, J., Mezes, C., Zhou, N., Balsara, R.D., and Castellino, F.J. (2015). Heteromerization of ligand binding domains of N-methyl-D-aspartate receptor requires both coagonists, L-glutamate and glycine. *Biochemistry* 54, 787-794.
- Chew, R.M., and Spencer, E. (1967). Development of metabolic response to cold in young mice of four species. *Comparative biochemistry and physiology* 22, 873-888.
- Chiang, J.L., Kirkman, M.S., Laffel, L.M., and Peters, A.L. (2014). Type 1 diabetes through the life span: a position statement of the American Diabetes Association. *Diabetes care* 37, 2034-2054.
- Chung, S.T., Chacko, S.K., Sunehag, A.L., and Haymond, M.W. (2015). Measurements of Gluconeogenesis and Glycogenolysis: A Methodological Review. *Diabetes* 64, 3996-4010.
- Cinti, S. (2002). Adipocyte differentiation and transdifferentiation: plasticity of the adipose organ. *Journal of endocrinological investigation* 25, 823-835.
- Collu-Marchese, M., Shuen, M., Pauly, M., Saleem, A., and Hood, D.A. (2015). The regulation of mitochondrial transcription factor A (Tfam) expression during skeletal muscle cell differentiation. *Bioscience reports* 35.
- Connolly, J.P., Gabrielsen, M., Goldstone, R.J., Grinter, R., Wang, D., Cogdell, R.J., Walker, D., Smith, D.G., and Roe, A.J. (2016). A Highly Conserved Bacterial D-Serine Uptake System Links Host Metabolism and Virulence. *PLoS Pathog* 12, e1005359.
- Connolly, J.P., Goldstone, R.J., Burgess, K., Cogdell, R.J., Beatson, S.A., Vollmer, W., Smith, D.G., and Roe, A.J. (2015). The host metabolite D-serine contributes to bacterial niche specificity through gene selection. *The ISME journal* 9, 1039-1051.

Cook, K.S., Min, H.Y., Johnson, D., Chaplinsky, R.J., Flier, J.S., Hunt, C.R., and Spiegelman, B.M. (1987). Adipsin: a circulating serine protease homolog secreted by adipose tissue and sciatic nerve. *Science (New York, NY)* 237, 402-405.

Cypess, A.M., Lehman, S., Williams, G., Tal, I., Rodman, D., Goldfine, A.B., Kuo, F.C., Palmer, E.L., Tseng, Y.H., Doria, A., *et al.* (2009). Identification and importance of brown adipose tissue in adult humans. *The New England journal of medicine* 360, 1509-1517.

Dadson, P., Landini, L., Helmio, M., Hannukainen, J.C., Immonen, H., Honka, M.J., Bucci, M., Savisto, N., Soinio, M., Salminen, P., *et al.* (2016). Effect of Bariatric Surgery on Adipose Tissue Glucose Metabolism in Different Depots in Patients With or Without Type 2 Diabetes. *Diabetes care* 39, 292-299.

de Jong, J.M., Larsson, O., Cannon, B., and Nedergaard, J. (2015). A stringent validation of mouse adipose tissue identity markers. *American journal of physiology Endocrinology and metabolism* 308, E1085-1105.

de Koning, T.J., Snell, K., Duran, M., Berger, R., Poll-The, B.T., and Surtees, R. (2003). L-serine in disease and development. *The Biochemical journal* 371, 653-661.

Dimitriadis, G., Mitrou, P., Lambadiari, V., Maratou, E., and Raptis, S.A. (2011). Insulin effects in muscle and adipose tissue. *Diabetes research and clinical practice* 93 *Suppl 1*, S52-59.

Edgar, R.C. (2013). UPARSE: highly accurate OTU sequences from microbial amplicon reads. *Nature methods* 10, 996-998.

El-Hattab, A.W. (2016). Serine biosynthesis and transport defects. *Molecular genetics and metabolism* 118, 153-159.

Falkenberg, M., Larsson, N.G., and Gustafsson, C.M. (2007). DNA replication and transcription in mammalian mitochondria. *Annual review of biochemistry* 76, 679-699.

Fedorenko, A., Lishko, P.V., and Kirichok, Y. (2012). Mechanism of fatty-acid-dependent UCP1 uncoupling in brown fat mitochondria. *Cell* 151, 400-413.

Felig, P. (1973). The glucose-alanine cycle. *Metabolism: clinical and experimental* 22, 179-207.

Finan, B., Yang, B., Ottaway, N., Stemmer, K., Muller, T.D., Yi, C.X., Habegger, K., Schriever, S.C., Garcia-Caceres, C., Kabra, D.G., *et al.* (2012). Targeted estrogen delivery reverses the metabolic syndrome. *Nature medicine* 18, 1847-1856.

Fischer, I.P., Irmeler, M., Meyer, C.W., Sachs, S.J., Neff, F., Hrabec de Angelis, M., Beckers, J., Tschop, M.H., Hofmann, S.M., and Ussar, S. (2018). A history of obesity leaves an inflammatory fingerprint in liver and adipose tissue. *International journal of obesity (2005)* 42, 507-517.

Flum, D.R., Belle, S.H., King, W.C., Wahed, A.S., Berk, P., Chapman, W., Pories, W., Courcoulas, A., McCloskey, C., Mitchell, J., *et al.* (2009). Perioperative safety in the longitudinal assessment of bariatric surgery. *The New England journal of medicine* 361, 445-454.

Foley, D.L., Mackinnon, A., Morgan, V.A., Watts, G.F., Castle, D.J., Waterreus, A., and Galletly, C.A. (2016). Common familial risk factors for schizophrenia and diabetes mellitus. *Aust N Z J Psychiatry* 50, 488-494.

Forest, C., Tordjman, J., Glorian, M., Duplus, E., Chauvet, G., Quette, J., Beale, E.G., and Antoine, B. (2003). Fatty acid recycling in adipocytes: a role for glyceroneogenesis and phosphoenolpyruvate carboxykinase. *Biochemical Society transactions* 31, 1125-1129.

Fukasawa, Y. (2000). Identification and Characterization of a Na<sup>+</sup>-independent Neutral Amino Acid Transporter That Associates with the 4F2 Heavy Chain and Exhibits Substrate Selectivity for Small Neutral D- and L-Amino Acids. *Journal of Biological Chemistry* 275, 9690-9698.

Galmozzi, A., Sonne, S.B., Altshuler-Keylin, S., Hasegawa, Y., Shinoda, K., Luijten, I.H.N., Chang, J.W., Sharp, L.Z., Cravatt, B.F., Saez, E., *et al.* (2014). ThermoMouse: an in vivo

model to identify modulators of UCP1 expression in brown adipose tissue. *Cell reports* 9, 1584-1593.

Garrow, T.A., Brenner, A.A., Whitehead, V.M., Chen, X.N., Duncan, R.G., Korenberg, J.R., and Shane, B. (1993). Cloning of human cDNAs encoding mitochondrial and cytosolic serine hydroxymethyltransferases and chromosomal localization. *J Biol Chem* 268, 11910-11916.

Gesta, S., Tseng, Y.H., and Kahn, C.R. (2007). Developmental origin of fat: tracking obesity to its source. *Cell* 131, 242-256.

Giordano, A., Frontini, A., and Cinti, S. (2016). Convertible visceral fat as a therapeutic target to curb obesity. *Nature reviews Drug discovery* 15, 405-424.

Golzarand, M., Toolabi, K., and Farid, R. (2017). The bariatric surgery and weight losing: a meta-analysis in the long- and very long-term effects of laparoscopic adjustable gastric banding, laparoscopic Roux-en-Y gastric bypass and laparoscopic sleeve gastrectomy on weight loss in adults. *Surgical endoscopy* 31, 4331-4345.

Groop, L. (2000). Pathogenesis of type 2 diabetes: the relative contribution of insulin resistance and impaired insulin secretion. *International journal of clinical practice Supplement*, 3-13.

Grosser, N., Oberle, S., Berndt, G., Erdmann, K., Hemmerle, A., and Schroder, H. (2004). Antioxidant action of L-alanine: heme oxygenase-1 and ferritin as possible mediators. *Biochemical and biophysical research communications* 314, 351-355.

Guard, D.B., Swartz, T.D., Ritter, R.C., Burns, G.A., and Covasa, M. (2009). NMDA NR2 receptors participate in CCK-induced reduction of food intake and hindbrain neuronal activation. *Brain research* 1266, 37-44.

Haines, W.R., Torres, G.E., Voigt, M.M., and Egan, T.M. (1999). Properties of the novel ATP-gated ionotropic receptor composed of the P2X(1) and P2X(5) isoforms. *Molecular pharmacology* 56, 720-727.

Hamdy, O., Porramatikul, S., and Al-Ozairi, E. (2006). Metabolic obesity: the paradox between visceral and subcutaneous fat. *Current diabetes reviews* 2, 367-373.

Hamilton, M.K., and Raybould, H.E. (2016). Bugs, guts and brains, and the regulation of food intake and body weight. *International Journal of Obesity Supplements* 6, S8-S14.

Harms, M., and Seale, P. (2013). Brown and beige fat: development, function and therapeutic potential. *Nature medicine* 19, 1252-1263.

Harms, M.J., Lim, H.W., Ho, Y., Shapira, S.N., Ishibashi, J., Rajakumari, S., Steger, D.J., Lazar, M.A., Won, K.J., and Seale, P. (2015). PRDM16 binds MED1 and controls chromatin architecture to determine a brown fat transcriptional program. *Genes Dev* 29, 298-307.

Heaton, J.M. (1972). The distribution of brown adipose tissue in the human. *Journal of anatomy* 112, 35-39.

Helboe, L., Egebjerg, J., Moller, M., and Thomsen, C. (2003). Distribution and pharmacology of alanine-serine-cysteine transporter 1 (asc-1) in rodent brain. *The European journal of neuroscience* 18, 2227-2238.

Hilton, C., Karpe, F., and Pinnick, K.E. (2015). Role of developmental transcription factors in white, brown and beige adipose tissues. *Biochimica et biophysica acta* 1851, 686-696.

Hin, N., Duvall, B., Berry, J.F., Ferraris, D.V., Rais, R., Alt, J., Rojas, C., Slusher, B.S., and Tsukamoto, T. (2016). D-Amino acid oxidase inhibitors based on the 5-hydroxy-1,2,4-triazin-6(1H)-one scaffold. *Bioorg Med Chem Lett* 26, 2088-2091.

Hirsch, L., Yang, J., Bresee, L., Jette, N., Patten, S., and Pringsheim, T. (2017). Second-Generation Antipsychotics and Metabolic Side Effects: A Systematic Review of Population-Based Studies. *Drug Saf.*

Hjorth, M.F., Ritz, C., Blaak, E.E., Saris, W.H., Langin, D., Poulsen, S.K., Larsen, T.M., Sorensen, T.I., Zohar, Y., and Astrup, A. (2017). Pretreatment fasting plasma glucose and insulin modify dietary weight loss success: results from 3 randomized clinical trials. *The American journal of clinical nutrition* 106, 499-505.

- Hogan-Cann, A.D., and Anderson, C.M. (2016). Physiological Roles of Non-Neuronal NMDA Receptors. *Trends in pharmacological sciences* 37, 750-767.
- Holm, L.J., Haupt-Jorgensen, M., Larsen, J., Giacobini, J.D., Bilgin, M., and Buschard, K. (2018). L-serine supplementation lowers diabetes incidence and improves blood glucose homeostasis in NOD mice. *PloS one* 13, e0194414.
- Horio, M., Kohno, M., Fujita, Y., Ishima, T., Inoue, R., Mori, H., and Hashimoto, K. (2011). Levels of D-serine in the brain and peripheral organs of serine racemase (Srr) knock-out mice. *Neurochemistry international* 59, 853-859.
- Horton, E.S. (1983). Role of environmental factors in the development of noninsulin-dependent diabetes mellitus. *The American journal of medicine* 75, 32-40.
- Hotamisligil, G.S., Shargill, N.S., and Spiegelman, B.M. (1993). Adipose expression of tumor necrosis factor- $\alpha$ : direct role in obesity-linked insulin resistance. *Science (New York, NY)* 259, 87-91.
- Huttlin, E.L., Jedrychowski, M.P., Elias, J.E., Goswami, T., Rad, R., Beausoleil, S.A., Villen, J., Haas, W., Sowa, M.E., and Gygi, S.P. (2010). A tissue-specific atlas of mouse protein phosphorylation and expression. *Cell* 143, 1174-1189.
- Ito, K., Dezaki, K., Yoshida, M., Yamada, H., Miura, R., Rita, R.S., Ookawara, S., Tabei, K., Kawakami, M., Hara, K., *et al.* (2017). Endogenous  $\alpha$ 2A-Adrenoceptor-Operated Sympathoadrenergic Tones Attenuate Insulin Secretion via cAMP/TRPM2 Signaling. *Diabetes* 66, 699-709.
- Ito, Y., Takahashi, S., Shen, M., Yamaguchi, K., and Satoh, M. (2014). Effects of L-serine ingestion on human sleep. *SpringerPlus* 3, 456.
- Jastroch, M., Divakaruni, A.S., Mookerjee, S., Treberg, J.R., and Brand, M.D. (2010). Mitochondrial proton and electron leaks. *Essays in biochemistry* 47, 53-67.
- Jastroch, M., Hirschberg, V., and Klingenspor, M. (2012). Functional characterization of UCP1 in mammalian HEK293 cells excludes mitochondrial uncoupling artefacts and reveals no contribution to basal proton leak. *Biochimica et biophysica acta* 1817, 1660-1670.
- Jeanson, Y., Carriere, A., and Casteilla, L. (2015). A New Role for Browning as a Redox and Stress Adaptive Mechanism? *Frontiers in endocrinology* 6, 158.
- Jeremic, N., Chaturvedi, P., and Tyagi, S.C. (2017). Browning of White Fat: Novel Insight Into Factors, Mechanisms, and Therapeutics. *Journal of cellular physiology* 232, 61-68.
- Kageyama, T., Imura, T., Matsuo, A., Minato, N., and Shimohama, S. (2000). Distribution of the 4F2 light chain, LAT1, in the mouse brain. *Neuroreport* 11, 3663-3666.
- Kantrowitz, J.T., Epstein, M.L., Beggel, O., Rohrig, S., Lehrfeld, J.M., Revheim, N., Lehrfeld, N.P., Reep, J., Parker, E., Silipo, G., *et al.* (2016). Neurophysiological mechanisms of cortical plasticity impairments in schizophrenia and modulation by the NMDA receptor agonist D-serine. *Brain* 139, 3281-3295.
- Kantrowitz, J.T., Woods, S.W., Petkova, E., Cornblatt, B., Corcoran, C.M., Chen, H., Silipo, G., and Javitt, D.C. (2015). D-serine for the treatment of negative symptoms in individuals at clinical high risk of schizophrenia: a pilot, double-blind, placebo-controlled, randomised parallel group mechanistic proof-of-concept trial. *The lancet Psychiatry* 2, 403-412.
- Kiefer, F.W. (2017). The significance of beige and brown fat in humans. *Endocrine connections* 6, R70-r79.
- Kiss, J.P., Zsilla, G., Mike, A., Zelles, T., Toth, E., Lajtha, A., and Vizi, E.S. (1995). Subtype-specificity of the presynaptic  $\alpha$  2-adrenoceptors modulating hippocampal norepinephrine release in rat. *Brain research* 674, 238-244.
- Klemm, D.J., Leitner, J.W., Watson, P., Nesterova, A., Reusch, J.E., Goalstone, M.L., and Draznin, B. (2001). Insulin-induced adipocyte differentiation. Activation of CREB rescues adipogenesis from the arrest caused by inhibition of prenylation. *J Biol Chem* 276, 28430-28435.

Klingenspor, M., Fromme, T., Hughes, D.A., Jr., Manzke, L., Polymeropoulos, E., Riemann, T., Trzcionka, M., Hirschberg, V., and Jastroch, M. (2008). An ancient look at UCP1. *Biochimica et biophysica acta* 1777, 637-641.

Labrie, V., Fukumura, R., Rastogi, A., Fick, L.J., Wang, W., Boutros, P.C., Kennedy, J.L., Semeralul, M.O., Lee, F.H., Baker, G.B., *et al.* (2009). Serine racemase is associated with schizophrenia susceptibility in humans and in a mouse model. *Human molecular genetics* 18, 3227-3243.

Labrie, V., Wang, W., Barger, S.W., Baker, G.B., and Roder, J.C. (2010). Genetic loss of D-amino acid oxidase activity reverses schizophrenia-like phenotypes in mice. *Genes, brain, and behavior* 9, 11-25.

Lane, H.Y., Lin, C.H., Green, M.F., Hellemann, G., Huang, C.C., Chen, P.W., Tun, R., Chang, Y.C., and Tsai, G.E. (2013). Add-on treatment of benzoate for schizophrenia: a randomized, double-blind, placebo-controlled trial of D-amino acid oxidase inhibitor. *JAMA psychiatry* 70, 1267-1275.

Le, K.T., Paquet, M., Nouel, D., Babinski, K., and Seguela, P. (1997). Primary structure and expression of a naturally truncated human P2X ATP receptor subunit from brain and immune system. *FEBS letters* 418, 195-199.

Lee, N.Y., Kim, Y., Ryu, H., and Kang, Y.S. (2017). The alteration of serine transporter activity in a cell line model of amyotrophic lateral sclerosis (ALS). *Biochemical and biophysical research communications* 483, 135-141.

Lee, Y.H., Petkova, A.P., Konkar, A.A., and Granneman, J.G. (2015). Cellular origins of cold-induced brown adipocytes in adult mice. *FASEB journal : official publication of the Federation of American Societies for Experimental Biology* 29, 286-299.

Leiden, J.M., Yang, L.H., Morle, G.D., June, C.H., Lindsten, T., Thompson, C.B., and Karpinski, B. (1989). The 4F2 heavy chain gene: a molecular model of inducible gene expression in human T cells. *Journal of autoimmunity* 2 *Suppl*, 67-79.

Leitao-Azevedo, C.L., Guimaraes, L.R., de Abreu, M.G., Gama, C.S., Lobato, M.I., and Belmonte-de-Abreu, P.S. (2006). Increased dyslipidemia in schizophrenic outpatients using new generation antipsychotics. *Revista brasileira de psiquiatria (Sao Paulo, Brazil : 1999)* 28, 301-304.

Li, G., and Lu, C.D. (2016). The Cryptic *dsdA* Gene Encodes a Functional D-Serine Dehydratase in *Pseudomonas aeruginosa* PAO1. *Curr Microbiol* 72, 788-794.

Li, G., Xie, C., Lu, S., Nichols, R.G., Tian, Y., Li, L., Patel, D., Ma, Y., Brocker, C.N., Yan, T., *et al.* (2017). Intermittent Fasting Promotes White Adipose Browning and Decreases Obesity by Shaping the Gut Microbiota. *Cell Metab* 26, 672-685 e674.

Lidell, M.E., Betz, M.J., Dahlqvist Leinhard, O., Heglind, M., Elander, L., Slawik, M., Mussack, T., Nilsson, D., Romu, T., Nuutila, P., *et al.* (2013). Evidence for two types of brown adipose tissue in humans. *Nature medicine* 19, 631-634.

Lin, L., Yee, S.W., Kim, R.B., and Giacomini, K.M. (2015). SLC transporters as therapeutic targets: emerging opportunities. *Nature reviews Drug discovery* 14, 543-560.

Liu, D., Bordicchia, M., Zhang, C., Fang, H., Wei, W., Li, J.L., Guilherme, A., Guntur, K., Czech, M.P., and Collins, S. (2016). Activation of mTORC1 is essential for beta-adrenergic stimulation of adipose browning. *J Clin Invest* 126, 1704-1716.

Liu, Z., Chen, O., Wall, J.B.J., Zheng, M., Zhou, Y., Wang, L., Ruth Vaseghi, H., Qian, L., and Liu, J. (2017). Systematic comparison of 2A peptides for cloning multi-genes in a polycistronic vector. *Sci Rep* 7, 2193.

Lo, K.A., and Sun, L. (2013). Turning WAT into BAT: a review on regulators controlling the browning of white adipocytes. *Bioscience reports* 33.

Locke, A.E., Kahali, B., Berndt, S.I., Justice, A.E., Pers, T.H., Day, F.R., Powell, C., Vedantam, S., Buchkovich, M.L., Yang, J., *et al.* (2015). Genetic studies of body mass index yield new insights for obesity biology. *Nature* 518, 197-206.

- Lockridge, A.D., Baumann, D.C., Akhaphong, B., Abrenica, A., Miller, R.F., and Alejandro, E.U. (2016). Serine racemase is expressed in islets and contributes to the regulation of glucose homeostasis. *Islets* 8, 195-206.
- Lopez-Soriano, F.J., and Alemany, M. (1987). Effect of cold-temperature exposure and acclimation on amino acid pool changes and enzyme activities of rat brown adipose tissue. *Biochimica et biophysica acta* 925, 265-271.
- Lu, X., Solmonson, A., Lodi, A., Nowinski, S.M., Sentandreu, E., Riley, C.L., Mills, E.M., and Tiziani, S. (2017). The early metabolomic response of adipose tissue during acute cold exposure in mice. *Sci Rep* 7, 3455.
- Madeira, C., Lourenco, M.V., Vargas-Lopes, C., Suemoto, C.K., Brandao, C.O., Reis, T., Leite, R.E., Laks, J., Jacob-Filho, W., Pasqualucci, C.A., *et al.* (2015). d-serine levels in Alzheimer's disease: implications for novel biomarker development. *Translational psychiatry* 5, e561.
- Mannion, B.A., Kolesnikova, T.V., Lin, S.H., Wang, S., Thompson, N.L., and Hemler, M.E. (1998). The light chain of CD98 is identified as E16/TA1 protein. *J Biol Chem* 273, 33127-33129.
- Marquard, J., Otter, S., Welters, A., Stirban, A., Fischer, A., Eglinger, J., Herebian, D., Kletke, O., Klemen, M.S., Stozler, A., *et al.* (2015). Characterization of pancreatic NMDA receptors as possible drug targets for diabetes treatment. *Nature medicine* 21, 363-372.
- Martinez-Sanchez, N., Moreno-Navarrete, J.M., Contreras, C., Rial-Pensado, E., Ferno, J., Nogueiras, R., Dieguez, C., Fernandez-Real, J.M., and Lopez, M. (2017). Thyroid hormones induce browning of white fat. *J Endocrinol* 232, 351-362.
- Masaki, T., Yoshimichi, G., Chiba, S., Yasuda, T., Noguchi, H., Kakuma, T., Sakata, T., and Yoshimatsu, H. (2003). Corticotropin-releasing hormone-mediated pathway of leptin to regulate feeding, adiposity, and uncoupling protein expression in mice. *Endocrinology* 144, 3547-3554.
- Mastroberardino, L., Spindler, B., Pfeiffer, R., Skelly, P.J., Loffing, J., Shoemaker, C.B., and Verrey, F. (1998). Amino-acid transport by heterodimers of 4F2hc/CD98 and members of a permease family. *Nature* 395, 288-291.
- Mathers, C.D., and Loncar, D. (2006). Projections of global mortality and burden of disease from 2002 to 2030. *PLoS medicine* 3, e442.
- McBride, H.M., Neuspiel, M., and Wasiak, S. (2006). Mitochondria: more than just a powerhouse. *Current biology* : CB 16, R551-560.
- McMurdie, P.J., and Holmes, S. (2013). phyloseq: an R package for reproducible interactive analysis and graphics of microbiome census data. *PloS one* 8, e61217.
- Metcalf, J.S., Dunlop, R.A., Powell, J.T., Banack, S.A., and Cox, P.A. (2018). L-Serine: a Naturally-Occurring Amino Acid with Therapeutic Potential. *Neurotoxicity research* 33, 213-221.
- Migliorini, R.H., Garofalo, M.A., and Kettelhut, I.C. (1997). Increased sympathetic activity in rat white adipose tissue during prolonged fasting. *The American journal of physiology* 272, R656-661.
- Milet, C., Bleher, M., Allbright, K., Orgeur, M., Couplier, F., Duprez, D., and Havis, E. (2017). *Egr1* deficiency induces browning of inguinal subcutaneous white adipose tissue in mice. *Sci Rep* 7, 16153.
- Mishra, R.C., Tripathy, S., Quest, D., Desai, K.M., Akhtar, J., Dattani, I.D., and Gopalakrishnan, V. (2008). L-Serine lowers while glycine increases blood pressure in chronic L-NAME-treated and spontaneously hypertensive rats. *Journal of hypertension* 26, 2339-2348.
- Montesinos Guevara, C., and Mani, A.R. (2016). The role of D-serine in peripheral tissues. *European journal of pharmacology* 780, 216-223.

- Murray, I., Sniderman, A.D., and Cianflone, K. (1999a). Mice lacking acylation stimulating protein (ASP) have delayed postprandial triglyceride clearance. *Journal of lipid research* *40*, 1671-1676.
- Murray, I., Sniderman, A.D., Havel, P.J., and Cianflone, K. (1999b). Acylation stimulating protein (ASP) deficiency alters postprandial and adipose tissue metabolism in male mice. *J Biol Chem* *274*, 36219-36225.
- Nakauchi, J., Matsuo, H., Kim, D.K., Goto, A., Chairoungdua, A., Cha, S.H., Inatomi, J., Shiokawa, Y., Yamaguchi, K., Saito, I., *et al.* (2000). Cloning and characterization of a human brain Na(+)-independent transporter for small neutral amino acids that transports D-serine with high affinity. *Neuroscience letters* *287*, 231-235.
- Ndiaye, F.K., Ortalli, A., Canouil, M., Huyvaert, M., Salazar-Cardozo, C., Lecoœur, C., Verbanck, M., Pawlowski, V., Boutry, R., Durand, E., *et al.* (2017). Expression and functional assessment of candidate type 2 diabetes susceptibility genes identify four new genes contributing to human insulin secretion. *Mol Metab* *6*, 459-470.
- Nedergaard, J., Golozoubova, V., Matthias, A., Asadi, A., Jacobsson, A., and Cannon, B. (2001). UCP1: the only protein able to mediate adaptive non-shivering thermogenesis and metabolic inefficiency. *Biochimica et biophysica acta* *1504*, 82-106.
- Newman, A.C., and Maddocks, O.D.K. (2017). Serine and Functional Metabolites in Cancer. *Trends in cell biology*.
- Ng, Y., Tan, S.X., Chia, S.Y., Tan, H.Y., Gun, S.Y., Sun, L., Hong, W., and Han, W. (2017). HOXC10 suppresses browning of white adipose tissues. *Experimental & molecular medicine* *49*, e292.
- Nishimura, Y., Tanaka, H., Ishida, T., Imai, S., Matsusue, Y., Agata, Y., and Horiike, K. (2014). Immunohistochemical localization of D-serine dehydratase in chicken tissues. *Acta histochemica* *116*, 702-707.
- O'Brien, P.E. (2010). Bariatric surgery: mechanisms, indications and outcomes. *Journal of gastroenterology and hepatology* *25*, 1358-1365.
- Ohno, H., Shinoda, K., Spiegelman, B.M., and Kajimura, S. (2012). PPARgamma agonists induce a white-to-brown fat conversion through stabilization of PRDM16 protein. *Cell Metab* *15*, 395-404.
- Okla, M., Kim, J., Koehler, K., and Chung, S. (2017). Dietary Factors Promoting Brown and Beige Fat Development and Thermogenesis. *Advances in nutrition (Bethesda, Md)* *8*, 473-483.
- Osundiji, M.A., and Evans, M.L. (2013). Brain control of insulin and glucagon secretion. *Endocrinology and metabolism clinics of North America* *42*, 1-14.
- Osundiji, M.A., Lam, D.D., Shaw, J., Yueh, C.Y., Markkula, S.P., Hurst, P., Colliva, C., Roda, A., Heisler, L.K., and Evans, M.L. (2012). Brain glucose sensors play a significant role in the regulation of pancreatic glucose-stimulated insulin secretion. *Diabetes* *61*, 321-328.
- Otte, D.M., Barcena de Arellano, M.L., Bilkei-Gorzo, A., Albayram, O., Imbeault, S., Jeung, H., Alferink, J., and Zimmer, A. (2013). Effects of Chronic D-Serine Elevation on Animal Models of Depression and Anxiety-Related Behavior. *PLoS one* *8*, e67131.
- Ouchi, N., Parker, J.L., Lugus, J.J., and Walsh, K. (2011). Adipokines in inflammation and metabolic disease. *Nature reviews Immunology* *11*, 85-97.
- Paley, C.A., and Johnson, M.I. (2018). Abdominal obesity and metabolic syndrome: exercise as medicine? *BMC sports science, medicine & rehabilitation* *10*, 7.
- Pardridge, W.M. (2005). The blood-brain barrier: bottleneck in brain drug development. *NeuroRx : the journal of the American Society for Experimental NeuroTherapeutics* *2*, 3-14.
- Paredes, S.D., Barriga, C., Reiter, R.J., and Rodriguez, A.B. (2009). Assessment of the Potential Role of Tryptophan as the Precursor of Serotonin and Melatonin for the Aged Sleep-wake Cycle and Immune Function: *Streptopelia Risoris* as a Model. *International journal of tryptophan research : IJTR* *2*, 23-36.



- Pasquali, L., Gaulton, K.J., Rodriguez-Segui, S.A., Mularoni, L., Miguel-Escalada, I., Akerman, I., Tena, J.J., Moran, I., Gomez-Marin, C., van de Bunt, M., *et al.* (2014). Pancreatic islet enhancer clusters enriched in type 2 diabetes risk-associated variants. *Nature genetics* *46*, 136-143.
- Peeters, A., Barendregt, J.J., Willekens, F., Mackenbach, J.P., Al Mamun, A., and Bonneux, L. (2003). Obesity in adulthood and its consequences for life expectancy: a life-table analysis. *Annals of internal medicine* *138*, 24-32.
- Pond, C.M. (1992). An evolutionary and functional view of mammalian adipose tissue. *The Proceedings of the Nutrition Society* *51*, 367-377.
- Preusser, M., Berghoff, A.S., Thallinger, C., and Zielinski, C. (2017). CECOG educational illustrations: the blood-brain barrier and its relevance for targeted cancer therapies and immuno-oncology. *ESMO open* *2*, e000194.
- Puigserver, P., Wu, Z., Park, C.W., Graves, R., Wright, M., and Spiegelman, B.M. (1998). A cold-inducible coactivator of nuclear receptors linked to adaptive thermogenesis. *Cell* *92*, 829-839.
- Quast, C., Pruesse, E., Yilmaz, P., Gerken, J., Schweer, T., Yarza, P., Peplies, J., and Glockner, F.O. (2013). The SILVA ribosomal RNA gene database project: improved data processing and web-based tools. *Nucleic acids research* *41*, D590-596.
- Rais, R., Thomas, A.G., Wozniak, K., Wu, Y., Jaaro-Peled, H., Sawa, A., Strick, C.A., Engle, S.J., Brandon, N.J., Rojas, C., *et al.* (2012). Pharmacokinetics of oral D-serine in D-amino acid oxidase knockout mice. *Drug metabolism and disposition: the biological fate of chemicals* *40*, 2067-2073.
- Rayner, D.V. (2001). The sympathetic nervous system in white adipose tissue regulation. *The Proceedings of the Nutrition Society* *60*, 357-364.
- Rehni, A.K., and Dave, K.R. (2018). Impact of Hypoglycemia on Brain Metabolism During Diabetes. *Molecular neurobiology*.
- Rexrode, K.M., Hennekens, C.H., Willett, W.C., Colditz, G.A., Stampfer, M.J., Rich-Edwards, J.W., Speizer, F.E., and Manson, J.E. (1997). A prospective study of body mass index, weight change, and risk of stroke in women. *Jama* *277*, 1539-1545.
- Rhea, E.M., Salameh, T.S., Logsdon, A.F., Hanson, A.J., Erickson, M.A., and Banks, W.A. (2017). Blood-Brain Barriers in Obesity. *The AAPS journal* *19*, 921-930.
- Ritter, R.C. (2011). A tale of two endings: modulation of satiation by NMDA receptors on or near central and peripheral vagal afferent terminals. *Physiology & behavior* *105*, 94-99.
- Rojo, L.E., Gaspar, P.A., Silva, H., Risco, L., Arena, P., Cubillos-Robles, K., and Jara, B. (2015). Metabolic syndrome and obesity among users of second generation antipsychotics: A global challenge for modern psychopharmacology. *Pharmacological research* *101*, 74-85.
- Rowe, A.H. (1923). INSULIN TREATMENT OF DIABETES MELLITUS. *California state journal of medicine* *21*, 204-208.
- Rutter, A.R., Fradley, R.L., Garrett, E.M., Chapman, K.L., Lawrence, J.M., Rosahl, T.W., and Patel, S. (2007). Evidence from gene knockout studies implicates Asc-1 as the primary transporter mediating d-serine reuptake in the mouse CNS. *The European journal of neuroscience* *25*, 1757-1766.
- Sacks, F.M., Bray, G.A., Carey, V.J., Smith, S.R., Ryan, D.H., Anton, S.D., McManus, K., Champagne, C.M., Bishop, L.M., Laranjo, N., *et al.* (2009). Comparison of weight-loss diets with different compositions of fat, protein, and carbohydrates. *The New England journal of medicine* *360*, 859-873.
- Safory, H., Neame, S., Shulman, Y., Zubedat, S., Radziszewsky, I., Rosenberg, D., Sason, H., Engelender, S., Avital, A., Hulsmann, S., *et al.* (2015). The alanine-serine-cysteine-1 (Asc-1) transporter controls glycine levels in the brain and is required for glycinergic inhibitory transmission. *EMBO reports* *16*, 590-598.

- Saito, M., Okamatsu-Ogura, Y., Matsushita, M., Watanabe, K., Yoneshiro, T., Nio-Kobayashi, J., Iwanaga, T., Miyagawa, M., Kameya, T., Nakada, K., *et al.* (2009). High incidence of metabolically active brown adipose tissue in healthy adult humans: effects of cold exposure and adiposity. *Diabetes* *58*, 1526-1531.
- Sakimura, K., Nakao, K., Yoshikawa, M., Suzuki, M., and Kimura, H. (2016). A novel Na<sup>+</sup> - Independent alanine-serine-cysteine transporter 1 inhibitor inhibits both influx and efflux of D-Serine. *Journal of neuroscience research*.
- Sanchez-Garrido, M.A., Brandt, S.J., Clemmensen, C., Muller, T.D., DiMarchi, R.D., and Tschop, M.H. (2017). GLP-1/glucagon receptor co-agonism for treatment of obesity. *Diabetologia* *60*, 1851-1861.
- Sarwar, N., Gao, P., Seshasai, S.R., Gobin, R., Kaptoge, S., Di Angelantonio, E., Ingelsson, E., Lawlor, D.A., Selvin, E., Stampfer, M., *et al.* (2010). Diabetes mellitus, fasting blood glucose concentration, and risk of vascular disease: a collaborative meta-analysis of 102 prospective studies. *Lancet (London, England)* *375*, 2215-2222.
- Sasaki, T., Kinoshita, Y., Matsui, S., Kakuta, S., Yokota-Hashimoto, H., Kinoshita, K., Iwasaki, Y., Kinoshita, T., Yada, T., Amano, N., *et al.* (2015). N-methyl-d-aspartate receptor coagonist d-serine suppresses intake of high-preference food. *American journal of physiology Regulatory, integrative and comparative physiology* *309*, R561-575.
- Sasaki, T., Matsui, S., and Kitamura, T. (2016). Control of Appetite and Food Preference by NMDA Receptor and Its Co-Agonist d-Serine. *Int J Mol Sci* *17*.
- Sason, H., Billard, J.M., Smith, G.P., Safory, H., Neame, S., Kaplan, E., Rosenberg, D., Zubedat, S., Foltyn, V.N., Christoffersen, C.T., *et al.* (2016). Asc-1 Transporter Regulation of Synaptic Activity via the Tonic Release of d-Serine in the Forebrain. *Cerebral cortex*.
- Scheller, J., Chalaris, A., Schmidt-Arras, D., and Rose-John, S. (2011). The pro- and anti-inflammatory properties of the cytokine interleukin-6. *Biochimica et biophysica acta* *1813*, 878-888.
- Schiffman, S.S., and Engelhard, H.H., 3rd (1976). Taste of dipeptides. *Physiology & behavior* *17*, 523-535.
- Schoettl, T., Fischer, I.P., and Ussar, S. (2018). Heterogeneity of adipose tissue in development and metabolic function. *The Journal of experimental biology* *221*.
- Schottl, T., Kappler, L., Braun, K., Fromme, T., and Klingenspor, M. (2015). Limited mitochondrial capacity of visceral versus subcutaneous white adipocytes in male C57BL/6N mice. *Endocrinology* *156*, 923-933.
- Seale, P., Bjork, B., Yang, W., Kajimura, S., Chin, S., Kuang, S., Scime, A., Devarakonda, S., Conroe, H.M., Erdjument-Bromage, H., *et al.* (2008). PRDM16 controls a brown fat/skeletal muscle switch. *Nature* *454*, 961-967.
- Sharma, B.K., Patil, M., and Satyanarayana, A. (2014). Negative regulators of brown adipose tissue (BAT)-mediated thermogenesis. *Journal of cellular physiology* *229*, 1901-1907.
- Sidossis, L., and Kajimura, S. (2015). Brown and beige fat in humans: thermogenic adipocytes that control energy and glucose homeostasis. *J Clin Invest* *125*, 478-486.
- Silbernagl, S., Volker, K., and Dantzer, W.H. (1999). D-Serine is reabsorbed in rat renal pars recta. *The American journal of physiology* *276*, F857-863.
- Sim, Y.B., Park, S.H., Kim, S.S., Lim, S.M., Jung, J.S., and Suh, H.W. (2014). Activation of spinal alpha2 adrenergic receptors induces hyperglycemia in mouse though activating sympathetic outflow. *European journal of pharmacology* *741*, 316-322.
- Singh, S., Narang, A.S., and Mahato, R.I. (2011). Subcellular fate and off-target effects of siRNA, shRNA, and miRNA. *Pharmaceutical research* *28*, 2996-3015.
- Steppan, C.M., Bailey, S.T., Bhat, S., Brown, E.J., Banerjee, R.R., Wright, C.M., Patel, H.R., Ahima, R.S., and Lazar, M.A. (2001). The hormone resistin links obesity to diabetes. *Nature* *409*, 307-312.

- Strasser, B., and Fuchs, D. (2016). Diet Versus Exercise in Weight Loss and Maintenance: Focus on Tryptophan. *International journal of tryptophan research : IJTR* 9, 9-16.
- Strychar, I. (2006). Diet in the management of weight loss. *CMAJ* 174, 56-63.
- Surwit, R.S., Kuhn, C.M., Cochrane, C., McCubbin, J.A., and Feinglos, M.N. (1988). Diet-induced type II diabetes in C57BL/6J mice. *Diabetes* 37, 1163-1167.
- Suvisaari, J., Partti, K., Perala, J., Viertio, S., Saarni, S.E., Lonnqvist, J., Saarni, S.I., and Harkanen, T. (2013). Mortality and its determinants in people with psychotic disorder. *Psychosom Med* 75, 60-67.
- Suwandhi, L., Hausmann, S., Braun, A., Gruber, T., Heinzmann, S.S., Gálvez, E.J.C., Buck, A., Legutko, B., Israel, A., Feuchtinger, A., *et al.* (2018). Chronic d-serine supplementation impairs insulin secretion. *Molecular Metabolism*.
- Tabatabaie, L., Klomp, L.W., Rubio-Gozalbo, M.E., Spaapen, L.J., Haagen, A.A., Dorland, L., and de Koning, T.J. (2011). Expanding the clinical spectrum of 3-phosphoglycerate dehydrogenase deficiency. *Journal of inherited metabolic disease* 34, 181-184.
- Tanahashi, S., Yamamura, S., Nakagawa, M., Motomura, E., and Okada, M. (2012). Clozapine, but not haloperidol, enhances glial D-serine and L-glutamate release in rat frontal cortex and primary cultured astrocytes. *Br J Pharmacol* 165, 1543-1555.
- Tang, Y., Axelsson, A.S., Spegel, P., Andersson, L.E., Mulder, H., Groop, L.C., Renstrom, E., and Rosengren, A.H. (2014). Genotype-based treatment of type 2 diabetes with an alpha2A-adrenergic receptor antagonist. *Science translational medicine* 6, 257ra139.
- Tarasov, A.I., Semplici, F., Ravier, M.A., Bellomo, E.A., Pullen, T.J., Gilon, P., Sekler, I., Rizzuto, R., and Rutter, G.A. (2012). The mitochondrial Ca<sup>2+</sup> uniporter MCU is essential for glucose-induced ATP increases in pancreatic beta-cells. *PLoS One* 7, e39722.
- Tejas-Juarez, J.G., Cruz-Martinez, A.M., Lopez-Alonso, V.E., Garcia-Iglesias, B., Mancilla-Diaz, J.M., Floran-Garduno, B., and Escartin-Perez, R.E. (2014). Stimulation of dopamine D4 receptors in the paraventricular nucleus of the hypothalamus of male rats induces hyperphagia: involvement of glutamate. *Physiology & behavior* 133, 272-281.
- Thiemann, S., Smit, N., Roy, U., Lesker, T.R., Galvez, E.J.C., Helmecke, J., Basic, M., Bleich, A., Goodman, A.L., Kalinke, U., *et al.* (2017). Enhancement of IFN $\gamma$  Production by Distinct Commensals Ameliorates Salmonella-Induced Disease. *Cell host & microbe* 21, 682-694.e685.
- Thwaites, D.T., and Anderson, C.M. (2011). The SLC36 family of proton-coupled amino acid transporters and their potential role in drug transport. *Br J Pharmacol* 164, 1802-1816.
- Toner, M.M., Holden, W.L., Foley, M.E., Bogart, J.E., and Pandolf, K.B. (1989). Influence of clothing and body-fat insulation on thermal adjustments to cold-water stress. *Aviation, space, and environmental medicine* 60, 957-963.
- Trayhurn, P., and Beattie, J.H. (2007). Physiological role of adipose tissue: white adipose tissue as an endocrine and secretory organ. *Proceedings of the Nutrition Society* 60, 329-339.
- Tsai, F.J., Yang, C.F., Chen, C.C., Chuang, L.M., Lu, C.H., Chang, C.T., Wang, T.Y., Chen, R.H., Shiu, C.F., Liu, Y.M., *et al.* (2010). A genome-wide association study identifies susceptibility variants for type 2 diabetes in Han Chinese. *PLoS genetics* 6, e1000847.
- Tsai, G., Yang, P., Chung, L.C., Lange, N., and Coyle, J.T. (1998). D-serine added to antipsychotics for the treatment of schizophrenia. *Biological psychiatry* 44, 1081-1089.
- Uhlen, S., Schioth, H.B., and Jahnsen, J.A. (2016). A new, simple and robust radioligand binding method used to determine kinetic off-rate constants for unlabeled ligands. Application at alpha2A- and alpha2C-adrenoceptors. *European journal of pharmacology* 788, 113-121.
- Unger, R.H., and Orci, L. (2002). Lipoapoptosis: its mechanism and its diseases. *Biochimica et biophysica acta* 1585, 202-212.
- Ussar, S., Fujisaka, S., and Kahn, C.R. (2016). Interactions between host genetics and gut microbiome in diabetes and metabolic syndrome. *Mol Metab* 5, 795-803.

- Ussar, S., Griffin, N.W., Bezy, O., Fujisaka, S., Vienberg, S., Softic, S., Deng, L., Bry, L., Gordon, J.I., and Kahn, C.R. (2015). Interactions between Gut Microbiota, Host Genetics and Diet Modulate the Predisposition to Obesity and Metabolic Syndrome. *Cell Metab* 22, 516-530.
- Ussar, S., Lee, K.Y., Dankel, S.N., Boucher, J., Haering, M.F., Kleinridders, A., Thomou, T., Xue, R., Macotela, Y., Cypess, A.M., *et al.* (2014). ASC-1, PAT2, and P2RX5 are cell surface markers for white, beige, and brown adipocytes. *Science translational medicine* 6, 247ra103.
- Utsunomiya-Tate, N., Endou, H., and Kanai, Y. (1996). Cloning and functional characterization of a system ASC-like Na<sup>+</sup>-dependent neutral amino acid transporter. *J Biol Chem* 271, 14883-14890.
- van der Stelt, I., Hoevenaars, F., Siroka, J., de Ronde, L., Friedecky, D., Keijer, J., and van Schothorst, E. (2017). Metabolic Response of Visceral White Adipose Tissue of Obese Mice Exposed for 5 Days to Human Room Temperature Compared to Mouse Thermoneutrality. *Frontiers in physiology* 8, 179.
- Van Harmelen, V., Reynisdottir, S., Cianflone, K., Degerman, E., Hoffstedt, J., Nilsell, K., Sniderman, A., and Arner, P. (1999). Mechanisms involved in the regulation of free fatty acid release from isolated human fat cells by acylation-stimulating protein and insulin. *J Biol Chem* 274, 18243-18251.
- Van Horn, M.R., Sild, M., and Ruthazer, E.S. (2013). D-serine as a gliotransmitter and its roles in brain development and disease. *Frontiers in cellular neuroscience* 7, 39.
- Verrey, F., Closs, E.I., Wagner, C.A., Palacin, M., Endou, H., and Kanai, Y. (2004). CATs and HATs: the SLC7 family of amino acid transporters. *Pflugers Archiv : European journal of physiology* 447, 532-542.
- Villarroya, F., and Vidal-Puig, A. (2013). Beyond the sympathetic tone: the new brown fat activators. *Cell Metab* 17, 638-643.
- Wang, Q., Garrity, G.M., Tiedje, J.M., and Cole, J.R. (2007). Naive Bayesian classifier for rapid assignment of rRNA sequences into the new bacterial taxonomy. *Applied and environmental microbiology* 73, 5261-5267.
- Wang, Q.A., Tao, C., Gupta, R.K., and Scherer, P.E. (2013). Tracking adipogenesis during white adipose tissue development, expansion and regeneration. *Nature medicine* 19, 1338-1344.
- Wang, S.C., Bednarski, B., Patel, S., Yan, A., Kohoyda-Inglis, C., Kennedy, T., Link, E., Rowe, S., Sochor, M., and Arbabi, S. (2003). Increased depth of subcutaneous fat is protective against abdominal injuries in motor vehicle collisions. *Annual proceedings Association for the Advancement of Automotive Medicine* 47, 545-559.
- Wang, W., and Seale, P. (2016). Control of brown and beige fat development. *Nature reviews Molecular cell biology* 17, 691-702.
- Watford, M. (2000). Functional glycerol kinase activity and the possibility of a major role for glyceroneogenesis in mammalian skeletal muscle. *Nutrition reviews* 58, 145-148.
- Wieser, V., Moschen, A.R., and Tilg, H. (2013). Inflammation, cytokines and insulin resistance: a clinical perspective. *Archivum immunologiae et therapeuticae experimentalis* 61, 119-125.
- Willer, C.J., Speliotes, E.K., Loos, R.J., Li, S., Lindgren, C.M., Heid, I.M., Berndt, S.I., Elliott, A.L., Jackson, A.U., Lamina, C., *et al.* (2009). Six new loci associated with body mass index highlight a neuronal influence on body weight regulation. *Nat Genet* 41, 25-34.
- Wolosker, H., Blackshaw, S., and Snyder, S.H. (1999). Serine racemase: a glial enzyme synthesizing D-serine to regulate glutamate-N-methyl-D-aspartate neurotransmission. *Proceedings of the National Academy of Sciences of the United States of America* 96, 13409-13414.
- Xie, X., Dumas, T., Tang, L., Brennan, T., Reeder, T., Thomas, W., Klein, R.D., Flores, J., O'Hara, B.F., Heller, H.C., *et al.* (2005). Lack of the alanine-serine-cysteine transporter 1 causes tremors, seizures, and early postnatal death in mice. *Brain research* 1052, 212-221.

Yamamori, H., Hashimoto, R., Fujita, Y., Numata, S., Yasuda, Y., Fujimoto, M., Ohi, K., Umeda-Yano, S., Ito, A., Ohmori, T., *et al.* (2014). Changes in plasma D-serine, L-serine, and glycine levels in treatment-resistant schizophrenia before and after clozapine treatment. *Neuroscience letters* 582, 93-98.

Yang, G., Li, C., Gong, Y., Fang, F., Tian, H., Li, J., and Cheng, X. (2016). Assessment of Insulin Resistance in Subjects with Normal Glucose Tolerance, Hyperinsulinemia with Normal Blood Glucose Tolerance, Impaired Glucose Tolerance, and Newly Diagnosed Type 2 Diabetes (Prediabetes Insulin Resistance Research). *Journal of diabetes research* 2016, 9270768.

Yin, J., Ren, W., Yang, G., Duan, J., Huang, X., Fang, R., Li, C., Li, T., Yin, Y., Hou, Y., *et al.* (2016). L-Cysteine metabolism and its nutritional implications. *Molecular nutrition & food research* 60, 134-146.

Yoshida, T., and Kikuchi, G. (1970). Major pathways of glycine and serine catabolism in rat liver. *Archives of biochemistry and biophysics* 139, 380-392.

Yue, J.T., Abraham, M.A., Bauer, P.V., LaPierre, M.P., Wang, P., Duca, F.A., Filippi, B.M., Chan, O., and Lam, T.K. (2016). Inhibition of glycine transporter-1 in the dorsal vagal complex improves metabolic homeostasis in diabetes and obesity. *Nat Commun* 7, 13501.

Zhang, Y., Proenca, R., Maffei, M., Barone, M., Leopold, L., and Friedman, J.M. (1994). Positional cloning of the mouse obese gene and its human homologue. *Nature* 372, 425-432.

Zhou, J., and Qin, G. (2012). Adipocyte dysfunction and hypertension. *American journal of cardiovascular disease* 2, 143-149.

Zietak, M., Kovatcheva-Datchary, P., Markiewicz, L.H., Stahlman, M., Kozak, L.P., and Backhed, F. (2016). Altered Microbiota Contributes to Reduced Diet-Induced Obesity upon Cold Exposure. *Cell Metab* 23, 1216-1223.

## VII Acknowledgements

At this point I would like to thank all people who made this work possible and supported me during my time as PhD student.

First, I want to thank Prof. Dr. Matthias Tschöp for providing a great research environment at the Institute of Diabetes and Obesity at the Helmholtz Center Munich. Second, I thank Prof. Dr. Johannes Beckers for taking over the role of my second adviser and for great and helpful discussions throughout my PhD thesis.

Special thanks go to my supervisor Dr. Siegfried Ussar for giving me the opportunity to perform my PhD thesis in his research group and for providing exciting projects. Under his supervision I got to know many methods, techniques and I learned a lot for my future life.

Of course I thank the whole Adipocyte and Metabolism group for scientific discussions, and, in particular, Andreas Israel and Ruth Karlina for performing several stainings. I especially thank Ingrid Fischer and Tim Gruber for proofreading my thesis and their helpful remarks.

I also want to thank all my collaboration partners for their contribution to publish my work. Dr. Simone Hausmann taught me how to isolate islets and perform *in vitro* GSIS. Tim Gruber, Beata Legutko and Cristina García Cáceres gave me insights into the brain, whereas Alexander Braun and Martin Elsner measured amino acids from cell and tissue extracts. Silke Heinzmann and Philippe Schmitt-Kopplin took over the liver metabolomics and I hope to continue the collaboration for the outstanding L-serine-project, where the liver metabolites seem to be altered drastically. Achim Buck, Annette Feuchtinger and Axel Walch generated MALDI images of labelled D-serine and helped evaluating islet and adipocyte cell size. Elizabeth Haythorne and Guy Rutter measured the membrane potential of isolated islets and thereby helped to prove the fact that D-serine does not directly act on beta cells. Eric Gálvez and Till Strowig performed the gut microbiota studies and welcomed me “back home” in Braunschweig, the city I received my Bachelor’s and Master’s degree in. It was a pleasure collaborating with you and to get an insight into your knowledge and methods which at the end helped me to see a bigger picture of the projects.

Finally, the biggest thank goes to my boyfriend Matthias Lehmann as well as my friends and family for their never-ending mental support. Especially my lab-colleges Dr. Simone Hausmann, Dr. Theresa Schöttl, Ingrid Fischer and Ines Pramme-Steinwachs became close friends and supported me during good and bad times. Thank you for always being there!







## IX Curriculum Vitae

**Lisa Siu-Lan Suwandhi, M.Sc.**

**Date of birth** 07/09/1989  
**Place of birth** Böblingen  
**Nationality** German

### Education

---

08/2014 – now: PhD Thesis; Helmholtz Center Munich, Institute for Diabetes and Obesity (Junior Research Group “Adipocytes and Metabolism”)

10/2013 - 05/2014: Master’s Thesis at Mediagnost Gesellschaft für Forschung und Herstellung von Diagnostica GmbH: „Validation of Insulin-like growth factor binding Protein-1 specific antibodies”

09/2012 – 05/2014: Master of Science in Biotechnology, Technical University of Braunschweig

07/2012 – 08/2012: Student assistant at the Institute for microbiology, Technical University of Braunschweig

04/2012 – 07/2012: Bachelor’s Thesis at the Institute of Microbiology, Technical University of Braunschweig „Analysis of Protein-Protein-Interaction between HemC and HemD from *Bacillus megaterium*”

09/2009 – 07/2012: Bachelor of Science in Biotechnology; Technical University of Braunschweig

09/2000 – 07/2009: Hegel-Gymnasium in Stuttgart, Germany  
Intensive courses: Biology and Chemistry